A Dissertation for the Degree of Doctor of Philosophy

Development of Complete Path Planning and Tracking Control Technologies for Autonomous Paddy field Tillage and Pudling·Leveling Operations

수도작 자율 경운 및 써레·정지 농작업을 위한 전역 경로 생성 및 탐색 제어 기술 개발

February 2022

Graduate School of College of Agriculture and Life Sciences
Seoul National University
Major in Biosystems Engineering

Chan-Woo Jeon

Development of Complete Path Planning and Tracking Control Technologies for Autonomous Paddy field Tillage and Pudling·Leveling Operations

Advisor: Prof. Hak-Jin Kim

Submitting a Ph.D. Dissertation of Biosystem Engineering
February 2022

Graduate School of College of Agriculture and Life Sciences
Seoul National University
Department of Biosystems Engineering

Chan-Woo Jeon

Confirming the Ph.D. Dissertation written by Chan-Woo Jeon
February 2022

Chair _____

Vice Chair _____

Examiner _____

Examiner _____

Examiner _____

Development of Complete Path Planning and Tracking Control Technologies for Autonomous Paddy field Tillage and Pudling·Leveling Operations

Chan-Woo Jeon

ABSTRACT

The agricultural sector is undergoing various challenges of farm management related to increasing agricultural production with limited resources. Driven by expectations for sustainable agricultural systems, autonomous agricultural machines equipped with path planning and tracking algorithms are a promising approach used to increase agricultural production and efficiency in a sustainable way. Successful adoption of an autonomous system in paddy fields depends on the abilities to generate a coverage path applicapable to various field shapes in the presence of an enclosing field boundary with a dedicated entrance and to control the motion of the tractor reflecting the dynamic navigational condition occurring because of the frequent headland turning on field with high soil moisture content or flooded water. This study reports on the development of a complete coverage-path planner (CPP) with an optimal sequence and an intelligent path tracking controller to cover a whole area with the high field efficiency for autonomous tillage and puddling·leveling tractors operating in

the polygonal paddy field. A full CPP that provides automatic generation of both inner and outer-work paths, and boundary corner turning methods applicable to irregular paddy fields was developed based on the proposed path models of tillage and puddling·leveling operations for an autonomous tractor. An optimation method for determining a sequence of inner tracks based on the genetic algorithm (GA) was implemented in the CPP to improve the path planning performance in terms of field efficiency by reducing the non-working distance. For a complete CPP that enables the tractor located at the entrance to automatically go to the start point of the full CPP and return to the entrance after completing agricultural tasks, a novel path planner for the entry and exit operations of an autonomous tractor was developed using the A* algorithm. To enhance the capability of the autonomous tractor based on a previously developed slip estimation-based steering control to keep the implement on the reference path at various speed conditions, an intelligent tracking controller was designed and developed using reinforcement learning (RL) by considering navigational conditions represented by lateral deviations and heading errors in real-time. The feasibility of using the developed algorithms was investigated via computer simulations followed by field tests with a 63.4-kW autonomous tractor equipped with the developed CPP and tracking controller in polygonal paddy fields. In path planning simulation, the CPP with optimal sequence showed the effect of increasing the field efficiency by reducing the

non-working distancee in three polygonal fields, i.e., 28 %, 33.9 %, and 45.0 %, as compared with those obtained with the previously developed CPP. From the validation, the full CPP demonstrated could guide the autonomous tractor with tracking accuracy that showed lateral and heading root-mean-squared errors (RMSEs) of < 10.1 cm and 2.2° and tillage performance with the skipped areas of < 1.7% of the total area in three different polygonal paddy fields: triangle, (3020.3 m^2), quadrilateral (3451.3 m^2), and pentagon (4361.3 m^2). In addition, when the autonomous puddling·leveling tractor equipped with the developed CPP navigated the paddy field where the water was flooded, the results showed lateral deviations ranging from -11.3 cm to 13.7 cm and heading errors ranging from -2.7 deg to 1.8 deg, respectively, and the system showed superior tracking performance in terms of travel distance and fuel consumption by reducing from 3039.6 m to 1940.1 m and 17.1 L to 16.3 L as compared with those of the manual operation. However, it was confirmed that it took about 20 minutes more time because it traveled at a slower average velocity (1.35 km/h) than the manual-driven tractor (2.75 km/h). Nevertheless, similar leveling performance was obtained with the altitude ranging from 39.61 m to 39.85 m (autonomous) and from 39.62 m to 39.81 m (manual), respectively. The autonomous tractor equipped with the RL-based intelligent path tracking controller without any stops or divergence with improved path-tracking accuracy (lateral and heading RMSEs of 12.9 cm

and 3.8 deg) as compared with those (lateral and heading RMSEs of 30.1 cm and 8.6 deg) obtained using the system with slip-estimation based tracking method at 4 km/h, thereby implying that the developed CPP and RL-based intelligent tracking controller would show the potential of the autonomous tillage and puddling·leveling tractor in paddy field.

Keywords: Autonomous tractor, paddy field, tillage, puddling and leveling, Coverage path planner, Optimal path planning, Path tracking, Reinforcement learning

Student Number : 2015-21508

TABLE OF CONTENTS

LIST OF FIGURES

LIST OF TABLES

CHAPTER 1
INTRODUCTION

BACKGROUND

The supply rate of large-horsepower medium to large agricultural machinery for efficient agricultural production, along with the demand for increased production due to the world population rise, has been continuously increasing as the decrease in and aging of the farm household population have become severe. Given those issues, automation technology that enables high productivity and convenient machine operation is being applied in various agricultural tasks, such as tillage, sowing, pest prevention, and harvesting. However, the agricultural production methods developed for the purpose of simply increasing the yield show limitations in terms of the sustainable development of agriculture because excessive amounts of fertilizers and pesticides are applied without considering the environment. To overcome these limitations, precision agricultural technology, which monitors the conditions of crops and soil in real time and accordingly inputs the proper amount of agricultural materials to the required place, is being introduced. Furthermore, based on the concept of precision agriculture, many studies are being conducted for the realization of intelligent agricultural machinery to which the Agriculture 4.0 paradigm fused with Internet of things (IoT), big data, robotics, and artificial intelligence (AI) is applied (Schrijver et al., 2016).

Automated driving technology is gaining significant attention as an automation and intelligence technology to improve efficiency across various industries (Thomasson et al., 2019). In particular, this technology has been actively explored

in the automobile field, leading to the development of many element technologies necessary for the automated driving of automobiles, such as navigation, route planning, and sensor fusion. Vehicles equipped with Level 2 ADAS (Advanced Driver Assistance Systems) are already on the market, and further development of Level 3 or higher autonomous vehicles and their element technologies is also actively underway. Because the development of these autonomous vehicles has resulted in the improved performance of related parts, such as sensors and boards, as well as the advancement of related technologies, it is highly encouraging in terms of improving the efficiency of development when these technologies are introduced into the autonomous agricultural machinery field. However, given the nature of automobiles, 1) the ground friction force or contact area of the road is mostly continuous without significant fluctuations because automobiles are driven on-road, and 2) automobiles must maintain a safe distance according to the driving velocity by themselves. In contrast, agricultural machines, such as tractors and combines, are ideal primary applications of automated driving technology because 1) they are driven at low velocity off-road, 2) they are relatively free from obstacles given the surrounding environment (farmland), and 3) they repeat tasks along a straight or curved path. Thus, if the robustness of navigation technology is further secured in an agricultural work environment in addition to the automated driving technology, it will be advantageous for applying automated driving or automation technology to agricultural machinery.

As civilian use of GPS technology was permitted in 1995, and the security code on selective availability that was available only to some authorized organizations was unlocked in 2000, the idea of precision agriculture emerged. The automated

driving technology for agricultural machinery since then has been developed for the purpose of effective resource management and production enhancement (Stafford, 2000). In the early stages, technological development started with a guide bar technology that guides the degree of deviation in real time in the form of driver assistance to improve the tracking performance, evolving to the development and distribution of automatic steering technology mounted on an electric motor or hydraulic valve interlocking actuator. Furthermore, autonomous tractors that automate most of the tasks required by existing workers, such as steering, velocity variation, and operation of machinery under limited farming conditions, have been developed and marketed since the 2010s. Related technologies have been recently developed in the direction of intelligent tractors, mainly led by large tractor manufacturers and national research institutes that provide data-driven integrated agricultural solutions covering all agricultural tasks, such as tillage, leveling, transplanting, sowing, weeding, harvesting, and post-harvest management. Furthermore, the problem of lack of economic feasibility for small- and medium-sized farms due to high-priced sensors and base technology was previously pointed out as a limitation of precision agriculture. However, this issue has been overcome by the commercially expanded distribution of core technologies and the drop in the price of GNSS (Global Navigation Satellite System), a core sensor, with the development of automated vehicle technology, resulting in the spread of autonomous tractors and element technologies (Figure 1).

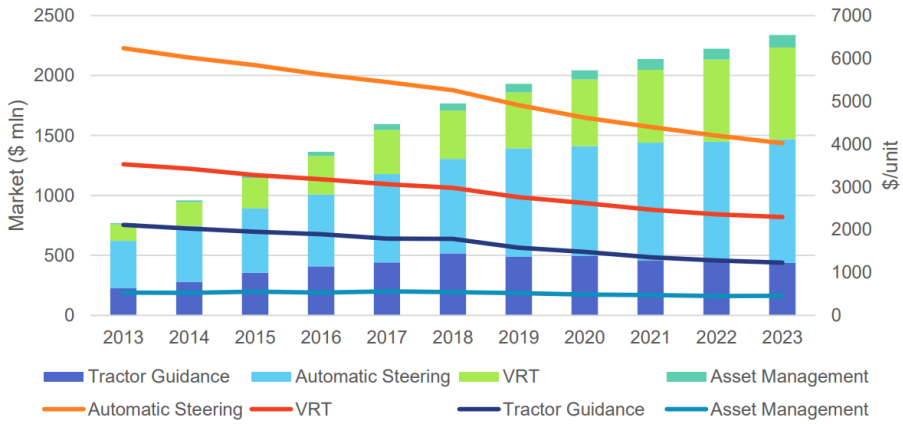

Figure 1. The market value for the GNSS receivers sold for agriculture purposes (Agricultural Robots and Drones 2016-2026: Technology, Markets, and Forecasts)

Autonomous Techonology in Agricultural Mahcinery

Unmanned mobile robot technology, along with AI and information and communications technology (ICT) technologies, is already being applied in the fields of manufacturing, logistics, medical care, rehabilitation, safety, and personal services, and its scope of application is further expanding in response to social demand for improved convenience. With the advancement of the technology itself, research and development (R&D) has been actively conducted at the level of autonomy that recognizes the situation by itself and finalizes optimal judgments through the convergence of cutting-edge IT technology and AI, departing from the conventional automation function that imitates humans. This robot technology has recently been introduced into the automation system of agricultural machinery, contributing to the enhanced operational efficiency and productivity. However, typical industrial robots operate to handle uniform and standardized tasks on a flat paved road, whereas agricultural robots mostly target non-uniform objects, such as soil and crops, and operate in difficult-to-control environments, such as irregular

road surfaces. In this respect, it is difficult to apply all the latest robot technologies to the agricultural field (R Shamshiri et al., 2018).

Investment in agricultural robot technology reflecting these environmental characteristics in agriculture has increased steadily by 80% or more annually since 2012, and the investment has been concentrated mostly on agricultural machinery automation technology (Oberti & Shapiro, 2016; Tillett, 2003). Over time, many agricultural tasks have been automated through large-horsepower autonomous tractors operating on limited cleared farmland. Furthermore, along with the technological developments, such as automatic steering and navigation control, automated machine control, automated headland turning, environment recognition, variable-rate application, mechanical operation optimization, swarm control, and IoT-based V2V (vehicle to vehicle) or V2X (vehicle to everything), Case IH presented the concept of an unmanned tractor, to which robot technology was applied, in 2016, thereby leading to the development of autonomous robot farming machinery exceeding the conventional automation functions (Oberti & Shapiro, 2016; Tillett, 2003).

Various autonomous operation tests must be performed in real environments to develop element technologies for autonomous tractors and further predict and analyze algorithm performance. However, there are many restrictions, including safety issues, difficulties in providing various artificial test environments. The need for a platform and an arable field to perform the tests. Nevertheless, the simulation technique among robot technologies can be utilized to efficiently verify the effectiveness of the path planner and tracker in a computer environment and optimize related parameters (Han, Kim, Jeon, & Kim, 2019). For example, the

actual farmland environment reflecting soil slip and slope can be configured in the simulator by adding the steering of the autonomous agricultural machinery and the responsiveness of the acceleration and deceleration device to easily predict the performance of the path planner and tracker. Thus, the related algorithms can be easily and quickly developed.

Core techonolgies of autonomous system of agricultural mahcinery

The core base technology for automated driving of agricultural machinery is divided into three categories: 1) an algorithm responsible for designing an operation strategy and calculating control commands and a higher-level controller technology corresponding to the “brain” with the developed algorithm installed, 2) automated driving platform technology for agricultural machinery that actually executes the commands, and 3) perception-based driving technology that senses the information from the surrounding environment.

The autonomous driving and cultivating technology is becoming automated and intelligent by the convergence with robotic technology. Its basic configuration includes 1) a GNSS sensor and inertial measurement unit (IMU) sensor to acquire the information on absolute position and posture and sensor fusion technology to improve sensor stability, 2) path planning algorithm that designs a strategy for operating a tractor in farmland considering the target farming environment, 3) path tracking technology that autonomously controls steering and velocity by utilizing the difference between the current and target positions and directional angles of the agricultural machinery as well as the real-time status information of the agricultural machinery, and 4) automated machine control technology according to driving, work status, and attribute information for each position (Figure 2).

Path planning technology, which directly affects work efficiency and level before actual operation in the field, requires superintelligence that exceeds that of the worker in presenting the optimized path based on extensiveness that can respond to the size and shape of the field, the type of agricultural task, and the production of agricultural machinery in use as well as the application of robot technology. Moreover, the path tracking technology related to performance in actual operation requires flexibility that can respond to variables, such as various situations that occur when driving on straight or curved paths depending on the specifications, velocity, and steering characteristics of the agricultural machinery, or slips that occur due to a phenomenon in which the soil collapses due to a failure to bear the weight of the agricultural machinery.

Stable sensor data collection technology and optimized hardware platform technology are essential to apply the developed path planning and tracking algorithm. Thus, to compensate for the instability of the absolute position detection of the GNSS sensor used as the basic sensor for automated driving of agricultural machinery, a technology for fusion with the relative position information collected from various sensors is being researched and developed. For example, the application of the Kalman filter through fusion with the IMU sensor is widely used in autonomous vehicles and mobile robots. However, it is difficult to introduce a technology for implementing autonomous agricultural machinery due to the absence of domestic base technologies for agricultural GNSS/INS Kalman filters considering the aspects of the agricultural work environment, such as irregular soil surfaces, and tractor operation characteristics. The recent spread of electronic tractors has enabled the application of CAN (Controller Area Network)

communication-based integrated controllers. However, the application of integrated controllers for automated driving additionally requires connection to a GNSS/INS sensor that recognizes a precise position as well as setting and monitoring electro-hydraulic steering and acceleration/deceleration devices for the automated tracking of environmental conditions for agricultural tasks. In particular, the image controller provides information on the work situation to the driver and further serves as an image input/output device that receives various work conditions and driving conditions for the automated control of agricultural machinery. It also acts as the brain that controls tractors and combines in performing autonomous driving according to the input information.

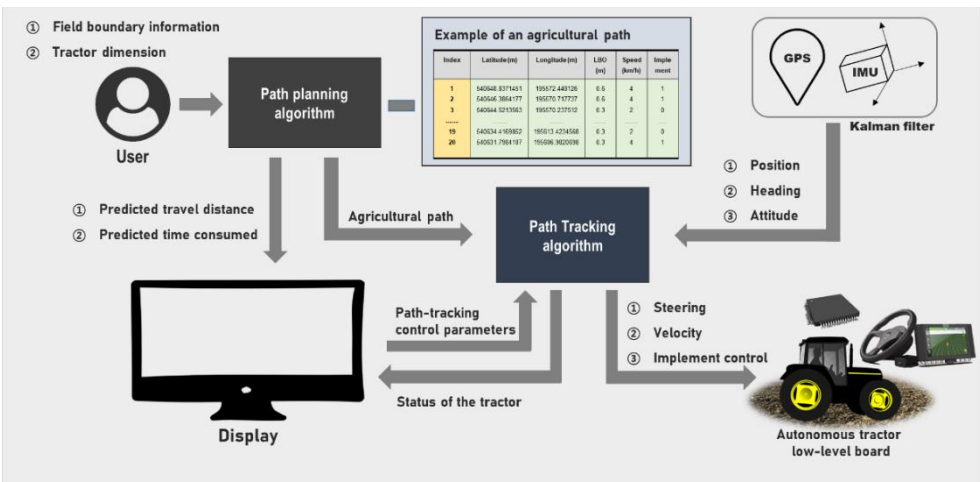

Figure 2. Schematic diagram of the autonomous system of agricultural machinery.

PROBLEM STATEMENT

Different agricultural conditions from developed countries

The global farmland area for cropping, including fields, paddies, and orchards, was approximately 1.6 billion ha in 2019 and the cultivated area in developed countries has decreased due to urbanization, whereas it has been steadily increasing

in developing countries (FAOSTAT, 2021). In particular, rice, which is the staple food for approximately 40% of the world's population, is an important food produced mainly in the East Asian region, whose annual product amounts to approximately 4.8 million tons from the area of 170 million hectare, corresponding to 11.2% of the global farmland (Watanabe, 2018). However, there is a need for an alternative solution to overcome the low production issue due to social problems, such as aging and labor shortage. Based on the FAO (The Food and Agriculture Organization) 2017 data, the leading East Asian countries in agriculture (Japan, China, South Korea, and India) account for 52.6% of the world's rice production, and they are striving to implement solutions by introducing automated driving technology. The paddy field, which plays an important role in global food production, is managed by intensive agriculture that utilizes the entire field within the farmland in a small-scale and compartmentalized manner due to the paddy levees that have been formed around the farmland through flooded water irrigation based on the advantages of nutrition supply to seedlings and weed management. Thus, it is necessary to develop a path planning technology that reflects turning within the farmland, boundary work on the paddy field according to the farmland shape, and the single entrance formed due to the topographical characteristics of paddy levees, as well as a control technology that sufficiently reflects the slip effect occurring because of the frequent turning and flooded environment.

The autonomous agricultural machinery technology, which has been developed mainly in developed countries, such as the United States and Europe, is used for automated driving work along the reciprocating path within large-compartment farmland of 10 ha or more for crops such as corn and soybeans. Although the work

performance of this large-scale agricultural machinery is excellent, its automated driving control system that has been distributed in the foreign environment cannot be directly applied to the domestic agricultural environment. This is because this control system is vulnerable to multiple variables that occur due to structural differences across agricultural machinery systems with various sizes, differences in compartment sizes, and intensive farming conditions. Thus, it is necessary to develop technology to achieve a high level of automation while performing universal functions corresponding to the specifications of traditional agricultural machinery that has been utilized under farming conditions with multiple restrictions, such as paddy fields.

R&D of technologies is underway in developed countries for expanding the application range of automated driving systems in farmland due to the demand for an environmentally friendly and sustainable agricultural production system with increased efficiency. As the world's population will rise to 9 billion by 2050, crop production is required to increase by 50–70% compared to the current level (Alexandratos & Bruinsma, 2012). This social demand for technology has resulted in the development of efficient management technologies that utilize the entire field within the farmland, such as the performance of agricultural tasks using multiple agricultural machinery, the production of crops using the headland area, and path planning to minimize the effect of soil compaction (Thomasson et al., 2019). These advanced path planning and control technologies, resulting from thissocial demand for technology, can share the development direction of the technology applicable to the paddy field, which has been developed in the form of intensive agriculture. These technologies have been developed and distributed

mainly by companies in developed countries in the case of automated headland turning, whereas it is necessary to investigate the tillage algorithm for agricultural tasks in the headland area that occurs due to turning within the field.

Non-linear and coupled operation of autonomous agricultural vehicle controller

The development of autonomous agricultural machinery is focused mainly on the automation function that replaces the driver's function, and the control values calculated according to rules set based on data collected from sensors, such as GNSS, camera, and radar, are transmitted to the actuator. In the case of the automobile industry where automated driving technology is mainly applied, automated driving technology is divided into Stages 0–5, depending on the level of automation technology: Stage 0 refers to the level at which the human driver has full control. The system has longitudinal and lateral control in operation at Stages 1–2, and it further obtains the ability to recognize and respond to problem situations at Stages 3–5 (Shergold et al., 2016). Automated driving of agricultural machinery is actively evolving toward full autonomy. The R&D in American and European agricultural machinery companies is mainly focused on reciprocation and automated headland management technology, while Japanese agricultural machinery companies are developing an AB line or curve, which has adapted reciprocating work path automation and automated technology for agricultural work and headland turning.

An autonomous system of agricultural machinery equipped with advanced automation technology is required under paddy farming conditions that utilize the entire farmland, and it must be accompanied by an appropriate automation strategy.

However, the expansion of agricultural conditions requires a complicated automation strategy. In particular, the automation technology that calculates the control values based on a predetermined strategy is insufficient for real-time situation changes occurring from the characteristics of agricultural machinery running off-road as well as the mechanical response of agricultural machinery systems at various horsepower ratings, which are used according to the applicable agricultural work and farmland conditions (Zhang et al., 2019). AI obtains a method to derive an optimized strategy by modifying rules based on data and answers rather than the traditional method of creating answers based on existing rules and data. Starting from the field of robotics requiring an unmanned autonomous decision-making system, AI is further gaining attention in the agriculture industry with the advent of Agriculture 4.0 (Saiz-Rubio & Rovira-Más, 2020). Thus, AI can be a solution to the difficulties in creating strategies, which inevitably arise due to various considerations in implementing a highly intelligent automated driving system. However, in order for AI technology to be applied to autonomous agricultural machinery, a rational research method is required to understand the agricultural work environment and interpret and quantify the data collected during driving.

OBJECTIVES

The objective of this research was to develop a complete coverage-path planner and intelligent path tracking controller for an autonomous tillage and puddling·leveling tractor system operating in a pologonal paddy field based on position information measured from GNSS sensors.

The specific objectives were as follows.

1) To develop a complete coverage path planner that provides automatic generation of optimal inner and outer-work paths, and boundary corner turning methods for an autonomous tillage and puddling·leveling tractor applicable to various shapes of polygonal paddy fields.
2) To develop an entry-exit planner that enables the tractor located at the entrance to automatically go to the start point of an operational path, perform an agricultural task along the planned optimal path, and return to the entrance after completing the work.
3) To design an intelligent path tracking algorithm based on adaptively situational awareness and response, enabling autonomous operation with increased field efficiency by intelligently interpreting surrounding driving environment factors when working with a tractor using a reinforcement learning method.
4) To validate the complete coverage-path planner and intelligent path tracking controller in field tests using the full-scale autonomous tractor equipped with a GPS/INS system

CHAPTER 2

LITERATURE REVIEW

OVERVIEW OF RESEARCH TREND

Domestic research trend

The overall domestic research on autonomous agricultural machinery has proceeded with continuous and active governmental support since the introduction of precision agriculture, which was initiated by the corporation in the 1990s. In the earlier days, the focus was on technology development, and algorithm research was actively conducted mainly by academics and national research institutes. As related technology advanced, the hardware element technologies, including tractors, rice transplanters, and combines required for the introduction of the autonomous system, power shift, continuously variable transmission (CVT), and electro-hydraulic actuator, was developed, in collaboration with domestic agricultural machinery companies to create added value. As a result, a combine, tractor, and rice transplanter equipped with an autonomous system were manufactured in the early 2000s, and on-site evaluation was performed. However, this effort failed to develop into a practical model due to the characteristics of the automated driving system requiring various element technologies (Table 2).

Table 1. Domestic research trends for an autonomous agricultural machine.

Year	Organization	Contents
1997	Seoul National University (SNU)	- Developent of an autonomous speed sprayer system based on Fuzzy logic control using ultrasonic sensor and DPGS.
2001	Seoul National University (SNU) Sunkunguan University (SKKU)	- Development and validation of an autonomous combine harvester based on fuzzy logic controller using DGPS, gyro sensor, and ultrasonic sensor. - Lateral deviation of < 30 cm in straight and < 50 cm in curved paths.
2004	Rural Development Administration (RDA) LS Cable & System Ltd.	- Development of a tractor that allows real-time rice field observation through the Internet. - Lateral deviation of < 20 cm in straight path
2004	TYM	- Development of high-function power shift tractors and unauthorized transmission for 100KW agricultural tractors since 2010. - Power transmission device using electronic hydraulic pressure essential for autonomous driving of a tractor.
2007	Rural Development Administration (RDA)	- Development of an autonomous rice transplanter equipped with a straight and turning control algorithm
2008	Chungnam National University (CNU) Kukje Machinery Co., Ltd	- Development and validation of an autonomous tillage tractor system with a route planning and tracking algorithms.
2013	Seoul National University (SNU) Unmanned Solution	- Development of an 63-kW autonomous tillage tractor equipped with full-coverage path planner and pure-pursuit based tracking controller. - Electric power steering, throlle control, and implement up/down control using CAN communication modules were developed to enable for the tractor to navigate and cover an arable area. - Lateral deviation and heading error of < 13 cm and 3.7 deg while performing tillage operation.
2015	Chonnam National University (CNU)	- Development of an autonomous lawn mowing system that is equipped with GNSS and vision sensors in 25 kW tractors to determine growth information of grass. But, lack of evaluation tests in various environments
2015	Seoul National University (SNU)	- Development of steering simulator to develop path planning algorithm. - Development of a simulator that can check the driving state under actual soil conditions in conjunction with the simulator.
2019	Korea Institute of Machinery & Materials (KIMM)	- Development of core technologies, i.e., path planning and path-tracking algorithms for an autonomous tractor operated in the feiel - The results of tracking performance showed that the autonomous tractor followed a straghit path with lateral deviation < 30 cm.
2019	Seoul National University (SNU)	- Development of a complete CPP for an autonomous tillage tractor that provides automatic generation of both inner and outer-work paths, and boundary corner turning methods applicable to polygonal-shaped paddy fields with various corner angles. - The autonomous tillage tractor successfully followed the whole paths with lateral and heading root-mean-squared errors ranging from 32 to 101 mm and 0.6° to 2.2°, respectively, and demonstrated superior tillage performance by reducing the skipped areas of 1.7% (triangle), 0.9% (quadrilateral), and 1.0% (pentagon) of the total area

As the concept of a semi-driverless tractor emerged in the 2010s, which automated reciprocating linear work based on the high-precision positioning technology of John Deere in the United States and FENDT in Europe (GuideConnect, 2012; Saiz-Rubio & Rovira-Más, 2020), complementary research on autonomous tractors began under the lead of the government, based on the previously developed core element technology. Based on industry–university cooperation, technology development close to commercial application has been achieved by universities dedicated to developing a path planning and tracking algorithm suitable for domestic agricultural characteristics and agricultural machinery companies involved in the establishment of autonomous tractor platforms and field verification (Fig. 4). In addition, as stable correction signal reception, which is a key to high-precision positioning, has become available to domestic agricultural machinery companies through collaboration with large companies SKT, KT, LG Uplus, and MBC, these machinery companies are striving to develop related technology with the goal of commercializing some functions. Based on the core technology obtained through the development of autonomous tractors, autonomous rice transplanters are being marketed, and further development and commercialization of autonomous combine technology are forthcoming.

Figure 3. View of autnomous tractor developed by TYM, unmanned solution, and SNU and field test.

Overseas research trend

Overseas research on autonomous tractors has been performed with a focus on core technologies for system development, corresponding hardware platform establishment, and the acquisition of a sensor system for the stable operation of algorithms. Recent studies have extended to the application of telematics technology for big data construction and analysis by acquiring information on crop growth status and surroundings of vehicles through computer vision and utilizing the information obtained from IoT. Based on these study achievements, larger tractor manufacturers are providing farming solutions, ranging from data collection to data analysis, prescription, and management. Thus, starting with AutoTrac of John Deere in the United States in 2002, products equipped with some of these functions have been commercialized, and they are currently utilized by 60–70% of farms in North America, 30–50% of farms in Europe, and 90% of farms in Australia.

Globally, investment in agriculture technology, which contains the largest proportion of automation and autonomous technology, has been led by large agricultural machinery manufacturers, increasing by 80% annually since 2012. Some of the automation technology has already been marketed, mainly regarding large-scale tractors operating in the farmland environment with soil preparation completed, and the convergence with robot technology is accelerating the realization of an autonomous agricultural machinery technology (Decker Walker, 2016). The main technologies applicable here include (1) optimal operation strategy planning technology for agricultural tasks, (2) automated vehicle and steering control technology, (3) automated machinery control technology, (4) automated technology for headland ordering and turning management, (5) surrounding environment

recognition technology, (6) crop recognition technology for variable work machine control, (7) optimal control technology for mechanical vehicles, (8) strategy design and control technology for simultaneous operation of vehicles, (9) vehicle-to-vehicle communication technology, and (10) stable sensor information acquisition technology (Thomasson et al., 2019). According to the data (Table 3) on the main functions of autonomous tractors of leading agricultural machinery manufacturers worldwide surveyed by the Grains Research and Development Corporation (GRDC) in 2017, the main functions for the autonomous tractor system include a total of 11 technologies after adding the communication technology with workers in the farmland to the 10 aforementioned technologies.

- (Autonomous system) Vehicle & steering control
- (Autonomous system) Path planner with optimal strategy for agricultural task and implement control
- (Hardware platform) Advanced hardware control function of electronic tractor
- (Hardware platform) Optimal control technology for vehicles
- (Hardware platform) Variable control of agricultural implements and ISOBUS
- (Sensor) Stable acquisition of sensor information

Table 2. Technology and product development for the six major tractor manufacturers relating to autonomy.

		Technology pathway to autonomy	Tractor manufacturer					
			John Deere	CNH	AGCO	CLASS	SAME Deutz-Fahr	Kubota
Fundamental Technology for autonomous tractor	Autonomous system	Automated tractor guidance	O	O	O	O	O	O
		Path planning	O	O	O	O	O (with Topcon)	O
		Auto control of implement functionality	O	O	O	O	O	O
	Hardware platform	Drive by wire functionality	O	O	O	O	O	O
		Performance optimization (Ex. CVT, IVT)	O	O	O	O	O	O
		Variable rate technology	O	O	O	O	O	O
	Sensor	GNSS solution	O	O (with Topcon)	O (with Topcon)	O (with Topcon)	O (with Topcon)	O
		Machine to Machine communication	O	O	O	X	O	X
		Sensing - perception	O	O	X	O	O	X
		Sensing – process monitoring	O	O	X	O	X	O
		Telematics	O	O	O	O	X	O
		Infield coms and data infrastructure	O	X	X	O	X	O
		Data management solution	O (JD Link)	O (PLM™ Connect)	O (Fuse)	O (CLAAS telematics solution)	O (SDF data managem ent)	O (KSAS)

Comparison of domestic and overseas autonomous system

John Deere, a leader in automated driving agricultural machinery, has utilized the satellite, wireless, and radio calibration signal network built by its subsidiary Navicom to establish and sell autonomous kits (AutoTrac) and installation-type autonomous tractors, based on an autonomous StarFire GNSS system possessing positioning precision with an error level of less than 10 cm without separate terrestrial reference stations. AutoTrac products provide driving functions for straight, curved, circular, and boundary tracks that follow the farmland boundary. It can autonomously set any appropriate path by changing the headland turning method, and the order of the reciprocating operation line sequence, depending on the boundary information input based on the worker`s experience, the work type, and the tractor`s horsepower. In addition, this product provides the user-input type skip pass and changes the pass functions in tracking the planned path to allow the worker to directly respond after recognizing situations, such as the emergence of obstacles, people, and animals. Furthermore, the premium product group provides an autonomous tractor system with a high level of automation (Fig. 5) by furnishing an automated turning function and a machinery-based driving control function (Table 4). However, to apply the autonomous work to the entire farmland area, the work should be separately performed for the headland area and the inner work area, and path planning is performed through predetermined logic based on the worker's setting. Thus, for the advancement of the automated driving system, autonomous work technology that can apply to the entire area within orthogonal or irregularly shaped farmland is required. The implementation of this technology

requires the development of an intelligent autonomous system that 1) can autonomously observe the farmland environment, 2) is practical, and 3) includes judgment technology to improve agricultural work efficiency.

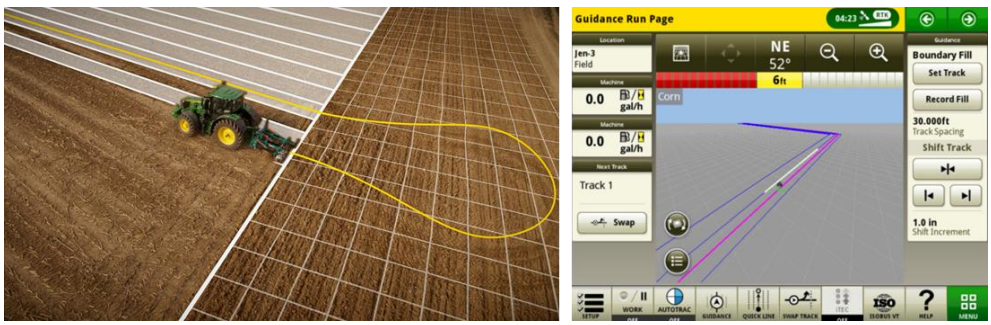

Figure 4. John Deere Autotrac

Japanese companies, such as Yanmar and Iseki, in addition to Kubota, the second largest tractor manufacturer worldwide, are exerting their efforts in R&D with the goal of developing automated driving systems for rice transplanters, tractors, and combines operated in paddy fields, which account for 50% or more of Japan's farming environment. Starting with Yanmar’s autonomous tractor in 2015, the most advanced automated driving systems as of 2020 are Yanmar’s Robot Tractor and Kubota’s Agrobot products, each of which supports a unique reciprocating work function, automated headland turning function, and automated work function for some of the headland area (Table 4). Kubota holds the technology to effectively respond to irregularly shaped field through diversified reciprocating routes, and automated headland turning technology in adjacent lines, and it provides a function to stop when an obstacle is found during autonomous operation by installing a safety device using vision. Yanmar`s products provide autonomous farming functions in irregularly shaped field and autonomous working functions in the

headland area except for the outermost areas through proper arrangement of straight reciprocating paths and headland turning in adjacent lines. However, it is necessary to improve the utility of the technology because it does not consider the fact that the autonomous work technology cannot be applied to the entire farmland due to the incomplete path path planner to cover the outer-work area and the environmental constraints caused by the fixed entrance that inevitably occur in a paddy field environment.

Figure 5. Kubota Agrobot (left) and Yanmar Robot tractor (right)

The domestic automated driving system succeeded in product development by securing core technology from the development of the autonomous straight rice transplanter by Daedong Industrial Co., Ltd. and the autonomous straight tractor by LS Mtron in 2019. However, there are difficulties in promoting their distribution because the technology is still in its infancy. Compared with overseas cases, although the domestic research has achieved technological advancement through various attempts, these technological achievements have not further developed into practical models because of deficiencies in the hardware platform technology, sensor stabilization technology, and automated driving system.

The major technologies of the automated driving systems described in previous studies, and held by tractor manufacturers, are contributing to the improvement of

the level of automation through the development of reciprocating work in irregularly shaped farmland, automated headland turning, and machinery control (Table 4). However, because the existing autonomous work technology for the headland area (back tillage technology) is incomplete, it may not be applicable to the entire farmland. Moreover, conventional automation technology may contribute to the precise control of overlapping and facilitate the monitoring of machinery and vehicle status, which is insufficient in achieving enhanced efficiency through optimization of agricultural tasks due to a lack of intelligence technology. In addition, although the fixed entrance, which is an inevitable characteristic in a paddy field environment, is an important factor in work efficiency, relatively few related studies on automated driving systems have considered this factor.

Table 3. Comparison of autonomy functions of autonomous tractor produced by oversea (JohnDeere, Kubota, Yanmar) and domestic tractor manufacturers.

Supported functions	Oversea tractor manufacturer			Domestic	
	John Deere (USA)	Kubota (Japan)	Yanmar (Japan)	Manufacturer	Research
Main target field	Upland field	Paddy field	Paddy field	Uncertainty	Paddy field
Boundary information	Manual	Manual	Manual	Manual	Manual
Field type	Rectangle & Irregular	Rectangle & Irregular	Rectangle & Irregular	-	Rectangle & Irregular
Consideration of Infield obstacle	O	X	X	X	X
Straight track	O	O	O	O	O

Curved track	O	O	X	X	X
Additional track (Ex. circle, adaptive)	O	X	X	X	X
Automatic headland turning	O	O	O	X	△ (partially)
Implement control	O	O	O	O	O
Automatic headland cultivation	△ (partially)	X	△ (partially)	X	△ (partially)
Autonomous decision making	X	X	X	X	X
Autonomous Full-coverage	X	X	X	X	X
Safety system (Obstacle detection)	△ (Operator perception and response)	O	X	X	X

PATH PLANNING

Chung et al. (1999) proposed two different path tracking algorithms that apply a minimum spanning tree by planning an optimal working path on a rectangular paddy field. Utilizing the selection method for the minimum time headland turning, and the calculation method for sequencing operation lines applying the brute-force method, they shortened the estimated mileage by approximately 78 m in comparison with the conventional planning method under the condition of 40 m × 100 m farmland.

Bochtis et al. (2009) developed a coverage path planner for self-driving lawnmower tractors using the tree hierarchy technique. They reported that it is possible to plan the automated headland turning path and reciprocating driving route for determining the minimum mileage by receiving user input of information on the farmland and vehicle. According to the result of an on-site evaluation using autonomous tractors, the non-working distance could be reduced by up to 50% compared to the conventional method.

D. Bochtis and C. G. Sørensen (2009) replaced the existing geometrical model formula-based path planning algorithm problem for agricultural tasks with the long-explored vehicle routing problem (VRP) to apply the metaheuristic methods (including the genetic algorithm and ant colony algorithm) that have been developed to solve the VRP. To reflect the agricultural work factors in the VRP, the types of agricultural performance factors were divided depending on the input/output of agricultural materials based on the agricultural machinery in planning the path, and based on this classification, a method for generating a reciprocating work path inside the irregularly shaped farmland was developed.

Jin and Tang (2010) compartmentalized the farmland to create alternating paths in the left and right directions in irregularly shaped farmland containing obstacles and investigated the determination of driving directions in each compartment to minimize the driving distance depending on four types of headland turning methods (Flat, U, Bulb, and Hook), which were mathematically defined. The headland turning model formula was geometrically defined by using the minimum turning radius of the tractor, the working width, and the headland turning width. When comparing the planned paths proposed for the three types of farmland shapes, and the driving

trajectory of skilled workers acquired during harvesting, a 0–9% reduction in turning distance was observed.

Seo et al. (2010) proposed a reciprocating work path generator for tillage work and divided the target areas into an inner reciprocating work area and a reciprocating work area, depending on the work width and the number of back tillage paths input by the user. The inner reciprocating work area was developed under the four categories of C-type, C-compartment-type, X-type, and R-type works. The input tractor and field variables were utilized to output the tillage path for each work type onto the screen and file, and the output data included the information that can be used in controlling the tractor's forward- and backward-moving and engine speed, the machinery's ascending/descending, and PTO ON/OFF, thereby enabling the report of the generation results in the virtual simulation. However, the developed algorithm failed to report the results generated from the field experiment on path tracking, and the limitations of the study lie in conducting path generation research on orthogonal farmland alone and missing a generation algorithm for the back tillage path.

Hameed et al. (2011) investigated the optimal reiprocating path generation algorithm in irregularly shaped farmland. The path optimization consisted of three steps. In the first step, the driving direction that minimizes the double work area that occurs after headland turning was determined based on the results from repeated input. In the second step, the operation line sequence that minimizes the non-working distance that occurs during headland turning was determined by a genetic algorithm. In the last step, an optimized path planning method was proposed by compartmentalizing the irregularly shaped farmland for efficient work and

minimizing the distance generated from movement between compartmentalized areas through a genetic algorithm. However, the effectiveness was not verified through field tests.

Matsuo et al. (2012) proposed a path planner for tillage work on orthogonal farmland and presented an algorithm for generating an autonomous working path for the entire area, including a straight reciprocating path area in the 45-degree diagonal and lengthwise directions, and a back tillage path area. An automated driving system was developed with the planner proposed by remodeling the forward- and backward-moving, working, and steering parts of a small-horsepower (24.3-Kw) tractor equipped with XNAV, an auto-tracking type surveying device. The path generation algorithm proposed in this study is a method of creating a diagonal reciprocating work path in the inner work area of the farmland and then generating an outer-work path in the outer work area of the field, depending on the directions of the four sides of the field. The results of an experiment conducted on orthogonal farmland of 18.5 x 50 m showed that the driving distance of the diagonal work path was 20% longer, whereas the driving efficiency was higher than that of the conventional work path when a 45-degree driving path angle was set.

Han et al. (2013) analyzed and modeled the domestic tillage work sequence and path types in an orthogonal paddy field environment and presented a path planning algorithm in response to various types of headland turning (C type, X type, and R type). Furthermore, they presented the Route Date Definition File (RDDF), including path point and tractor control information for applying the waypoint navigation algorithm, and performed the field verification, thereby indicating that

the average and maximum errors were found to be within 11cm and 21.4, respectively, on a straight path.

Ibrahim A Hameed et al. (2013) compartmentalized the field to deal with fixed obstacles in irregularly shaped farmland in planning the path and presented a reciprocating work path for each area as well as an optimal sequence planning algorithm using a genetic algorithm. According to the result of applying the proposed algorithm to the field with round-shaped obstacles within a 5.54-ha area for work scenario evaluation, it took 0.18 sec to create a path. The same study decided that it is a path planning method with high work efficiency in terms of work time and cost. However, there is no headland turning path, and the results were not verified through field tests.

Zhou et al. (2014) presented a back tillage path planning algorithm for an inner reciprocating work area in a multiple fixed obstacle environment in irregularly shaped farmland through compartmentalization. Path planning consisted of three steps. In the first step, the inner and back tillage areas were divided based on the agricultural work width, the number of back tillage paths input by the user, and the number of user input rounds, and an operation line was created in each area. In the second step, the area was divided based on farmland and obstacle boundaries. In the final step, the connection sequence of each compartment was optimized by using the ant colony algorithm. When comparing the workers` trajectories acquired during the formation of a potato ridge, and plowing work, and the path created using the algorithm on two irregularly shaped farmlands for scenario evaluation, the developed path planning algorithm was determined to be a highly efficient path planning method in terms of working distance. However, this algorithm's application to

autonomous tractors is limited because there is no headland turning path, and the results were not verified through field tests.

Backman et al. (2015) examined the automated generation method for a turning path by applying the maximum steering speed term to the Dubins curve model. In the conventional Dubins curve model, which does not reflect the steering angular velocity of the tractor, the tracking velocity is continuous, while the tracking precision decreases due to the control commands generated discretely, which has been improved by utilizing a numerical optimization method. The same study further reported the possibility of creating a path that can increase time efficiency for the C-type, X-type, and Fishtail-type headland turning methods in a simulation environment.

Hameed et al. (2016) investigated a three-dimensional (3D) path planning method using digital elevation model (DEM) information of the target farmland to minimize the unworked area that occurs due to the change in the tractor postures during driving in an irregular agricultural work environment. The path generated using the conventional two-dimensional (2D) planner was updated through projection according to the height information of the DEM, and the interpolation method was utilized to compensate for the increased distance between the path points by increasing the dimension. According to the study, an unworked or overlapping area occurred because the distance between adjacent paths increased or decreased depending on the sloped ground. The application of a suitable driving direction could enhance the field efficiency by 2–14%.

Edwards et al. (2017) presented the modularization results of an optimal path planning algorithm for lawnmower tractors that was previously in the research

stage. The path planning module proposed in the study can create a lengthwise reciprocating work path in the inner work area of farmland and present a C-type Omega-based headland turning pattern. The study aimed to present a path by minimizing the unworked distance that occurs during headland turning. As a result of comparing the trajectories of skilled workers acquired from 12 fields of various shapes and sizes and the presented paths, the distance was reduced by 0.2–18.3%. When the field was compartmentalized into 5x5 m^2, the average number of passes per area was reported to decrease. However, its results were not verified due to the absence of field test results using autonomous tractors.

Rodias et al. (2017) analyzed the optimized performance of a path planning algorithm in irregularly shaped farmland, including inner reciprocating work path, headland turning, and back tillage path, in terms of energy saving. They selected the optimal operation line that minimizes the unworked distance through iterative calculations using the mathematical model of headland turning. The fuel efficiency of five farmlands was further investigated by utilizing the calculation formula for standard fuel consumption per agricultural work, presented by the American Society of Agricultural and Biological Engineers (ASABE). Compared to the conventional planning method of working around the entire farmland in a clockwise or counterclockwise direction, there was an improvement by 9.19% in fuel efficiency during the tillage.

Rahman et al. (2019) presented an automated farmland boundary information acquisition method for path planning in irregularly shaped farmland. The study primarily indicated that most of the path planning algorithms operate by receiving information on the vertices of the field corners as farmland boundary information,

whereas there is a limit to defining the environment boundary of real-world farmland with a straight line connecting the corner points. The same study automatically acquired farmland information by using the driving trajectories obtained along the boundary and the convex hull method. This approach was reported to increase the time efficiency in applying the automated driving system and reduce the unworked area through on-site evaluation in convex- and concave-shaped paddy fields.

As summarized in Table 5, regarding the literature on path creation, previous studies have investigated path planning algorithms to optimize the driving direction and operation line to improve driving efficiency and reduce fuel consumption in 2D or 3D environments. However, most of the studies reported the results by comparing and verifying the worker trajectory and the ideal path through a virtual scenario, while the effectiveness was not verified under the conditions of actual agricultural machines, such as a tractor. In addition, unworked land would occur because the back tillage turning method around the corner was not presented in irregularly shaped farmland, and the results of autonomous work in the entire farmland were also limited to the orthogonal type. In terms of intelligent algorithms, research on path planning algorithms was relatively insufficient, which reflected the single entrance occurring due to the topographical characteristics of ridges in a paddy field environment. Thus, the following are necessary in a paddy field environment: 1) the development of a path planning technology for the entire area in irregularly shaped farmland, including a complete back tillage path through high-level automation to improve work efficiency, and 2) the application of intelligent optimization technology reflecting the environmental specificity of paddy fields to increase time and distance efficiency and reduce fuel consumption.

Table 4. Summary of literature review on path planning researches.

	Previous	Needs
Field shape	Polygonal field shape	Polygonal field shape
Full-coverage path planning	- Full-coverage path planning technology in pologonal field shape - Limitaion of covering performance in corner area of the field - Insufficient coverage path planning technology	- Full-coverage path planning technology in pologonal field shape - Precise covering strategy algorithm especially in the corner area of the field
Advanced automation technology		- Entry & exit path - Complete coverage path
Inteligence & Optimization	- Optimal path generation - Increase of field efficiency (travel distance or time consumed) by applying the intelligence technique such as the genetic algorithm and the ant colony algorithm	- Intelligent path planning that reflects the condition of a paddy field (field boundary, single entrance, etc.).
Test methods	- Virtual simulation - Field test	- Virtual simulation - Field test - Comparision of the tracking and covering performances with the skilled worker

PATH TRACKING

Lee (1998) explored path tracking and control algorithms using DGPS, an unmanned driving system configuration of an ultrasonic sensor-based speed sprayer, and a fuzzy controller in an orchard environment. They calculated the steering angle by comparing the direction information received from the DGPS and the reference

path direction. They also developed an obstacle response algorithm during driving by utilizing the judgment principle of the tracking fuzzy controller by receiving distance values from four ultrasonic sensors. They conducted a field experiment to compare the performance of a controller using DGPS alone and a tracking controller combining DGPS and the ultrasonic sensor, each of which was compared to the reference path to present the straight path tracking performance within 48 cm and 39 cm of the maximum square root error, respectively.

Noguchi et al. (1998) developed an automated driving system combining the steering angle generation software, which calculates the steering angle by the difference from the reference path based on GNSS antenna position change compensation according to the roll, pitch, and heading of vehicles and the precise location information acquired with RTK-GPS as well as an agricultural robot hardware platform equipped with a sensor module based on RTK-GPS, fiber optic gyroscope (FOG), and IMU. Tillage work was performed in a straight section of 140 m, presenting the performance with a maximum error of 7 cm and a square root error of 2.9 cm.

Cho (2000) developed a fuzzy control technology utilizing a geomagnetic sensor and machine vision for an autonomous tillage tractor system. They applied the Hough transform to the image obtained from the color CCD (charge-coupled device) camera to calculate the steering angle consisting of left, right, and neutral stages using the direction angle, the direction angle obtained from the geomagnetic sensor, and the distance difference from the reference path in the image as input to the fuzzy controller. Steering was performed using a cylinder. The maximum RMS position

error was reported to be 23.2 cm according to the lateral displacement measured along straight navigation using the DGPS receiver in an actual field environment.

Kise et al. (2001) investigated an autonomous tractor using RTK-GPS, FOG, and IMU sensors. To obtain stable direction angle information, the FOG time drift compensation method was applied by utilizing the extended Kalman filter method. To generate the steering angle, the distance and direction angle error with respect to the reference path were calculated and used in the proportional control-based non-model controller. For a driving experiment, a straight path was set as the reference path in the field, and a rotary operation was performed at low and high speeds of 0.2 km/h and 1.6 km/h, respectively, to obtain the maximum square root distance error of 8 cm and the maximum square root direction angle error of 1.9 degrees.

Zhang and Qiu (2004) proposed a dynamic look-ahead distance tracking controller to improve the reference path tracking performance of an autonomous tractor. The developed tracking controller automatically adjusted the look-ahead distance in response to the speed, error with the reference path, and curvature of the adjacent reference path. When autonomous driving was performed after the turning of an autonomous tractor equipped with RTK-GPS and FOG sensors on asphalt and actual field at a tracking speed of 1.0 m/s and 1.8 m/s along the straight path, respectively, tracking precision of 80 cm or less in the entrance section after turning and a square root distance error of 10 cm or less was obtained in the straight section.

Lenain et al. (2005) proposed a real-time slip predictor and a method of calculating the predicted slip-reflected steering angle to improve the performance of automated vehicles applied to agricultural environments. The slip was observed in real time by applying the existing observer algorithm to the extended kinematic model, including

the slip angle. When the tracking experiment was conducted with an autonomous tractor equipped with RTK-GPS and IMU along a W-shaped reference path at 8 km/h in a grass environment, the error of approximately ±60 cm before the application of the observer was reduced to ±15 cm or less.

Huang et al. (2009) explored the improved pure pursuit method by presenting a method of determining the dynamic look-ahead distance based on neural network theory to improve the path tracking performance in a straight path as well as headland turning with different driving environment characteristics. They set the lateral distance and velocity between the vehicle and the reference path as input variables to create a look-ahead distance determination strategy, assigning the look-ahead distance as the output variable. The training was performed through 148 samples designated by humans, and in this case, the range of lateral displacement and velocity were set to ±1 and 0.3–0.4 m/s, respectively, and the look-ahead distance was accordingly discretized as 0.01, 0.5, and 1 m. The simulation study showed that as the fixed look-ahead distance dynamically was varied, driving time and space decreased, and driving efficiency increased in the headland turning area in addition to driving.

Fang et al. (2011) attempted to develop a robustness control algorithm to predict the cornering stiffness between the tire and the road surface of a driving platform. The tire stiffness was predicted based on the robustness of Luenberger observers by measuring the lateral acceleration and rotational change rate, and the predicted slip angle was reflected in the steering logic developed based on the continuous system to conduct the experiment. The convergence of the algorithm was confirmed through

simulation, and the lateral error was ±20 cm and the direction error was ±5 deg in actual driving.

Kraus et al. (2013) conducted a study on the development of an MHE-NMPC frame for autonomous tractor tracking based on longitudinal and lateral slip factors and an adaptive mode. Development MHE is a method that can estimate model parameters in real time for unknown soil condition changes. NMPC showed control output close to optimal based on the estimation results provided by MHE. It was reported that the MHE performance provided an accurate estimation of the parameters, enabling the path tracking performance of the NMPC controller.

Han et al. (2013) proposed a mathematical model of a tillage work path based on C-, X-, and R-type headland turning and proposed an RDDF including path points and control commands calculated through the model, thereby providing a reference path. Moreover, a program equipped with a look-ahead distance method-based path tracking algorithm was reported through a simulation environment and on-site evaluation. However, there was no verification of the tillage work performance, effect of slip by degree, or tracking precision of path points upon entry into the operation road after turning driving.

Han et al. (2015) created a reference path using the field information acquired from the paddy field conditions through the C-type headland turning-based path generation algorithm and conducted a tracking verification experiment with a 60-kw-class autonomous tractor platform equipped with RTK-GPS, IMU, and a path tracking algorithm based on the look-ahead distance method. Prior to on-site evaluation, the look-ahead distance, velocity, and turning path point interval required for automated driving were optimized based on the tracking performance through a

simulator capable of implementing the slip phenomenon. When driving along ten 70-m operation lines in dry and wet paddy field environments at 2 km/h, a square root error of 12.8 cm or less was obtained in the straight section.

Zhang et al. (2019) utilized the double-DQN method, one of the types of reinforcement learning, to propose an intelligent path tracking algorithm that can respond to both straight and turning sections by self-learning an optimal control strategy based on on-site data. For controller learning, lateral displacement relative to the reference path, direction angle error, and velocity were input as explanatory factors of the surrounding environment, and the steering angle was generated as the output. For performance evaluation, Huskey's robot platform was used to compare the figure-eight-shaped reference path tracking performance in a grass environment with the pure pursuit control technique based on look-ahead distance. According to the result of the experiment, the entry error decreased after turning, and the maximum error decreased by approximately 40% due to the shortened stabilization time after entry, whereas the reference path entry time increased due to the continuous path tracking characteristics.

Han, Kim, Jeon, Moon, et al. (2019) proposed a path follower based on a kinematic model formula that predicts slip depending on the real-time state of the tractor and reflects it in the steering angle calculation by utilizing the state-observer technique. The observer-based tracking controller was verified of the effectiveness in the simulation capable of slip implementation and actual tillage verification through a virtual simulator in a paddy field environment. In addition, after attaching a dynamometer to a three-point hitch, an unworked area was analyzed by creating a precision tillage map. When performing autonomous tillage by driving at 3 km/h in

an 80 x 30 m rectangle, tracking performance with a square root error within 23 cm and work performance of 91.5% were reported in the straight work section.

Chen and Chan (2020) proposed a path tracker that converges the proximal policy optimization (PPO) method applied with the actor & critic method among deep reinforcement learning using deep neural network techniques and the conventional pure pursuit method based on look-ahead distance. The study aimed to compensate for the disadvantages of reinforcement learning, which cannot converge in some cases, and the disadvantages of pure pursuit, which is vulnerable in responding to real-time changes in the surrounding environment. The basic formula for calculating steering angle and velocity followed the existing pure pursuit, while environment-defined input variables defined with lateral displacement and direction angle with respect to the reference path and velocity were utilized to create and add compensation variables. When path tracking simulation was performed based on the irregular S-shaped reference, the tracking performance of the proposed tracking controller was determined to be better than the pure pursuit method and model predictive control (MPC) method under various conditions of velocity and reference path shapes due to the learning effect.

Wang et al. (2019) proposed a velocity and steering calculation method that converges the Q-table among reinforcement learning methods and the PID (Proportional-Integral-Differential) technique most commonly used for controlling a two-wheeled mobile robot. To overcome the shortcomings of PID, which can be applied to simple situations but struggles to analyze complicated situations, by utilizing reinforcement learning, whose strength lies in the real-time analysis of complicated situations, the control values calculated by each method were used as

command values. The Q-table technique was trained for the situation where precision tracking was impossible through PID control by receiving environment-defining input variables defined with lateral displacement with respect to the reference path, directional angle error, and velocity. According to the result of experiments in a simulation environment, the proposed algorithm indicated better performance in velocity and accuracy of convergence to the reference path than that in the existing PID.

Table 6 analyzes and summarizes the literature on path tracking. The previous studies in the field of agricultural machinery have been focused mainly upon non-modeling-type tracking algorithms, such as pure pursuit and the Stanley method, as well as nonlinear driving model-based path tracking algorithms, such as the bicycle model and the Ackerman model. Furthermore, the control algorithm for overcoming the slip phenomenon, which has been extensively studied in the field of robotics, has been reported to effectively respond to soil environmental factors that inevitably occur frequently in off-road environments, including paddy fields. Recent studies have been conducted by employing reinforcement learning among deep learning methods for precision tracking that requires various environmental interpretations.

However, most of the studies have not verified the effectiveness through onsite tests, and some cases of on-site evaluations even reported unsatisfactory results. In particular, because various environmental changes occur in paddy fields that require frequent turning due to compartmentalization under conditions of relatively high soil moisture content, further research on path trackers capable of complicated environmental analysis is required for precision tracking. In addition, because most of the studies have focused on driving rather than work, steering and speed control

were calculated based on the center of gravity of the tractor rather than the machinery related to actual work. Therefore, further studies focused on machinery are needed to significantly improve the efficiency of agricultural tasks.

Table 5. Summary of literature review on path tracking researches.

	Previous study	**Needs**
Steering control	- Kinematic, geometric, and model based tracking controller - Slip-estimation based controller - Validation test in the paddy field	- Intelligent tracking controller equipped with the steering logic based on the implement - Adaptive Path following controller that can respond to mechanical responses of a tractor according to real-time situation changes, applied agricultural work, and farmland conditions (steering, speed) - Improving stability and environmental responsiveness through convergence with existing mechanical model-based controllers.
Velocity contorl	- Pre-defined velocity map	- Adaptive velocity controller
Navigational environment (Target control point)	- Interpretation of driving status using a single target point - Lateral deviation and heading error at a target point	- Interpretation of driving status using various information - Array of lateral deviation and heading error - Change of control point to an implement position where an agricultural task is performed actually

CHAPTER 3
PADDY FIELD FULL-COVERAGE PATH PLANNER FOR AN AUTONOMOUS TILLAGE TRACTOR

ABSTRACT

Successful use of an autonomous agricultural machine in paddy fields depends on the ability to generate a full-coverage path consisting of inner and outer-work paths adapted to various field shapes in the presence of an enclosing field boundary. To enhance the performance of a coverage path planner (CPP) developed in our previous study, this article describes the development of a complete CPP for an autonomous tillage tractor that provides automatic generation of both inner and outer-work paths, and boundary corner turning methods applicable to polygonal-shaped paddy fields with various corner angles. Computer simulation of the developed turning manoeuvres was conducted using a 3D tractor-driving simulator by analysing the trajectories of a virtual tractor on ground under varying corner angle conditions. A field evaluation was performed with a 60-kW autonomous tillage tractor equipped with the developed CPP algorithm in three different shapes of paddy fields. The results of the computer simulation confirmed that the designed boundary corner turning methods could provide an acceptable level of tracking performance with lateral deviations < 70 mm when following boundary corner turning paths. In the field tests, the autonomous tillage tractor successfully followed the whole paths with lateral and heading root-mean-squared errors ranging from 32 to 101 mm and 0.6° to 2.2°, respectively, and demonstrated

superior tillage performance by reducing the skipped areas of 1.7% (triangle), 0.9% (quadrilateral), and 1.0% (pentagon) of the total area as compared with that of 8.5% obtained with the previously developed system.

Keywords: Coverage path planning (CPP); Autonomous tillage tractor; Paddy field; Boundary corner turning; Skipped area

INTRODUCTION

The increasing demand for farming products and environmental considerations has led to the agricultural industry seeking cost efficiency measures from diverse solutions involving various academic fields, e.g. agronomy, geology, genetics, and engineering (Tilman et al., 2002). To achieve higher productivity even with lower energy consumption and less terrestrial field degradation, engineering has been focused on the development of advanced technologies in terms of auto-guidance systems and optimal fieldwork management (Gebbers & Adamchuk, 2010).

Recently, many automated agricultural applications, such as auto-steering (e.g. Agco AutoGuide, Agrocom E-drive, Ag Leader SteerCommand, Case IH AccuGuide, John Deere AutoTrac, Trimble Autopilot, etc.) and automatic implement guidance (e.g. John Deere iGuide, New Holland TrueGuide), have been commercialised (Han, Kim, Jeon, Moon, et al., 2019; Scarlett, 2001; Thomasson et al., 2019). Auto-guidance systems for agricultural machinery, in particular, have been comprehensively developed to aid or support the operator to allow more accurate control of the vehicle whilst operating the various implements (Groover & Grisso, 2009; Han et al., 2015). For example, when using an auto-steering system

with an autonomous variable rate boom sprayer, a 16% potential reduction in travel distance and associated fuel use was estimated compared with a conventional broadcast treatment (Hoy et al., 2014). Furthermore, automation can improve the farmer's comfort and relieve fatigue (Lenain et al., 2006).

Currently, most commercially available steering guidance systems for agricultural tasks are, in theory, capable of achieving high performance in terms of fuel, time efficiency, and operational quality (D. D. Bochtis & C. G. Sørensen, 2009). A measure of field operation performance is field efficiency (E_f), defined as the ratio of the productivity of the machine under field conditions to the theoretical maximum produced at its full rate (Bochtis & Vougioukas, 2008). Field efficiency is affected by various factors such as the size and shape of the field, the dimensions of the machine and implement, the strategies of field operation (path planning), the soil condition, and the crop yield. Among these, the strategies of agricultural routing problem (ARP) adaptively applied to various field shapes considering the mechanical characteristics of an autonomous tractor system directly affects the quality of the agricultural operation (Bochtis & Sørensen, 2010). Bergerman et al. (2013) stated that the design of an operational path is one of the critical tasks in farm management to improve field efficiency. Zandonadi (2012) suggested that the proper planning of field operations reduces agricultural operational costs with the use of high-end technology.

Several researchers have developed models to describe ARP by substituting it for a form of the coverage path planning (CPP) problem that generates a route that passes over all waypoints of a region. Researchers in this domain have focused on issues such as generating sub-fields due to physical obstacles or complex field

shapes (I. A. Hameed et al., 2013; I. A. Hameed et al., 2010; Oksanen & Visala, 2009), determining the orientation of the tracks and headland-turning patterns or track sequences (Bochtis et al., 2009; Bochtis & Vougioukas, 2008; Hameed et al., 2011; Jin & Tang, 2010), minimising the turning cost (Backman et al., 2015; Sabelhaus et al., 2013; Yu et al., 2015), representing 3D coverage paths based on pre-acquired digital elevation maps (Hameed, 2013; Hameed et al., 2016; Jin & Tang, 2011), and operating strategies for multiple machines (Bochtis & Sørensen, 2010; Conesa-Muñoz et al., 2016; Jensen et al., 2012; Johnson et al., 2009; Seyyedhasani & Dvorak, 2017).

For example, (Jin & Tang, 2010) presented a method for the geometrical presentation of a field combined with a path-planning algorithm for optimal field decomposition into sub-regions and determination of the driving direction in each sub-region. (Hameed et al., 2011) developed an effective coverage planner to derive the driving angle for minimising the overlapped area in a headland field and to arrange the track and block sequence using a genetic algorithm to minimise the non-working distance. (Jensen et al., 2012) proposed a path planning method for a transport unit in cooperation with a primary unit (e.g. a harvester) in agricultural operations involving inner-field paths by implementing Dijkstra's algorithm to solve the single-source shortest path problem on a metric map.

When evaluating the performance of a path planner for an autonomous tractor applied in a paddy field, the infield-coverage path, including inner- and outer-work paths for agricultural tasks and headland turning, is the main factor that directly affects the quality of the agricultural operation. In general, a paddy field is commonly segmented by embankments around 300 mm to hold flood water for

growing rice. Therefore, the planner should propose an operational path with strategies to avoid collisions with field borders while cultivating the whole area even in a polygonal paddy field. To do that, the outer-work paths generated in the headland areas adjacent to the embankments should be precisely designed based on each corner shape and the manoeuvring characteristics of the tractor.

Several researchers have presented methods to deal with infield path planning (Edwards et al., 2017; Hameed, Bochtis, & Sørensen, 2013; Han et al., 2013; Spekken & de Bruin, 2012; Zhou, Leck Jensen, Sørensen, Busato, & Bochtis, 2014). For example, Spekken and de Bruin (2012) presented a path planning method to design a geometrical route for inner-field and headland turning within the field boundary to minimise the time spent on machine servicing (loading or offloading agricultural input and output). Han et al. (2013) developed a coverage path planner for an autonomous tillage tractor to enable the vehicle to till in sequential tracks and carry out headland turning with fixed spacing within the rectangular paddy field. Edwards et al. (2017) proposed and evaluated an infield coverage planner prototype designed for mowing operations; it demonstrated good performance in terms of reducing the predicted travel distance by up to 50% in comparison with that obtained when a professional operator drove the tractor in the same fields. Although infield coverage paths have been proposed by many researchers, the performance of the agricultural operation has not yet been demonstrated or guaranteed when an autonomous tractor travelled the whole path in the field test. Han et al. (2019b) performed an autonomous tillage operation by navigating a 60-kW autonomous tractor equipped with a slip-estimation-based path-tracking controller on a map generated using a previously developed path

planning algorithm (Han et al., 2013). However, the algorithm could only generate a path in a rectangular paddy field. In addition, a large amount of skipped area occurred near the corners of the field due to incomplete strategies when generating the outer-work paths, especially in the boundary corner area, revealing the need for a more precise and improved path generation method covering the whole area of the paddy field.

Thus, to improve the performance of the previously developed system (Han et al., 2019), the ultimate goal of this study was to develop a complete field-coverage path planner for an autonomous tillage tractor applicable to various shapes of polygonal paddy fields.

The specific objectives for this chapter are to

1) Develop a complete paddy field-CPP that generates both inner- and outer-work tracks for a GNSS-based autonomous tractor to fully perform the tillage operations of polygonal paddy field.
2) Implement boundary corner turning methods for enhancing covering performance on the corner areas compared to the previous study, regardless of the various shapes of polygonal corners.
3) Validate the feasibility of the developed path planner by analysing the trajectories and field coverage efficiencies in simulation and the field tests.

MATERIALS AND METHODS

Design of the complete paddy field-coverage path planner

Tillage path model

The paddy-coverage path consists of inner-tracks with headland turning and outer-work paths with boundary corner, and the sequence varies depending on the type of agricultural task. The tillage and puddling·leveling paths were modeled using the information obtained from International Rice Research Institude (IRRI) and the results of previous studies (Bochtis et al., 2015; Han, Kim, Jeon, Moon, et al., 2019; Seo et al., 2010).

Figure 6 shows a conceptual diagram representing a tillage path model. The tractor started tillage operation at one corner of the inner area (Stage 1), entered the next inner-work track via a headland turning path (C, X, R, Ω types) determined by the width of the implement and the minimum turning radius of the tractor (Stage 2) (Jin & Tang, 2010). In addition, depending on the type of rotary cultivator or plow, the sequence of inner-work track was determined according to the aim of the plowing operation to collect or push the soil, and the pattern of headland turning was also identified. After finishing the agricultural task in an arable area of the inner-work area, the tractor exit to the outer-work area via the connection path, performs a tillage operation by traversing headland passes connected with a boundary corner turning path (Stage 3) and covers the cultivation work in all areas of farmland (Stage 4).

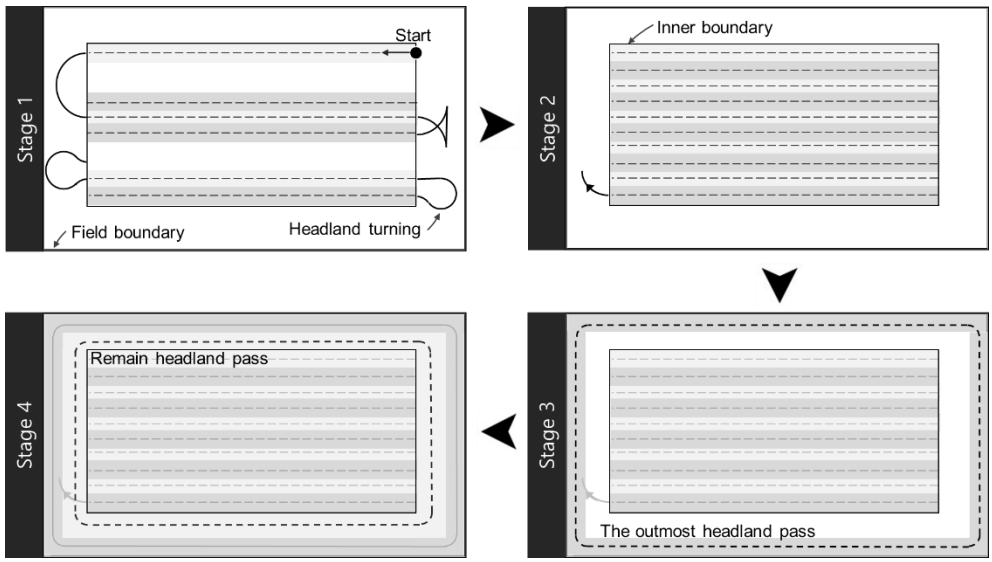

Figure 6. Process of the tillage operation for the autonomous tractor equipped with the ratary cultivator.

Architecture of the path planner

Guiding an autonomous tractor in a paddy field in the study was based on the generation of a combination of waypoint data and operational commands for the tractor with an implement when information about the field boundary and tractor dimensions is provided. Figure 7 shows the sequence of two different separate operations in series, i.e., the generation of inner- and outer-work paths, and the creation of the waypoint data and implement commands in RDDF (route data definition file) format (Table 6). An example of RDDF generated as the reference information for path tracking and agricultural task. The input data includes a set of coordinates of the points on the field boundary, the width of the implement, the number of headland passes, the overlap length, the headland turning pattern, and the driving direction defined as the angle between the driving direction and the horizontal axis of the transverse Mercator coordinate system.

In the 1st stage, the path was decomposed into two sub-regions, i.e., inner- and outer- work areas. The inner-work path includes straight tracks and headland turns, whilst the outer-work path included headland passes, boundary corner turning paths, and connection paths. On the inner-work path, the straight tracks were filled with the minimum boundary box (MBB) in the direction of the driving angle, which is the same as the long side of the field boundary, with parallel swaths, and the headland turns sequentially connects the straight paths at their ends. On the outer-work path, the headland passes were generated sequentially from outside to inside by inwardly moving the field boundary, and the boundary corner turning paths were generated by incorporating reversing to connect the headland passes. The connection path is used to connect the inner-work and outer-work paths. Two diagnostic algorithms were designed to investigate whether the waypoints generated on the outer-work path are located within the field boundary and whether they can cause an impossibly sharp turning manoeuvre for the autonomous tractor to follow due to the narrow outer-work area. The first diagnostic algorithm was implemented by inwardly moving the field boundary by half of the implement width to limit the area where the waypoints can be generated to allow the autonomous tractor to perform agricultural tasks without colliding with the field boundary. The second algorithm calculated the direction change of sequential three vectors consisting of consecutive four waypoints. When errors were detected, the number of headland passes was increased to obtain a wider headland area.

In the 2nd stage, the path generated during the first stage included waypoint data in RDDF format on their latitude and longitude coordinates, LBOs (limits of the boundary offset), traveling velocities (working and turning velocities), and

implement on/off operations. This file contains the input reference path and control strategies for the tracking method developed in our previous study (Han et al., 2019b). In principle, the tractor searched for the next waypoint when it reaches a waypoint within the offset distance, which was predefined in terms of LBO (Han et al., 2013). In addition, the predicted time and travel distance on the path when the tractor ideally navigated the proposed path was also provided as useful information.

Table 6. An example of RDDF generated as the reference information for path tracking and agricultural task.

Index	Northing (m)	Easting (m)	LBO (m)	Velocity (km/h)	Rotary cultivator up/down	Wing harrows folding/unfolding
1	410296.5	212973.3	0.1	4	1	0
2	410206.1	212965.2	0.1	2	1	0
…						
n-1	410290.5	212985.7	0.1	2	1	1
n	410289.5	212984.9	0.1	4	1	1

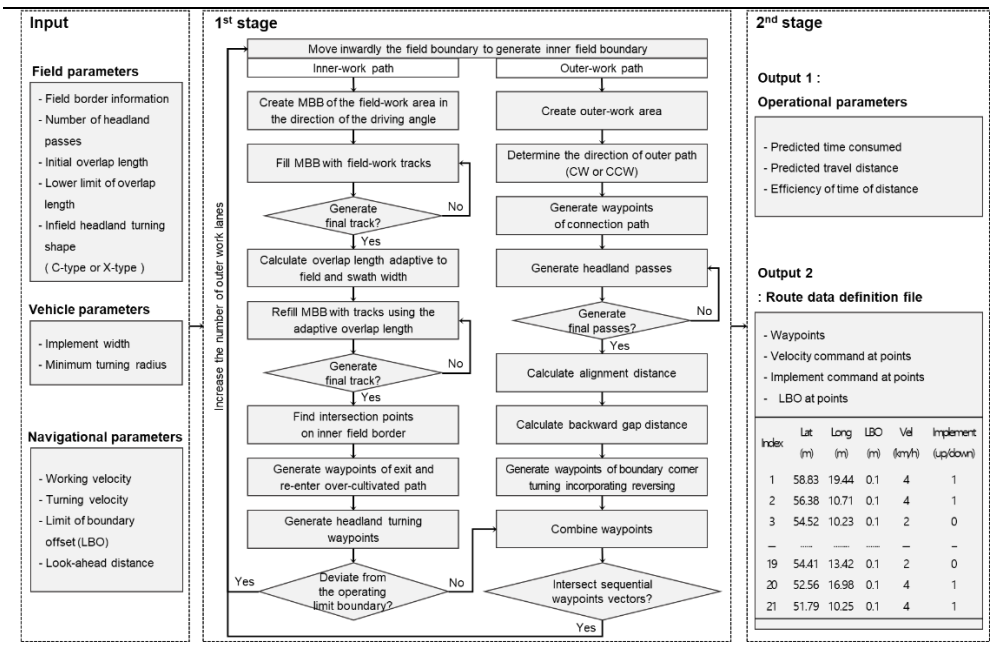

Figure 7. Flowchart of the complete paddy field-coverage path generation algorithm developed in the study.

Geometrical representation of the infield full-coverage path

Inner-work path with optimal overlap length

Inner-work tracks with adaptive overlap length

As shown in Figure 8, the border of the inner-work area was set by inwardly moving the field boundary by length (d_{HL}), which was defined based on the number of headland passes (n_h), the implement width (w), and the initial overlap length (w_{o-init}) (eq. 3.1), and the headland area between the field boundary and the inner-field border was then created at the same time. The approach for the generation of the inner-work tracks was based on the MBB method (I. A. Hameed et al., 2010; O'Rourke, 1985), which is the minimum-area rectangle enclosing the vertices of the field to concisely express a complex field shape. The bounding rectangle was oriented in the same direction as the driving angle. Straight segments were aligned in the driving direction fill the MBB with parallel swaths calculated using the implement width and overlap length. The method determined intersection points on the inner-field border to identify the inner-work tracks depending on whether they were inside or outside the inside working area. If they are outside the area, they were discarded. Otherwise, the line segment was indexed (i) as the inner-work track and the number of the inner-work tracks (n_i) was calculated.

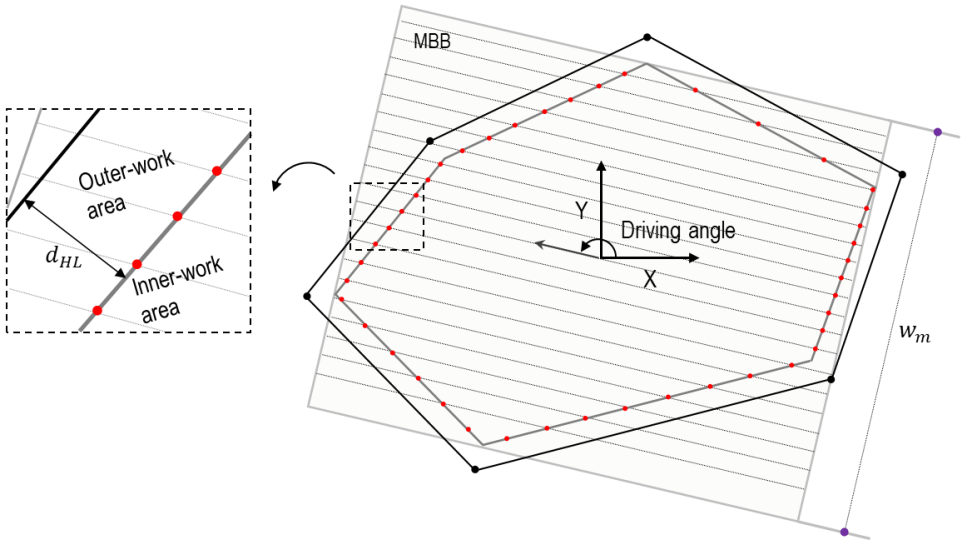

Figure 8. Geometrical representation of the inner-work tracks based on the minimum boundary box (MBB) method for the full coverage of the inner-work area.

$$d_{HL} = n_h(w - w_{o-init}) + w_{o-init} \qquad (3.1)$$

In this study, to prevent skipped or over-tilled areas, an overlap length, generally defined as zero (Hameed et al., 2016; Jensen et al., 2015; Oksanen & Visala, 2009; Spekken & de Bruin, 2012) or constant (Han et al., 2013; Han, Kim, Jeon, & Kim, 2019; Han et al., 2015), was calculated adaptively for the field and implement widths. Figure 9 (a) shows a flowchart for calculating the adaptive overlap length (w_o) using the number of the inner-work tracks (n_i), the implement width (w), the initial overlap length (w_{o-init}), the lower limit of overlap length (w_{limit}), and the width of a MBB's edge placed in the perpendicular direction of the driving angle (w_m). In this method, the remaining width was calculated to determine whether it could be evenly distributed to another overlap length (Figure 9 (b)). If it is possible, the overlap length is recalculated adaptively, and the number of inner-work tracks was reduced to increase the work efficiency (Figure 9 (c)). For practical operations,

the lower limit of the overlap length was set to prevent the skipped area (which can be caused by slippage on soil), a delay in the actuator, or a GPS error. In the opposite case, the number of inner -work tracks was maintained and the remaining width was evenly distributed over all of the overlap lengths.

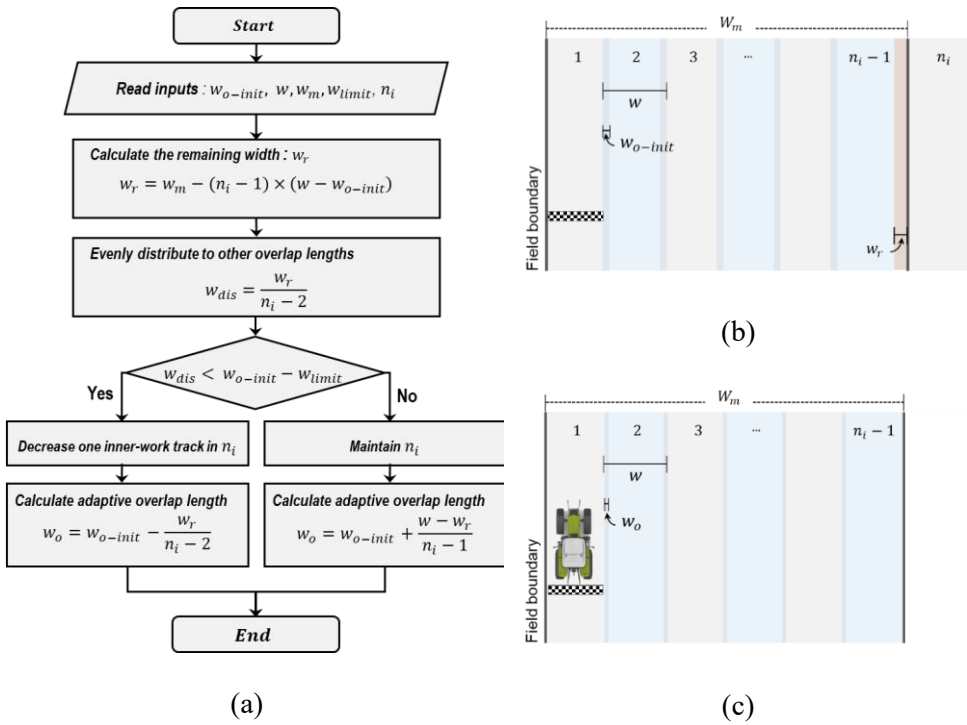

Figure 9. Notation for calculating the adaptive overlap length. (a) A flowchart of the calculation and schematics of (b) when the remaining width ($\boldsymbol{w_r}$) is distributed to the inner-work tracks and (c) when the number of inner-work tracks is then decreased.

Infield headland turning

According to headland patterns used in a agricultural operation for paddy fields proposed by the International Rice Research Institute (IRRI) (Figure 10), two different headland patterns, i.e., one-way and gathering (CASTRO, 1970) are commonly used to minimise the number of turns and maximise the length of the agricultural task runs. When the one-way pattern is used, the tractor follows a

series of parallel tracks sequentially from one boundary of the inner-field border and traverses all parallel tracks using R-type, X-type, or Ω-type headland turning according to the kinematic restrictions of the machine (Hunt, 2008; Witney, 1988) (Figure 10 (a)). The selection of the turning method is based on the skill of the driver and the available space in the headland area (Bochtis & Vougioukas, 2008). As shown in Figure 10 (b), the gathering pattern with C-type headland turning requires the tractor to recursively till tracks located parallel to each other at around half the width of the field. In this study, X-type and C-type, which demand a smaller space for completing the turning manoeuvre than R-type and Ω-type (Spekken et al., 2015), were adopted to generate the infield headland-turning paths because the headland area where the headland turning is executed can be relatively limited in the boundary of the paddy field.

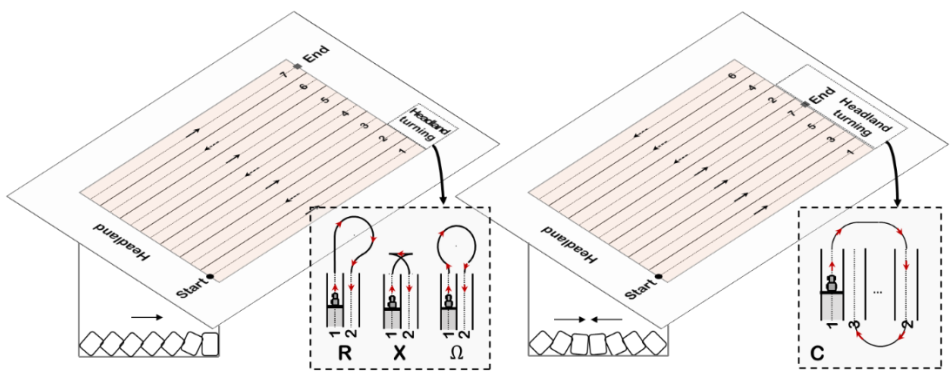

(a) (b)

Figure 10. The classic headland patterns: (a) one-way (R, X, and Ω types) and (b) gathering (C-type).

To achieve the generic solution for the CPP in the paddy field, irregularities of field boundaries were considered by generating the waypoints located on the line stretching the inner-work tracks for guiding the autonomous tractor to keep moving

straight ahead until the point is reached while performing the agricultural operation (Figure 11). As described in eq. 3.2, two different over-covered lengths for the tractor to till additionally when exiting (h_{exit}) and re-entering ($h_{re-enter}$) the inner-work area, respectively, are defined using two angles of the intersection of an inner-work track and the field boundary, i.e., θ_{exit} and $\theta_{re-enter}$. Mathematical models for the over-covered lengths representing three different angle cases are derived as a function of the implement width (w), the adaptive overlap length (w_o), the intersection angles (θ_{exit} and $\theta_{re-enter}$), the distance between the track and the vertex of the inner-field border near it (w'), and the intersection angle between the track and the other segment of the boundary (θ'_{exit} and $\theta'_{re-enter}$).

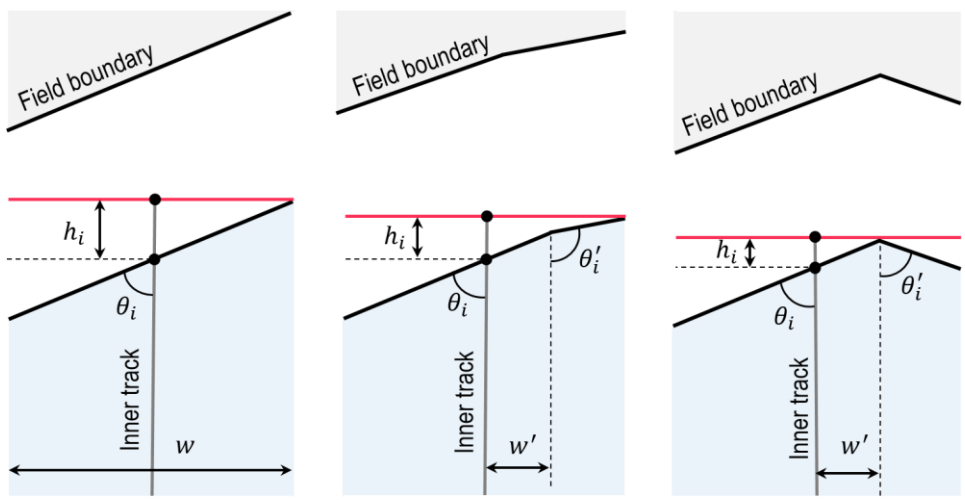

(a) $\theta'_i = 0^o$ (B) $\theta'_i \geq 90^o$ (C) $\theta'_i < 90^o$

Figure 11. Modelling of an over-covered length (h_{exit} and $h_{re-enter}$) according to the shape of the field boundary

$$h_i = \begin{cases} 0.5w\ arctan(-|\theta_i - 0.5\pi| + 0.5\pi) & (\theta_i' = 0^o) \\ w'\ arctan(-|\theta_i - 0.5\pi| + 0.5\pi) + (0.5w - w')\ arctan(-|\theta_i' - 0.5\pi| + 0.5\pi) & (\theta_i' \geq 90^o) \\ w'\ arctan(-|\theta_i - 0.5\pi| + 0.5\pi) & (\theta_i' < 90^o) \end{cases}$$

$$,i \in [exit, re-enter] \quad (3.2)$$

Figure 12 shows the implementation of X and C-shaped infield headland turning manoeuvres by accounting for exiting and re-entering the fieldwork area using the inner-work tracks. In both turning methods, the tractor followed the track and kept moving straight ahead while performing agricultural tasks until the centre of the implement reaches point 1 to avoid generating skipping areas using the over-covered length (h_{exit} and $h_{re-enter}$). After driving along the headland turning path, the tractor started to re-enter the inner-work area from point 4 with the implement running. The vehicle then followed the X-shaped turning path incorporating the two arcs (1-2 and 3-4) created using the minimum turning radius of the tractor (R) and reversing from point 2 to point 3. In the C-shaped turn, for the tractor to enter the next the inner-work track of an irregular polygonal paddy field, some straight lines and arcs with a radius of R as many as segment of the field boundary and corners were generated along the operating limit boundary (d_{OL}) created from the offset of the half of implement width defined using eq. 3.3 and the vehicle continues following it, as shown in Figure 12 (b). In addition, using the calculated lengths of h_{exit} and $h_{re-enter}$, which affect the width of the outer-work area, the diagnostic algorithm developed in the study determines whether the waypoints of the infield headland turn were located outside of the operating limit boundary created from the offset of the half of implement width, thereby increasing the number of headland passes (n_h) until all waypoints were within the boundary that prevents the tractor colliding with the field border.

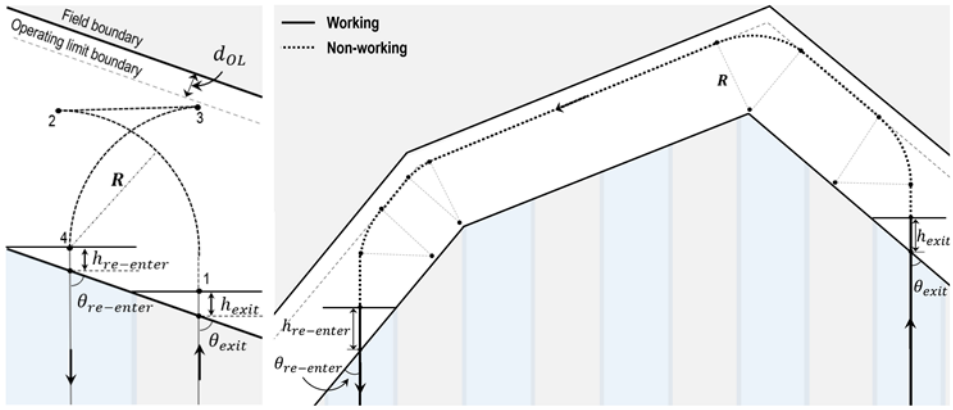

(a) X-type (b) C-type

Figure 12. (a) X and (b) C-shaped infield headland-turning manoeuvre.

$$d_{OL} = \ 0.5(w - w_{o-init}) + w_{o-init} \quad (3.3)$$

Outer-work path with boundary corner turning

Headland passes and boundary corner turning

The outer-work area between the field boundary and the inner-work area was filled with headland passes parallel to each boundary segment at an interval of constant swathing (L_c) based on the implement width (w), the initial overlap length (w_{o-init}), and the number of the headland passes (n_h) using Eq. 4. To cover this area, the tractor navigated around the entire field by repeating the headland passes operation parallel to each boundary segment and boundary corner turning operation to connect each pass in the sequence, whereby the tractor started to perform the agricultural from the outermost headland pass and gradually entered the inner headland pass. In this paper, headland and boundary corner turning methods are proposed for effectively covering the headland and corner areas regardless of the various shapes of polygonal corners.

Figure 13 shows a manoeuvre incorporating the reversing for covering the outer-work area developed in this study. When the tractor finished the agricultural operation on the headland pass from point 1 until the look-ahead point reached point 2; the navigational parameter of the tracking algorithm developed in our previous study (Han, Kim, Jeon, Moon, et al., 2019) such as the lateral deviation and heading error for calculating the steering angle. The tractor then deactivated the implement and navigates the boundary corner turning path generated with radius $R_{req_{c,k}}$ from points 2 to 3, which was calculated differently depending on the indexes of the boundary corners (k) and the headland passes (c) (eq. 3.5). Before reversing to cover the boundary corner area, the tractor continued along an additional straight path (3-4; the red line in Figure), referred to as the alignment path of length $l_{c,k}$, to give the autonomous tractor sufficient length to align its attitude with the next target line. Length $l_{c,k}$ is defined in two cases based on the difference in length between two radii, $R_{req_{c,k}}$ and R (Eq. 7): $R_{req_{c,k}} > R$ results in the generation of the boundary corner path the tractor can follow whereas $R_{req_{c,k}} < R$ needs an additional straight path of length $l_{c,k}$. In the first case, $l_{c,k}$ was set to the look-ahead distance ($l_{look-ahead}$) to perform reversing immediately after the centre of the tractor reaches point 3. When $R_{req_{c,k}} < R$ due to the headland pass being located inwardly, the generic solution for calculating the length of the alignment path even in the irregular field shape and various tractor type was designed using the difference in chord length ($H_{c,k}$) between two arcs drawn with radii of $R_{req_{c,k}}$ and R defined using eq. 3.6, the corner angle between adjacent boundary segments (θ_k), the radius of the boundary corner

turning path ($R_{req_{c,k}}$), and the minimum turning radius of the tractor (R) using eq. 3.7. After the tractor drove along the alignment path, it started to perform reversing from point 4 until the centre of the implement reaches point 5. To prevent a collision between the rear of the agricultural implement and the field boundary whilst reversing in the polygonal field, a reversing gap (p_k) was generated at each boundary corner using eq. 3.8. The vehicle then started to follow the next headland pass while activating the implement (5-6).

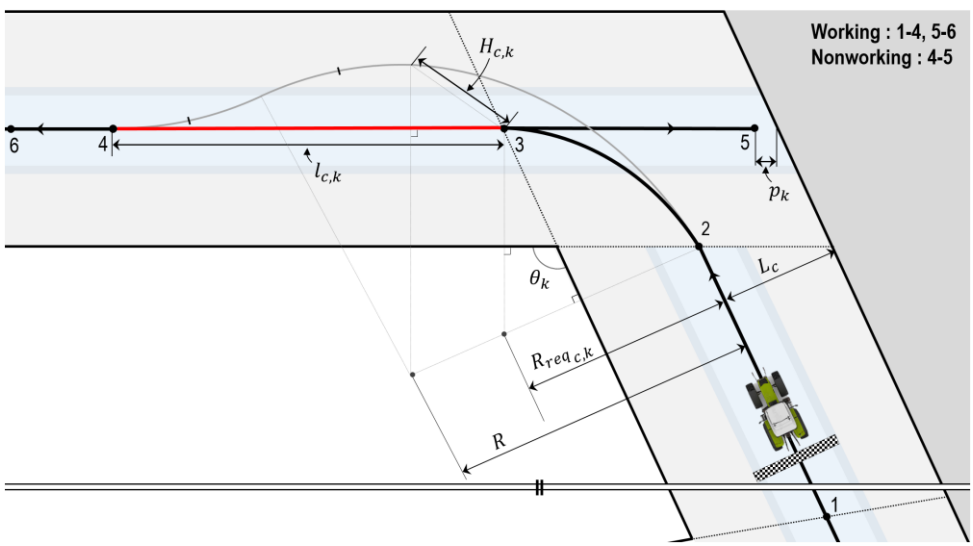

Figure 13. Manoeuvring in the headland passes and boundary corner turning.

$$L_c = \{(n_h - c)(w - w_{0-init}) + 0.5w\};\ \mathrm{c} = \{1,2,\dots,\mathrm{n_h}\} \quad (3.4)$$

$$R_{req_{c,k}} = \tan(0.5\theta_k)L_c\csc(\theta_k)\sqrt{2 - 2\,cos(\theta_k)};\ \ k = \{1,2,\dots,n_s\} \quad (3.5)$$

$$H_{c,k} = R\,tan(0.5\theta_k) - L_c\csc(\theta_k)\sqrt{2 - 2cos(\theta_k)} \quad (3.6)$$

$$l_{c,k} = \begin{cases} l_{look-ahead} & \left(R - R_{req_{c,k}} \le 0\right) \\ H_{c,k}sin(0.5\theta_k) + \sqrt{4Rcos(0.5\theta_k) - H_{c,k}cos^2(0.5\theta_k)} & \left(R - R_{req_{c,k}} > 0\right) \end{cases} \quad (3.7)$$

$$p_k = 0.5(w - w_{o-init})|cot(\theta_k)| \quad (3.8)$$

Connection path between the inner-work and outer-work areas

A connection path that transits from the inner-work to the outer-work area was generated in a similar way to the algorithm that created the infield C-shaped turning method, as shown in Figure 14. When the tractor left the last track, it continued to carry out agricultural task until the centre of the implement reached point 2, thus giving full coverage of the inner-work area. The tractor then raised the implement and navigated a straight path. The proposed method determined the rounding direction for covering the outer-work area, i.e., clockwise or counter clockwise, which affects the turning direction of the tractor at point 3, based on the location of the last track. To obtain the space where the path for entering the first headland pass from points 3 to 5, the direction was selected and the arc was based on the minimum turning radius of the tractor (R) and the straight path are generated using an operating limit boundary (d_{OL}) created from an offset, which is determined to be the half of the implement width apart from the field boundary (Eq. (7)). After boundary corner turning without reversing from points 5 to 6, the tractor started to till at the first headland pass.

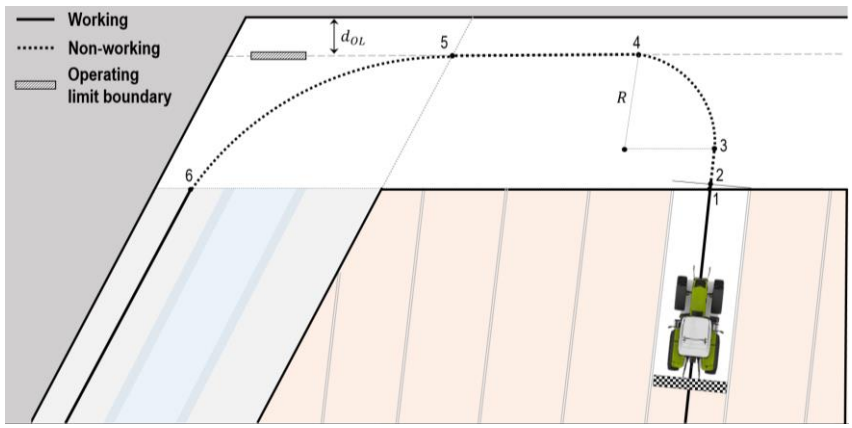

Figure 14. Manoeuvring on the connection path.

3D tractor driving simulator

As shown in Figure 15(a), the simulator architecture consists of a server developed with the RoboticsLab 2009 (ver. 1.10, Simlab Co., Seoul, Korea) based on an extended kinematic model and a path planning and tracking client implemented with Labview 2015. In the server environment, the motion of a 3D tractor simulator was determined using a dynamic vehicle model that considers the varing side force acting on front and rear wheel affected by the corresponding cornering stiffness coefficients of front (C_f) and rear tires (C_f) whensteering angles, velocities, and implement up/down commands were obtained from the client. As shown in Figure 15(b), the simulator could display the path imported from the RDDF (red line), allowing the user to observe a navigational trajectory of the virtual tractor in real-time. In addition, a graphic function was used to display the swath of the implement attached to the virtual tractor such that the working and non-

working area of the implement could be visually identified during the navigation (yellow grids). In the client environment, the path generated by the complete paddy field-CPP developed in LabVIEW (ver. 15, National Instruments, TX, USA), consisting of waypoints previously created in RDDF format, was imposed on the simulator using TCP/IP protocol as a desired position and direction for the tractor. The steering angles required for the tractor to follow the path were generated using a slide-estimation based path-tracking algorithm (Han, Kim, Jeon, Moon, et al., 2019).

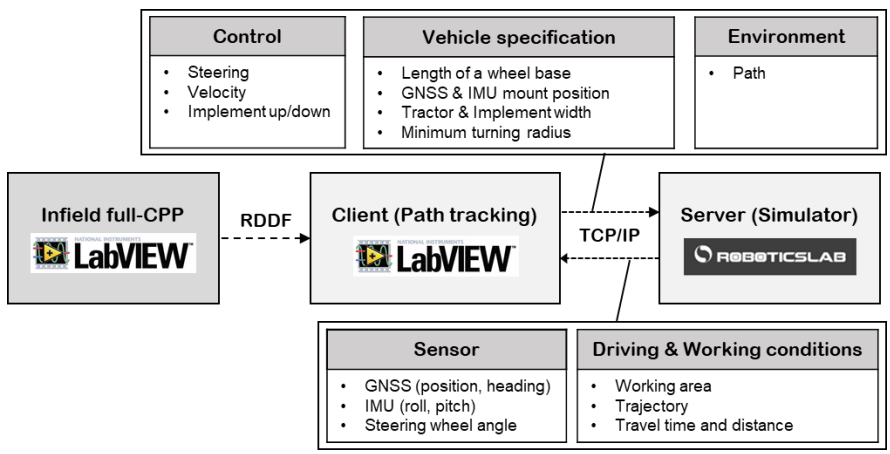

(a)

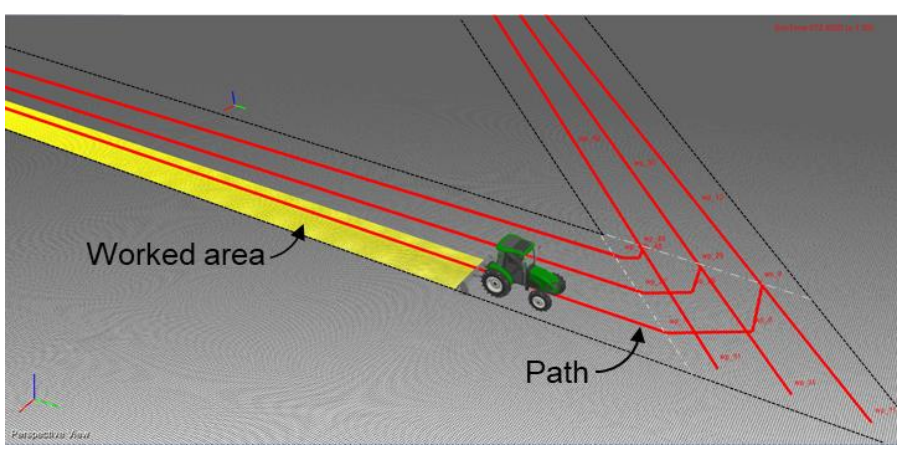

(b)

Figure 15. Architecture of the simulator, consisting of a path planning and tracking client and a vehicle motion server (a) and view of the 3D virtual tractor following the desired path (red line) displaying the swath of the implement (yellow grids) (b)

Autonomous tractor system

Test platform, TX853

The platform for the field tests was built using a 63.4-kW tractor (TX853, TYM., Seoul, Republic of Korea; Figure 16 (a)). The TX853 tractor, which is weighing 3421 kg, is a four-wheel with front-wheel steering, 24-level forward and reverse speeds. The wheelbase, the length between front and rear axles, and the height of the tractor are 2.2 m, 2.24 m, and 2.71 m, respectively. Specific information of the tractor was described in Table 7. An integrated navigation controller for high- and low-level controller (MXE-5501, ADLINK, Taiwan) for path-tracking algorithm was used to control the autonomous tractor of steering angle, travelling velocity, and implement up/down status (Table 8). The steering angle for path-tracking was calculated based on the slip-estimation method programmed in Labview 2018 on the navigation controller mounted on the cabin of the tractor.

(a) (b)

Figure 16 View of 63-kW autonomous tractor (TX853, TYM) (a) outside and (b) inside

Table 7. Specifications of the TX853 tractor used in this study

Items		Specifications
Engine	Type	Cummins 3.3L 4-cyl diesel
	Cylinders	4
	Displacement cubic	402.5 ci
	Fuel Tank Capacity	110.1 L
Electrical	Battery Capacity	12V 65AH
	Alternator	12V 65A
Transmission	Type	24-speed
	Numberf of Gears/Speeds	24 forward and reverse
Steering	Type	Hydrostatic Power
Brake type	Type	Wet disc

Table 8. Specifications of the navigational controller

Items	Specifications
Processor	Intel® Core™ i7-6820EQ
Memory	DDR4 2133 8GB
I/O	Ethernet 4x Intel GbE ports Serial Ports 6x COM (2x RS-232 + 4x RS-232/422/485) USB 4x USB 2.0 + 4x USB 3.0 DIO Isolated 8 DI + 8 DO Audio Mic-in
Weight	4 Kg
Operating Temperature	-20°C to 60°C
Humidity	Approx. 95% @40°C
Input voltage	9-32 Vdc

GNSS/INS system

A global navigation satellite system/inertial navigation system (GNSS/INS) (Ellipse-D, SBG SYSTEMS., France, Table 9) was mounted on a roof canopy of the tractor. Table 9 shows the speficifation of the GNSS/INS system. Differential correction data provided by a network-RTK device (MRD-1000T, SYNEREX., Republic of Korea) based on the long-term evolution (LTE) wireless network, were then transmitted to the rover via networked transport of Radio Technical Commission for Maritime Services (RTCM) using Internet protocol (NTRIP) to achieve 2 cm positioning and to observe the heading angle within ±0.1o accuracy during 60 s outage at a sampling frequency of 20 Hz. Before autonomous agricultural operations, an initialization process of the RTK-GNSS/INS sensor was performed by guiding the vehicle to navigate farm roads with a change in acceleration of $2\mathrm{m}/\mathrm{s}^2$ to measure and predict the tractor position, velocity, and heading.

(a) (b) (c)

Figure 17. (a) GNSS system used in this study, (b) triple frequency antenna, and (c) network-RTK device for collecting a differential correction data.

Table 9. Specifications of the GNSS system

Items	Specifications
42G1215A-XT-1-2-CERT Antenna	Frequency: L1, L2 Performance: LNA Gain (dB) Tracking: L-Band, SBAS, QZSS Max. number of frequency: Dual Input voltage: 2.5 to 24 VDC Consumption: 35 mA VSWR:<2.0:1
Ellipse-D	-Position & Heading accuracy RTK: 1 cm+1 ppm Heading accuracy < 1.3 deg -Data rate Measurements: 20Hz Position: 20Hz
MRD-1000T	- Format : RTCM 3.x (RTK) - Power : DC 5V/1A - Weight : 50 g - Operating temperature : -25 ~ 85oC - Communication : LTE

Steering control module

An electrical power steering (EPS) system (Unmanned Solution Co., Seoul, Republic of Korea, Figure 18 (a)) consisting of motor and control units (Figure 18 (b)) was installed on the tractor to change the orientation of the tractor during the autonomous navigation. An angle sensor (Steer sensor, ComeSys, Republic of Korea) was installed on the centre of the front kingpin. Input voltage of the motor is 12 V and a drive torque of EPS is 2.5 Nm (Table 10).

(a) (b)

Figure 18 (a) EPS module and (b) control board

Table 10. Specifications of the EPS module

Items	Specifications
Power	12V / 7A
Drive Torque	2.5 Nm
Reduction Ratio	1:15
Rotational Speed (No load)	150 RPM
Weight	3.05Kg
Operating Temperature	20ºC~80 ºC
Control Board	Baud rate : 500kbps Analog Input 2 channel 0Vdc, 5Vdc Output DIO 2 channel RS232 1 channel CAN 1 channel
Input of Steering Angle Sensor	Analog 0V: 100º / 2.5V : 0º

Throttle control actuator

As shown in Figure 19, an electic motor mounted in the bonnet (MX-106R, Dynamixel,. Korea) was used to control a velocity of the tractor by pulling the tractor hand throttle using the steel cable as shown in Figure 19 (b). The motor consists of a reducer, controller, driver, and network functions integrally and communicated through RS485 (Table 11).

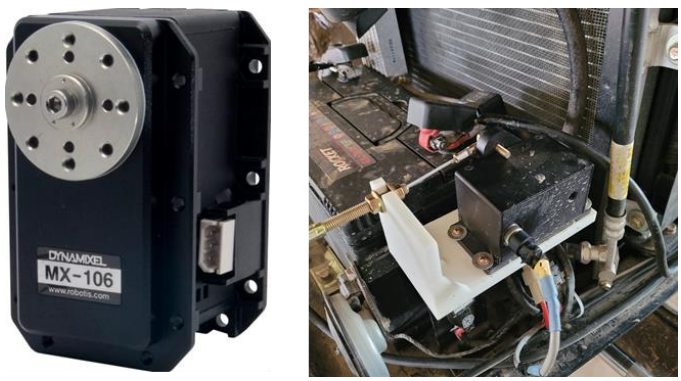

(a) (b)

Figure 19 (a) Dynamixel motor for throttle control and (b) design of the actuator

Table 11. Specifications of the dynamixel motor

Items	Specifications
Model Name	MX-106R
Size	40.2mm × 65.1mm × 46mm
Gear Ratio	225:1
Operation Voltage	12 V
Stall Torque	8.4 Nm
Stall Current	5.2 A
No Load Speed	345 RPM
Range of Motion	360 Degree
Operating Temperature	-5°C ~ +80°C
Communication Protocol	RS485 Asynchronous Serial
Position Sensor	Contactless absolute encoder

Evaluation of tracking and covering performance of the tillage coverage-path planner

Feaibility and validation test of the autonomous tillage path planner

Simulation study of the tracking and covering performance

As one scenario for studying the developed the outer-work path algorithm under various corner conditions, the virtual tractor navigated the paths generated with varying corner angles ranging from 30° to 150° at 10° intervals and with three headland passes, which formed two 20 m rows before and after the boundary corner turning path at a certain angle (Figure 20). The values for path generation parameters used in this study were 0.1 m, 0.07 m, 4 m, and 3 for the initial overlap length (w_{o-init}), lower limit of overlap length (w_m), the minimum turning radius of the tractor (R), and the number of headland passes (n_h), respectively. Navigational parameters such as the working and turning speed, look-ahead distance, implement width, and look-ahead distance, LBO, and the proportional-derivative (PD) control gains for the slide-estimation based path-tracking algorithm were the same as in our previous studies (Han, Kim, Jeon, Moon, et al., 2019).

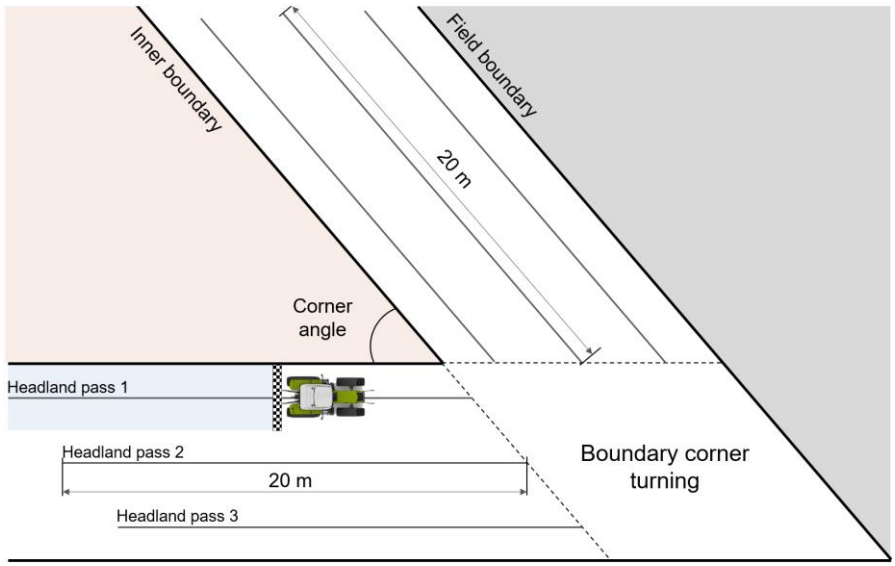

Figure 20 Setup for the simulation test for studying the developed outer-work path algorithm

Field testing on autonomous tillage in paddy fields

Two field tests were conducted with the autonomous tillage tractor. The first test was for validating the results obtained from the first simulation study, which was performed to investigate the performance of using the proposed method to generate an outer-work path, in a trapezoid field (586.7 m^2,+36°17’30.75’’ E, +127°8’22.07’’ N) with two acute (61.6° (corner 1) and 76.8° (corner 3)) and two obtuse (102.3° (corner 2) and 119.3° (corner 4)) corner angles, as shown in Figure 21 (a). Assuming that the autonomous tractor followed the path consisting of three outer work lanes with boundary corner turnings at each of the corners, the performance was evaluated by measuring the lateral deviations when the tractor navigate the generated paths while performing tillage operations. The second test was a full-scale tillage experiment for navigating a complete paddy field-CPP generated in three different polygonal paddy fields located at Chungnam, South

Korea: triangular (3020.3 m^2, +36°18’00.18’’ E, +127°09’31.84’’ N), quadrilateral (3451.3 m^2, +36°17’58.36’’ E, +127°09’34.74’’ N), and pentagonal (4361.3 m^2, +36°18’01.73’’ E, +127°09’34.85’’ N), as shown in Figure 21 (b). The corners of the field boundary were measured with the RTK-GPS mounted on the tractor and translated inwardly by half of the implement width. To generate the paths, the algorithm programmed in Labview 2015 was run on an i7-5500U CPU at 2.4-GHz Intel Centrino Mobile Workstation with 8 GB RAM. A navigation controller developed by Han et al. (2019b) was used to calculate the steering angle. The tillage implement control algorithm (Han, Kim, Jeon, & Kim, 2019), which reduced the not-tilled or overtilled areas by enabling a three-point hitch to be raised or lowered with appropriate delay times, was implemented in the tracking algorithm. The parameters for the path generation and path tracking used here were the same as in the simulation study.

(a)

(b)

Figure 21. View of (a) the fundamental field test for validating the developed outer-work path and (b) Google map image showing the three target fields located in Chungnam, South Korea: triangular (red), pentagonal (green), quadrilateral fields (orange), respectively.

Parameters of tracking performance

The driving RMSE of the autonomous tractor was evaluated by Equation (3.9) amd (3.10) using lateral distances measured from the tractor's position coordinates perpendicular to the pre-defined paths and heading errors. The lateral and heading errors were defined as the positive error on the right side and the negative error on the left side along the driving direction.

$$Lateral\ \ RMSE = \sqrt{\frac{\sum_{i=1}^{n}(y_i - \hat{y}_i)^2}{n-1}} \tag{3.9}$$

where y_i and $\hat{y}_i$ are the measured and the desired positions, respectively, and n is the total number of samples.

$$Heading\ \ RMSE = \sqrt{\frac{\sum_{i=1}^{m}(\theta_i - \hat{\theta}_i)^2}{m-1}} \tag{3.10}$$

where θ_i and $\hat{\theta}_i$ are the measured and the desired headings, respectively, and m is the total number of samples.

The field efficiency of the time and distance in Equation (3.11) and (3.12) was calculated using the effective and total working times and distances, defined as the times that the tractor spends in the area of in-field working and the total field, respectively.

$$\varepsilon_t = \frac{T_w}{T_t} \times 100\% \tag{3.11}$$

Where ε_t is the field efficiency of the time, T_w is the effective field time (s), and T_t is the total field time (s).

$$\varepsilon_d = \frac{D_w}{D_t} \times 100\% \tag{3.12}$$

Where ε_d is the field efficiency of the distance, D_w is the effective field distance (m), and D_t is the total field distance (m).

RESUTLS AND DISCUSSION

Feasibility testing of the boundary corner turning methods

Feasibility testing of the boundary corner turning methods

Figure 22 (a) shows the trajectories for the virtual tractor obtained when following the outer-work paths consisting of headland passes and boundary corner turnings at corner angles of 30° and 150°. Overall, it was possible for the autonomous tractor to follow the generated paths without any stops or crossing of the boundary at steep or smooth corners. However, as the 3 m-look-ahead point reached and updated the waypoint before the tractor position, an error occurred during the turning performed in advance just before entering the boundary corner, which increased when following the corner path at 30° rather than the one at 150° and navigating

the inside pass (Figure 22 (b)). This error proportionally caused a non-tilled zone labelled A and an over-tilled zone labelled C, as shown in Figure 22 (c). In addition, non-tilled zones (labelled B), which could have occurred even if a farmer had been driving the tractor, were inevitably found because it was impossible to drive back to the end of the field boundary to prevent the implement from destroying the embankment via a collision. Nevertheless, when the tractor navigated any boundary corner paths formed with alignment distances of 10.3, 10.9, and 11.5 m at the 30° boundary corner path and 3, 3, and 3 m at the 150° boundary corner path for each pass, the location significantly deviated and the heading of the tractor caused by steep boundary corner turning was adjusted accurately for the path during reversing within ± 50 mm.

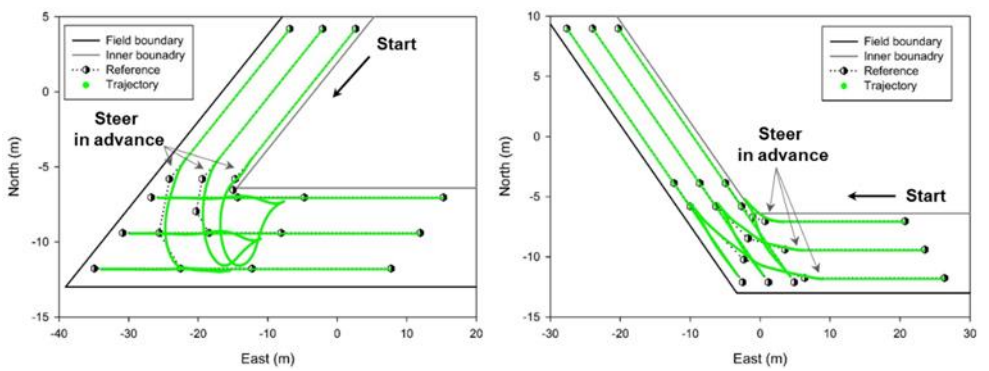

(a)

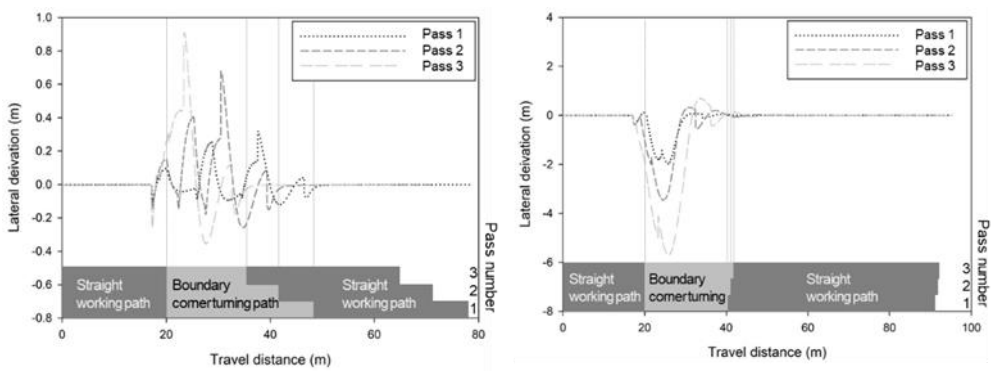

(b)

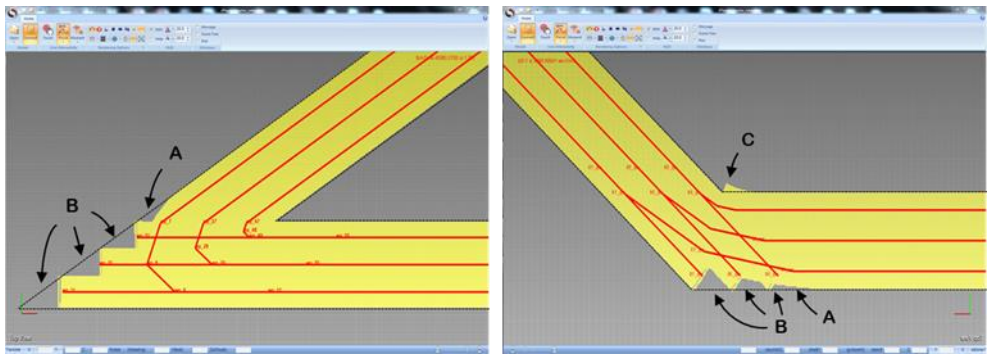

(c)

Figure 22. Simulation results of (a) the tracking trajectories, (b) lateral deviations, and (c) the tilled swath for the outer-work path at boundary corners of 30° and 150°.

Figure 23 a comparison of the effect of the corner angle and pass number on the tracking performance obtained when following the developed path. According to the aforementioned studies implemented for 30° and 150° corners, it was apparent that the root-mean-squared error (RMSE) in the lateral deviation was increased from 26 to 69 mm due to the characteristics of the look-ahead tracking method when the virtual tractor navigated around the boundary corner path at a smaller angle. However, even when following the path at the steepest corner with the most significant error, the tillage operation was conducted with an acceptable coverage efficiency because the alignment distance was adaptively calculated for the corner angle and the location of the headland pass, implying that the operation could be completed without additional non-tilled areas within the polygonal field boundary.

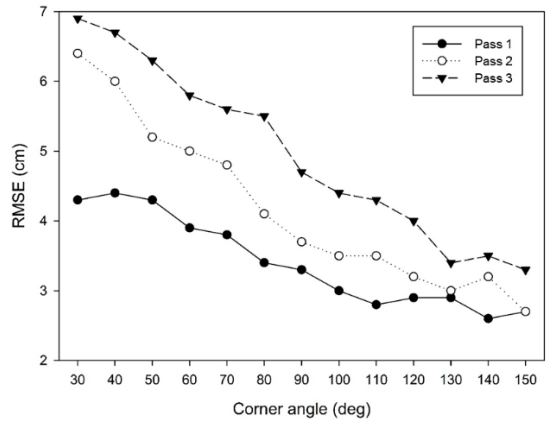

(a)

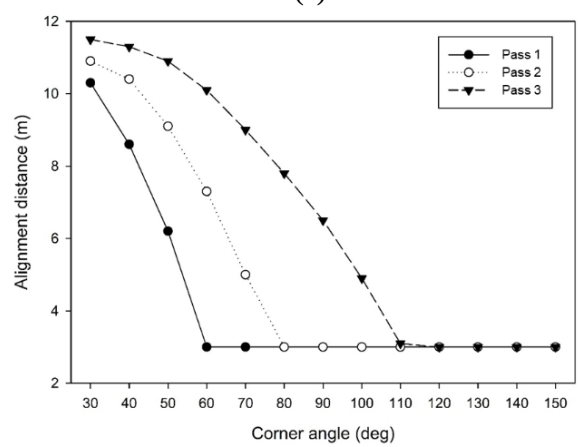

(b)

Figure 23. (a) Root-mean-squared error (RMSE) of lateral deviation of virtual tractor following the outer-work path (i.e., two 20-m rows after the boundary corner turning path) and (b) the alignment distance for various boundary corner angles.

Validation testing of outer path with boundary corner turning

Figure 27 shows the results for the trajectories of the autonomous tractor following the work path obtained from the developed path generation algorithm in a trapezoidal field when applied to four field corners with four different turning angles of 61.6°, 102.3°, 76.8°, and 119.3°. Similar to the results of the simulation study, the proposed path enabled the autonomous tractor to show acceptable tracking performance when following the straight working passes (Figure 27(a)). For example, as shown in Figure 27(b), when the system navigated the

autonomous tractor around corner 3, which is the steepest corner, the autonomous tractor successfully reached the end of the reversing path with an acceptable tracking level ranging from -30 to 70 mm even though the lateral deviations ranging from -1026 to 35 mm, -1767 to 212 mm, and -3479 to 507 mm were obtained along the turning paths on passes 1, 2, and 3, respectively. The RMSEs of each straight working pass were within 100 mm, implying that using the developed path effectively covered the outer-work area even in the polygonal field.

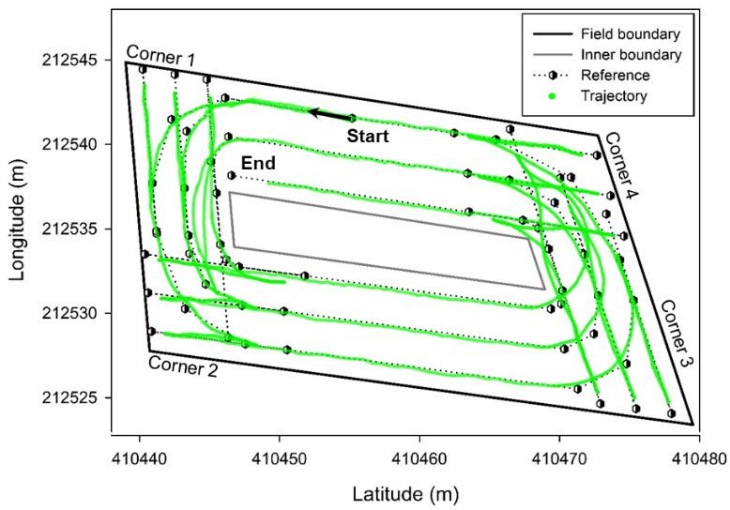

(a)

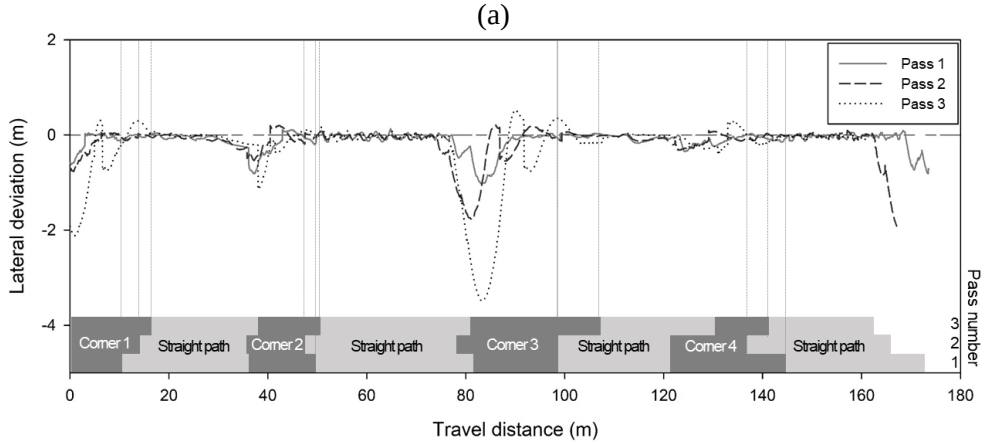

(b)

Figure 24. Results of (a) the tracking trajectory and (b) the lateral deviation of the tractor following the outer-work path in the field

Three case studies of full tillage paths

Generation of full tillage paths for the three different paddy field shapes

Figure 25 shows predefined maps of reference paths obtained with X- and C-type headland-turning patterns in three different fields. The inner-work tracks generated in the same direction as the longest segment of the field boundary completely filled the fieldwork area at regular swaths using an adaptive overlap length ranging from 73 to 178 mm in three types of field (Table 12). It is noticeable that the overlap length in the quadrilateral field was adjusted to be smaller than the initial overlap length (100 mm) in two turning patterns such that the number of inner-work tracks also decreased from 20 to 19, thereby resulting in decreases in the predicted time and travel distance compared to those obtained when the path was generated with an overlap length of 100 mm.

In addition, because the developed planner could automatically adjust the number of headland passes (n_h) depending on whether the headland-turning path was outside of the inner-work area, the whole paths were successfully generated within the field boundaries when not only the C-type but also the X-type pattern was used as the turning method. Even though it was difficult to determine an exact relationship between n_h and the headland-turning pattern, it was apparent that a bigger n_h would be needed when using the X-type turning method, as shown in the outer-work path of the pentagonal field in Figure 25. This was because the arc angle is adaptively calculated during C-type turning rather than constantly using

90° during X-type turning. In addition, when comparing operational paths of the triangular and quadrilateral field, n_h was strongly affected by the intersection angles between exiting or re-entering the inner-work track and the boundary, thus the closer the angle to the vertical, the smaller the required n_h (Figure 25 (b)).

The predicted travel distance and time based on separate calculations of the times required to travel the distances of the straight and curved paths and assuming that the tractor operates at 4 and 2 km h^{-1}, respectively, are highly related to n_h, n_i, and the headland-turning pattern, as reported in Table 12. For example, when the complete coverage tillage path was generated in the triangular and quadrilateral field where n_h and n_i were the same regardless of the turning pattern, the estimated total travel distances and times for the tillage operation for the operational path based on the C-type headland pattern (2229.2 m and 3086.3 s, and 2828.3 m and 3398.8 s, respectively) and X-type turning (2035.2 m and 3050.9 s, and 2567.2 m and 3373.9 s, respectively) were similar. The reason for the slight difference between the paths based on C- and X-type turning patterns is that the tractor should always travel approximately half of the field width to enter another track with C-type based headland turning whereas the X-type turning method requires the tractor to reverse for a relatively small distance. However, in the pentagonal field, bigger n_h caused by the X-type turning pattern requiring a wider area significantly increased the predicted travel distance and time for the tillage operation from 2392.8 to 2439.4 m and 2904.8 to 3714.2 s, respectively, indicating that the minimization of n_h, which is roughly inversely proportional to n_i, should be guaranteed to improve the performance of the proposed path planner.

(a) X-type

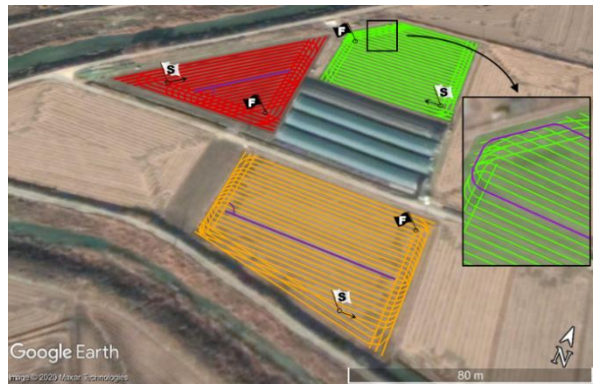

(b) C-type

Figure 25. Views of the operational paths in the three field shapes based on the (a) X-type and (b) C-type headland-turning patterns.

Table 12. Comparison of the operational parameters for the complete coverage paths for the three field shapes with X and C-type headland-turning patterns.

Field Shape	Headland Turn	Predicted Time (s)				Predicted Travel Distance (m)				w_o (mm)	n_h	n_i
		Inner-work	Headland turning	Outer-work	Total	Inner-work	Headland turning	Outer-work	Total			
Triangle	X	443.7	597.3	2009.8	3050.9	493.0	241.0	1301.2	2035.2	143	4	14
	C	443.7	663.0	1979.7	3086.3	493.0	435.3	1300.9	2229.2	143	4	14
Quadrilateral	X	1011.0	829.6	1450.9	3291.5	1126.4	346.7	1042.8	2515.9	73	3	19
	C	1011.0	964.6	1469.8	3445.4	1126.4	621.3	1083.7	2831.4	73	3	19
Quadrilateral (100 mm overlap)	X	1098.2	844.4	1488.3	3430.9	1216.3	353.0	1055.3	2624.6	100	3	20
	C	1098.2	1041.8	1477.5	3617.5	1216.3	648.4	1076.2	2940.9	100	3	20
Pentagon	X	647.5	735.1	2331.6	3714.2	715.9	294.8	1428.7	2439.4	178	4	17
	C	780.8	802.9	1321.1	2904.8	867.5	504.1	1021.2	2392.8	158	3	19

n_h, number of headland passes; n_i, number of fieldwork tracks; w_o, adaptive overlap length

Simulation of the automatic full tillage operation

Figure 26(a) shows a comparison of the reference paths of the autonomous tillage operation in three shape fields based on C-type turning patterns, with trajectories of a 3D virtual tractor operated in those paths. In all types of field, the virtual tractor performed complete tillage operation without any stops or collisions with the field boundary during the simulation, thus showing an acceptable performance with lateral RMSE ranging from 40 to 46 mm and heading RMSE ranging from 0.8° to 1.3°.

Figure 26(b) shows the coverage maps obtained using a display swath function to show the tilled area (yellow grid) in the simulator. The inner-work areas were almost completely covered in all field types because the waypoints (the crosses in Figure 26(a)) for the tractor additionally perform tillage operation until the tractor exited the inner-work area were elaborately designed with consideration for the irregularity of the field boundary. The skipped zones with areas of 46.2, 21.5, and 31.1 m^2, accounting for 1.53%, 0.62%, and 0.71% in triangular, quadrilateral, and pentagonal fields, respectively, were found at each boundary corner (Figure 26(b)) and inevitably occurred due to the outer-work path with a reversing gap to prevent collisions between the implement and the field boundary. In addition, the skipped zones labelled A (Figure 26(b)) were discovered for the same reason during boundary corner turning where the maximum and minimum errors were measured, implying that the algorithm for the determination of the look-ahead distance needs to be improved to effectively cover the polygonal field.

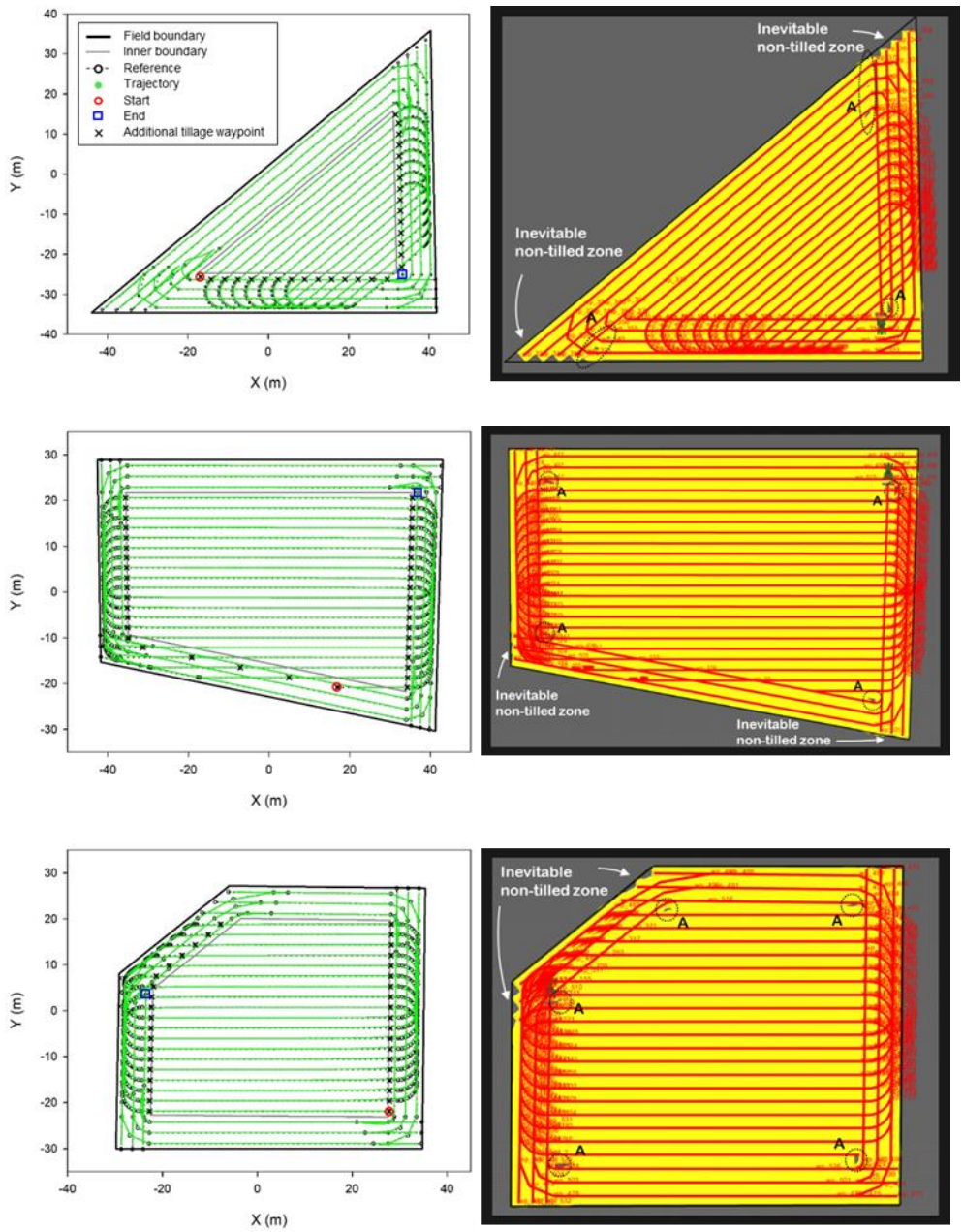

(a) (b)

Figure 26. Comparison of reference paths with trajectories of the autonomous tractor performing complete coverage tillage operations in three different polygonal fields based on C-type turning pattern and (b) views of the coverage maps obtained using the display swath function of the simulator.

Validation testing of outer path with boundary corner turning

Figure 27 shows the results for the trajectories of the autonomous tractor following the work path obtained from the developed path generation algorithm in a trapezoidal field when applied to four field corners with four different turning angles of 61.6°, 102.3°, 76.8°, and 119.3°. Similar to the results of the simulation study, the proposed path enabled the autonomous tractor to show acceptable tracking performance when following the straight working passes (Figure 27(a)). For example, as shown in Figure 27(b), when the system navigated the autonomous tractor around corner 3, which is the steepest corner, the autonomous tractor successfully reached the end of the reversing path with an acceptable tracking level ranging from -30 to 70 mm even though the lateral deviations ranging from -1026 to 35 mm, -1767 to 212 mm, and -3479 to 507 mm were obtained along the turning paths on passes 1, 2, and 3, respectively. The RMSEs of each straight working pass were within 100 mm, implying that using the developed path effectively covered the outer-work area even in the polygonal field.

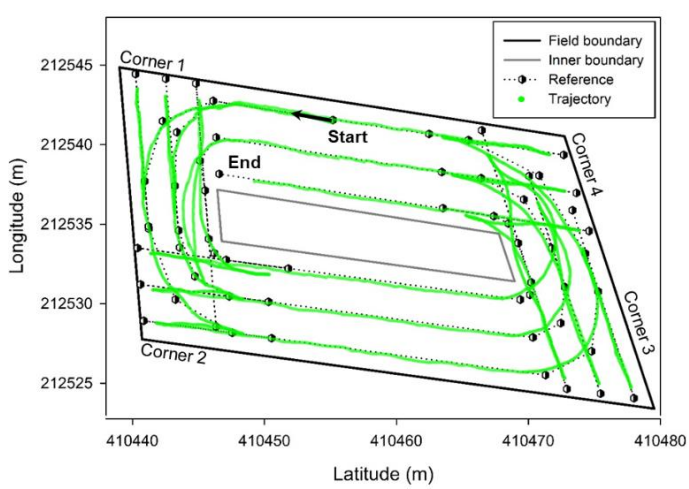

(a)

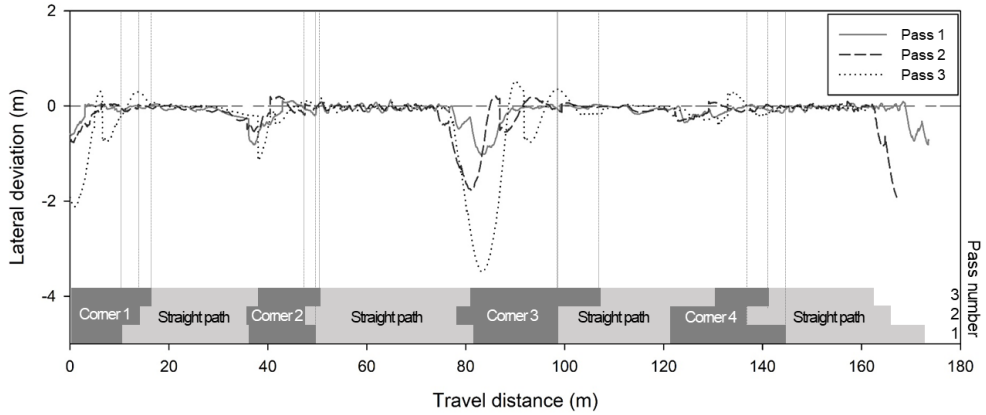

(b)

Figure 27. Results of (a) the tracking trajectory and (b) the lateral deviation of the tractor following the outer-work path in the field

Field tests of autonomous tillage operation in three different paddy fields

Figure 28 shows the trajectories of the autonomous tractor following operational paths with C-type headland turning for three different field shapes (triangle, quadrilateral , and pentagon) and the associated coverage maps drawn by the ArcGIS program (version 10.1, ESRI, Redlands, USA). Even though the field shapes were varied, which affects the strategies of the path generation algorithm and results in dynamic navigation behaviour of the tractor, autonomous tilling was successfully completed with an acceptable level of lateral deviation and heading error RMSEs measured for each working pass, ranging from 32 to 101 mm and 0.6 to 2.2 °, respectively, as shown in Figure 29. The autonomous tractor successfully navigated the full paths without colliding with the field boundary in 73.6, 96.2, and 75.0 min for the triangular, quadrilateral, and pentagonal fields,

respectively. The untilled areas of the full-scale tillage operation (labelled A, B, and C) were calculated to be 51.6 (triangle), 38.1 (quadrilateral), and 33.7 (pentagon) m^2, thereby accounting for 1.7%, 0.9%, and 1.0% of the total area. The results indicate that there was a significant decrease in skipped area compared with our previous study (Han, Kim, Jeon, Moon, et al., 2019) with a skipped area of 204.3 m^2, which corresponded to 8.5% of the total field area obtained in the field test using the same autonomous tractor in this study. Nevertheless, as obtained in the simulation study, the symmetrical skipped areas labelled A (9.2, 12.7, and 9.7 m^2) occurred at each boundary corner, implying that the time response of the steering system should be improved. At the end of the reversing path in the outer-work path, an untilled area labelled B (20.4, 21.9, and 9.5 m^2) also occurred because the autonomous tractor inevitably stopped before the edge of the implement reached the field boundary for the same reason as the simulation result. The possible causes for the skipped areas labelled C (4.1, 17.9, and 18.9 m^2) could be due to occasionally increased draft force on the rotary cultivator making the autonomous tractor oscillate and inaccurate GPS information, which was confirmed by the fact that the skipped areas were found in the area where the implement moved down and the trajectory section was non-continuous. Nevertheless, the fact that the autonomous tractor fully navigated the coverage path automatically and tilled more than 98.3% of the whole area in the polygonal paddy field without colliding with

the boundary indicates a significant enhancement in the guidance tractor system.

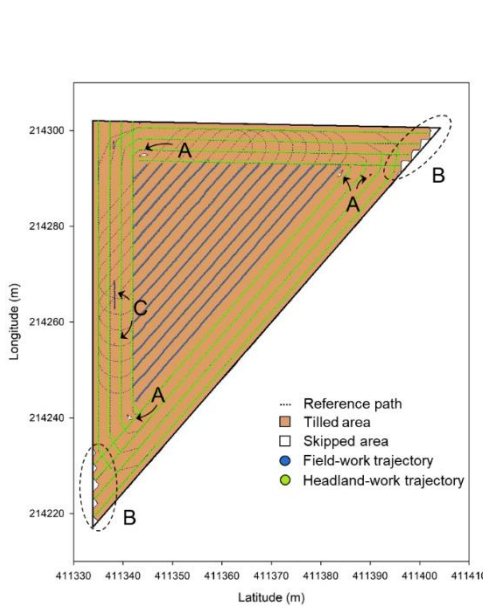

(a)

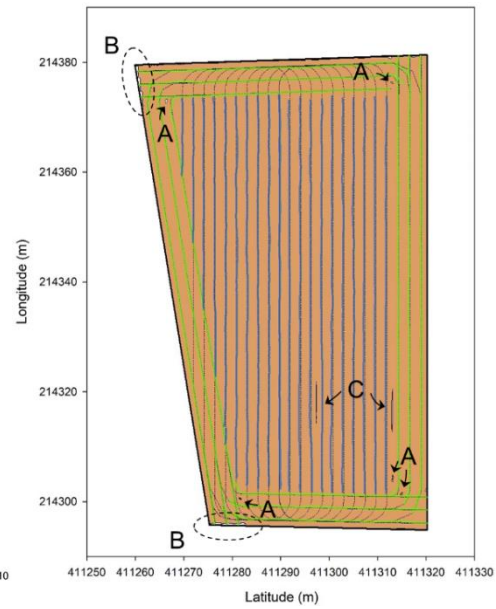

(b)

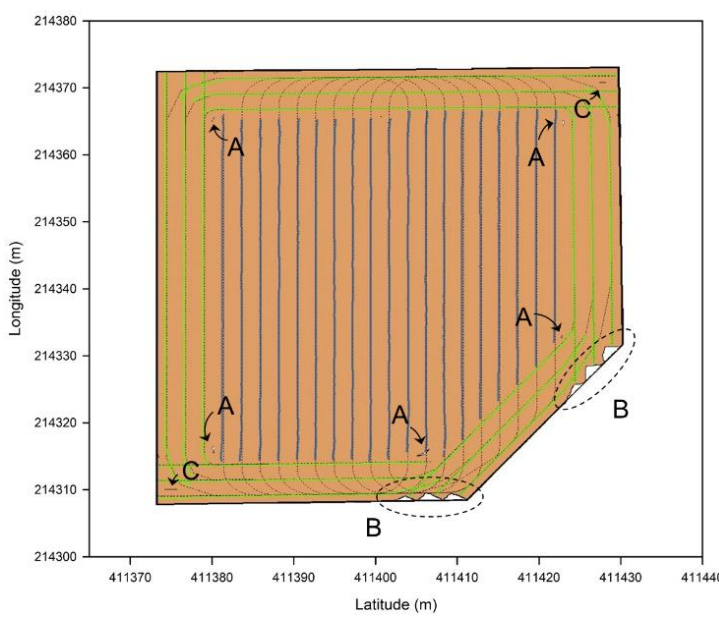

(c)

Figure 28. Trajectories and coverage maps of the autonomous tractor performing the tillage operation in the (a) triangular, (b) quadrilateral, and (c) pentagonal paddy fields.

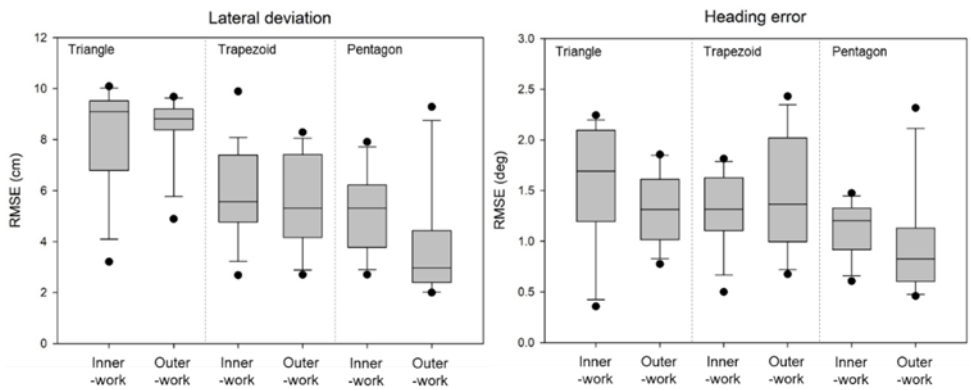

(a) (b)

Figure 29. RMSEs of (a) lateral deviations and (b) heading errors obtained when the autonomous tractor navigated the fieldwork and outer-work areas in three different polygonal paddy fields.

CONCLUSIONS

In this study, a complete paddy field-coverage path planner for an autonomous tillage tractor was designed and its performance was validated via both simulation and field testing. The main contribution of this study was to illustrate how inner and outer paths in various shapes of polygonal fields are automatically generated to enhance the coverage performance of an autonomous tractor when compared to our previously developed system. We proposed methods for generating the inner-path with an adaptive overlap length combined with C- and X-type headland-turning patterns and the outer-work path with a boundary corner path. The feasibility of using the path generation algorithms for autonomous tilling was investigated via a

3D graphic computer simulator. Field tests were conducted to validate the enhancement and potential of the fully automated tilling performance using a 63.4-kW autonomous tractor equipped with an INS system. The following conclusions can be drawn from the tests.

- An outer-work path generation method was designed to enable an autonomous tractor to automatically navigate the boundary corners connected with headland passes in the presence of an enclosing field boundary and to till the headland area. In this method, a geometrical model applicable to polygonal paddy fields was derived using the tractor's characteristics and field shape conditions. The results of the validation test showed that the proposed method could provide an acceptable level of coverage performance in terms of lateral deviations ranging from -30 to 70 mm at various corner angles (61.6°, 102.3°, 76.8°, and 119.3°).

- The proposed planner for an autonomous tillage tractor could provide an increase in coverage efficiency because the outer-work path including the alignment distance and a reversing gap was elaborately designed. In the field test, the autonomous tractor successfully followed (lateral and heading RMSEs < 10.1 m and 2.2°) and tilled the whole path with more than a 98.3% coverage efficiency in three different-shaped paddy fields. In future studies, we will develop an entry-exit path planner by considering the start and end points corresponding to a single entrance of the paddy field, in order to enable the autonomous tractor located at the entrance to automatically go to the starting location

of the operational path, perform the agricultural task within the field boundary, and return to the entrance.

CHAPTER 4

FULL-COVERAGE PATH PLANNER FOR AN AUTONOMOUS PUDDLING AND LEVELING TRACTOR IN PADDY FIELDS

ABSTRACT

Land puddling and leveling operations are required on every cropping season and are one of the most important strategies for paddy field management as they improve weed control and water efficiency which help produce high-quality yield. Application of autonomous tractor technology equipped with an effective coverage path planner (CPP) is necessary to perform puddling and leveling with an improved field efficiency in paddy fields where it is difficult to secure the driver's sight because of flooded waters. Therefore, this study describes the development of a complete CPP for an autonomous puddling and leveling tractor that automatically generates the inner- and outer- work path applicable to irregular fields. In addition, this study performed a field evaluation of using autonomous puddling and leveling CPP by comparing the tracking and leveling performance of an autonomous tractor with that of a skilled worker in the same conditions (e.g., test field and platform). An operational path-mapping model composed of a four-stage configuration was designed for an autonomous tractor equipped with a rotary cultivator and a wing harrow, which provides important benefits to the optimal track sequence derived by a genetic algorithm. The feasibility of using the developed algorithm was investigated via simulation studies in three fields followed by a field test with a 63-kW autonomous tractor. To evaluate the leveling performances, the height maps

generated using megapixel images were acquired from an unmanned aerial vehicle. The results of a computer simulation confirmed that the designed puddling and leveling CPP confirmed a planning performance by reducing the headland turning distance in three fields by 28 %, 33.9 %, and 45.0 %, as compared with that obtained with CPP from the previously developed track sequence. In the field test, the autonomous tractor successfully navigated the whole path with a lateral deviation ranging from -11.3 cm to 13.7 cm and a heading error ranging from -2.7 deg to 1.8 deg, respectively, and demonstrated superior tracking performance in terms of travel distance and fuel consumption by reducing from 3039.6 m to 1940.1 m and from 17.1 L to 16.3 L as compared with those of the manual operation because of refined traversal sequence using precise position information. However, it was confirmed that it took approximately 20 minutes more because it traveled at a slower average velocity (1.35 km/h) than the manual-driven tractor (2.75 km/h). Especially, the results of the leveling performance via height map showed the capacity of the autonomous tractor with a similar variability ranging from 39.61 m to 39.85 m (autonomous) and from 39.62 m to 39.81 m (manual).

Keywords: Path planning; Puddling and Leveling; Paddy field; Autonomous tractor

INTRODUCTION

The agricultural sectors, including the industrial and academic fields, are undergoing various challenges of farm management related because of the increase in agricultural production with limited resources (Tilman, Cassman, Matson,

Naylor, & Polasky, 2002). Driven by expectations for sustainable operation of food and agricultural system, Agriculture 4.0 brought a new concept of agriculture based on the introduction of automation, artificial intelligence, and robotics into the agricultural processes to overcome the problems that agriculture is facing. In this regard, self-driving agricultural machines play a relevant role to increase both production and efficiency in a sustainable way (Mazzia, Salvetti, Aghi, & Chiaberge, 2021). With the rapid adoption of automatic guidance systems in agriculture, agricultural routing planning (ARP) (Utamima, Reiners, & Ansaripoor, 2019), which is employed to optimize the logistics of the agricultural machines concerning their movements in the field and farm facilities, is a core task for efficient management to optimize resource utilization (i.e., electricity, fertilizer, fuel, human resource, and water) and the schedule needed to manage field operations with reduced environmental impacts (D. D. Bochtis, Sørensen, & Busato, 2014).

Researchers in ARP have worked on issues such as minimizing the input resource (e.g., time consumed, travel distance, fuel consumption, and traffic intensity) required for the machine to navigate all the requisite routes by optimizing track sequences (D. Bochtis, Vougioukas, & Griepentrog, 2009; Spekken & de Bruin, 2013; Utamima et al., 2019), headland turning patterns (D. Bochtis & Vougioukas, 2008; X. Han, Kim, Jeon, & Kim, 2019), and the orientation of the tracks (Edwards et al., 2017; I. Hameed, Bochtis, Sørensen, Jensen, & Larsen, 2013), representing 3D coverage path map (I. A. Hameed, la Cour-Harbo, & Osen, 2016; Jin & Tang, 2011; Vahdanjoo, Zhou, & Sørensen, 2020), and dealing with constraints (e.g., sub-fields, limited machine capacity, infield obstacles, and soil compaction risk)

(Augustin, Kuhwald, Brunotte, & Duttmann, 2020; D. D. Bochtis, Sørensen, & Green, 2012; Conesa-Muñoz, Pajares, & Ribeiro, 2016; Jensen, Bochtis, & Sørensen, 2015; Seyyedhasani & Dvorak, 2017). For instance, D. Bochtis et al. (2009) developed the B-pattern method which algorithmically determined sequences of field-work tracks for completely covered areas with a minimum total or non-working distance and was tested on an autonomous agricultural vehicle. (Spekken & de Bruin, 2013) proposed an optimal coverage path planner with an infield headland turning maneuver designed for an agricultural machine by minimizing the time needed for turning between tracks while accounting for time loss because of machine services.

Currently, several researchers have developed the planner to solve ARP problems in a paddy field by replacing it with coverage path planning (CPP) that generate routes that lead the machine to traverse all waypoints while performing agricultural tasks such as tillage (X. Han, Kim, Jeon, Moon, et al., 2019; C.-W. Jeon, Kim, Yun, Han, & Kim, 2021), puddling and leveling, planting (Nagasaka et al., 2009; Yin, Du, Noguchi, Yang, & Jin, 2018), weeding (Adhikari, Kim, & Kim, 2020; Choi et al., 2015), and harvesting (C. W. Jeon, Kim, Han, & Kim, 2017; Kurita, Iida, Cho, & Suguri, 2017). Among those agricultural tasks performed in paddy fields, puddling and leveling (i.e., wetland preparation), are required on nearly every cropping season, and they help improve weed control and facilitate the incorporation of nutrients in the soil to obtain high yields and is the general way of preparing lowland fields (Chauhan, 2013). When planning strategies to perform wetland preparation, there are two land leveling philosophies: (1) to provide a slope that fits a water supply; and (2) to level the field to its best condition with

minimal earth movement and then vary the water supply for the field condition (Walker, 1989). However, because of the operational environment where a field is flooded with water when performing the puddling and leveling operation, it is difficult for workers to distinguish between worked and non-worked zones visually. As a result, there is a high possibility that there will be multiple non-worked areas, which could cause large or no earth movements. An autonomous agricultural machine equipped with an effective CPP that navigates along with a pre-defined map while performing agricultural work based on position data measured from a global navigation satellite system (GNSS) sensor can be a good solution to this problem. In a previous study (C.-W. Jeon et al., 2021), we developed the complete paddy field CPP and validated its algorithm by a field test in three irregular-shaped fields using a 63-kW autonomous tractor. However, there was a limitation that the design of the path planner was based on the path model of the tillage operation.

Thus, to enhance the performance of the full CPP for the autonomous tractor system developed in our previous study (C.-W. Jeon et al., 2021), the ultimate goal of this study is to develop a complete field-CPP for an autonomous puddling and leveling tractor. In addition, to increase the field efficiency (e.g., travel distance and time consumed) of the pre-defined map, a determination of the optimal track sequence for puddling and leveling operation was proposed using a genetic algorithm (GA).

The specific objectives were to

- 1) Design the model of an autonomous puddling and leveling operation

- 2) Implement the path planner with the determination method of optimal sequence based on the proposed model
- 3) Investigate the feasibility of the developed path planner by analyzing its tracking and covering its performance via simulation studies
- 4) Validate the puddling and leveling path planner by comparing the tracking and puddling & leveling performance of the autonomous tractor with a skilled worker during the field test.

MATERIALS AND METHODS

Generation of puddling and leveling path

Modelling of puddling and leveling path

To guide the autonomous tractor in a paddy field to perform the puddling and leveling operations systemically, a CPP was designed to generate waypoint data and operational commands for the autonomous tractor. In this study, an agricultural model was proposed for the autonomous tractor equipped with a rotary cultivator and a paddy drive harrow with foldable wings. The swath of the harrow could be extended by unfolding the wing harrows to cover a wider area in a single drive to ensure a well-leveled field. According to the process of the puddling and leveling (wetland preparation) for paddy fields proposed by the International Rice Research Institute, the puddling, works the soil clods and incorporates weeds, straw, and stubble into the mud for the field to be flattened evenly, by preceded the leveling. Such that when performing the puddling and leveling operation with the implement

used in this study, there is a condition to be observed: the area covered by the unfolded wings should be chunked in advance.

To describe an agricultural routing problem by substituting it for a form of the CPP problem, a model for the puddling and leveling was designed. Assuming that the direction of the inner-work tracks, an inner-work area was already determined along the longest side of the field, the proposed model is composed of a four-stage configuration as illustrated in Figure 30. In the first stage, the autonomous tractor placed in a corner of the paddy field starts driving along the outmost headland passes located in the outer-work area, while operating a rotary cultivator and the paddy drive harrow with the folded wings to collect soil from the edge of the field inward. In the second stage, the tractor entering the inner-work area via the first track performs puddling and leveling operation by traversing tracks indexed by an odd number (e.g. 1, 3, 5,…) with the purpose of churning and pre-leveling these areas. In the third stage, the wing harrows are unfolded and the remaining inner tracks indexed by an even number (e.g. 2, 4, 6,…) were puddled and leveled by the tractor while leveling the softened area in the second stage once more. Given a such traversal strategy, a C-type headland turning pattern was used because the consecutive tracks to be covered by the tractor are non-adjacent. After covering the inner work area, the tractor returned to the outer-work area to finish the land preparation task following subsequent headland passes with the boundary corner turning. In this stage, the remaining areas including the headland area damaged by the machine when performing headland turning while the implement was raised, were re-leveled by using the wing harrows. Therefore, the proposed model allows

the autonomous tractor to perform one puddling and two leveling operations for the entire paddy field.

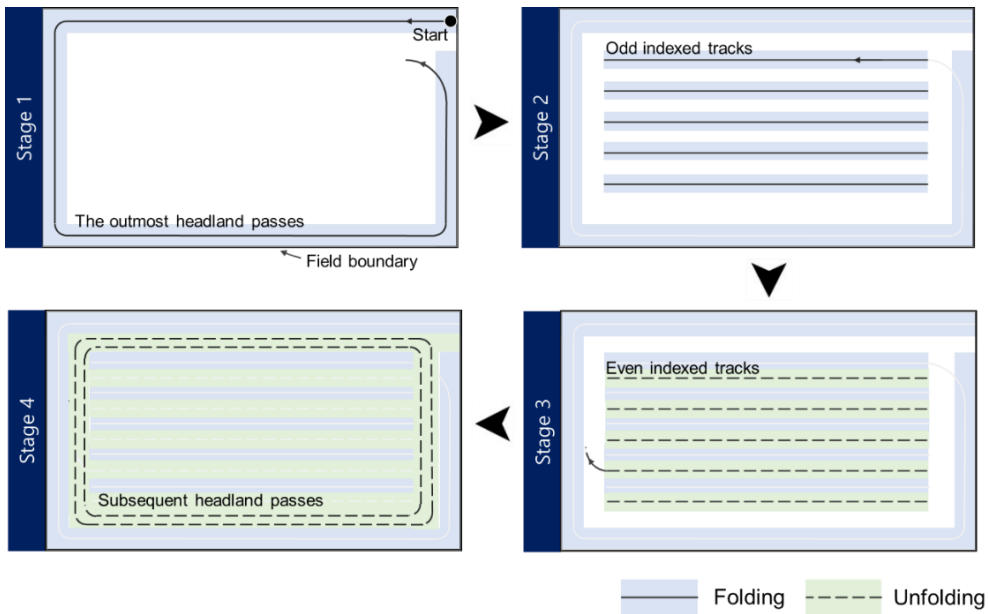

Figure 30. Process of puddling and leveling operation for the autonomous tractor equipped with the rotary cultivator and the paddy drive harrow with foldable wings.Figure 31 illustrates the process of generating the puddling and leveling path. In the path planner, the desired path described by a set of waypoints was generated based on the puddling strategy proposed in this study, using information about the coordinates of the boundary corners, the width of the implement, the overlap length, the minimum turning radius of the tractor, and navigational parameters such as working and turning velocity. The vertices of the boundary corners are given in the form of a text file as a closed polygon in a transverse Mercator (TM) coordinate system. In the proposed autonomous puddling and leveling model, the path is decomposed into two sub-regions, i.e., inner- and outer-work areas. The inner-work path includes odd & even tracks and C-type headland turns, while the outer-work paths consist of outmost- and subsequent-headland

passes with the boundary corner turning paths to connect them, and two connection paths to guide the tractor from the outmost outer-path to odd-indexed inner-tracks and from even-indexed tracks to the subsequent outer-path. In this study, the path planner provided an optimal track sequence of the inner tracks using a GA.

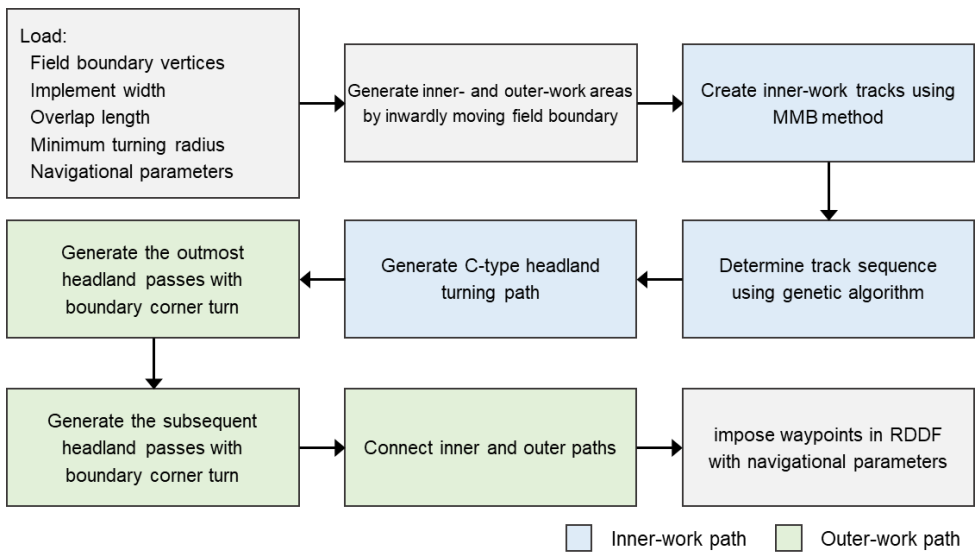

Figure 31. The architecture of the geometrical representation of the wet lend preparation path

Geometrical representation of inner and outer-work paths

The autonomous puddling and leveling path was geometrically represented by modifying the path planning approach proposed in our previous study (C.-W. Jeon et al., 2021). To secure a space where the tractor could execute the infield-headland turning maneuver, a boundary of an inner-work area, i.e. inner-field boundary, was generated based on the number of headland passes. The approach for the generation of the inner-work tracks is based on the MBB (Minimum bounding box) method (I. Hameed, Bochtis, Sørensen, & Nøremark, 2010; O'Rourke, 1985), which is a rectangle with a minimum-area enclosing the vertices of the field to

concisely express a complex field shape. The straight segment aligned in the direction of the longest side of the field filled the MBB with parallel swaths calculated using the implement width and overlap length to identify the inner work tracks as presented in Figure 32. Let H = {1, 2, 3, 4, …} be the arbitrarily ordered set of the inner-work track indices. A C-type headland pattern was used to connect each inner track at their ends because the tracks on the model of the puddling and leveling path were listed non-adjacently (odd and even tracks). The travel distance during the headland turning maneuver from the i[th] track to j[th] track ($d_{turning}(i,j)$), was computed based on the minimum turning radius of the tractor (R), exit and two angles of the intersection of an inner-work track and the field boundary, i.e., θ_{exit} and $\theta_{re-enter}$, and the swath (w) using Eq. 4.1.

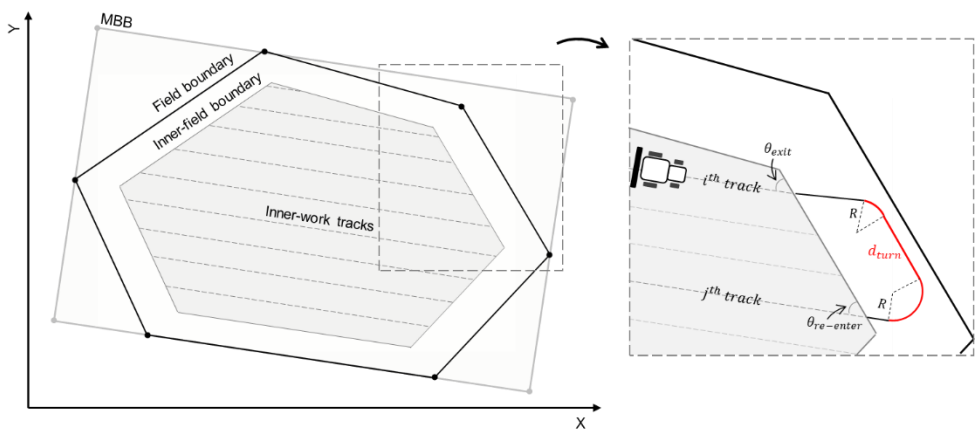

Figure 32. Geometrical representation of inner-work tracks and C-shaped infield headland turning maneuver.

$$d_{turning}(i,j) = 0.5w[\tan(-|\theta_{exit} - 0.5\pi| + 0.5\pi) + \tan(-|\theta_{re-enter} - 0.5\pi| + 0.5\pi)] + d_{turn} \quad i,j \in \{1,2,,\dots,\|H\|\} \quad (4.1)$$

On the outer-work paths, the headland passes including the outmost and subsequent passes and the boundary corner turning paths which incorporate

reversing to connect those passes at field boundary corners were generated as presented in Figure 33. In this process, to align its attitude with the next target line before reversing to cover the boundary corner area, the path planner provides the autonomous tractor an alignment path based on the index of the headland passes, the boundary corner angle, and the minimum turning radius of the tractor. In addition, two connection paths that transit between the inner-work and outer-work paths by connecting the outmost and subsequent headland were passed to the odd-indexed and even-indexed tracks, respectively, and were generated to navigate the tractor full-coverage puddling and leveling path. Detailed equations and derivation processes of the inner and outer paths can be found in our previous studies (C.-W. Jeon et al., 2021).

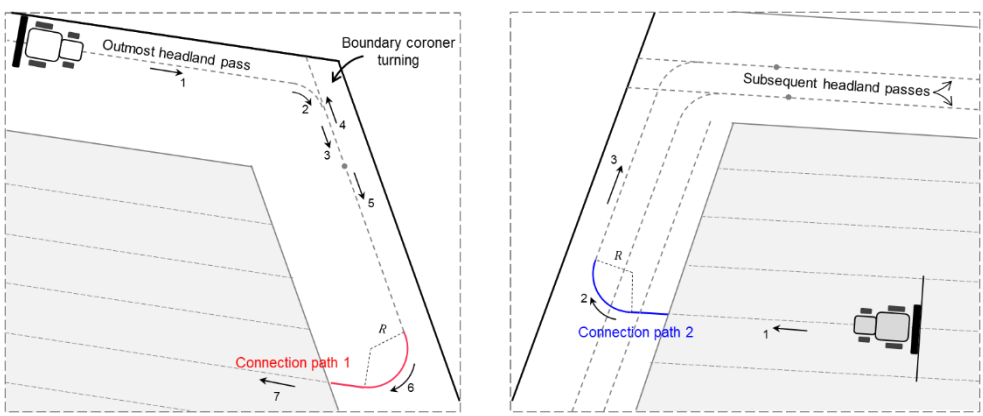

Figure 33. Geometrical representation of outer-work paths with two connection paths.

Optimal Path Planning algorithm using Genetic Algorithm

Travelling salesman problem and Genetic algorithm

The GA published by Goldberg and Holland (1988) have been widely used in solving the optimization problem of the path planning algorithm for various

contexts such as a mobile robot, an unmanned aerial vehicle (UAV), and an unmanned surface vehicle (Kim et al., 2017; Noguchi & Terao, 1997; Roberge et al., 2012), was implemented to find the optimal sequence($\sigma *$). Based on the genetic theory of Darwin evolution, the GA simulates the evolution of a population of solutions to optimize a problem: evaluation, selection, crossover, mutation, and replacement. Similar to living organisms that adapt to their environment by providing their strong genes to have a greater opportunity to pass their genes to future generations via reproduction, the solutions in the GA adapt to a fitness function over an iterative process using biology-like operators such as the crossovers of chromosomes, the mutations of genes, and the inversions of genes. The travelling salesman problem (TSP) is a representative application of the GA and Chatterjee et al. (1996) proposed a method to solve the TSP using GA. Given a set of cities and distances between every pair of cities, the problem is to find the shortest possible route that visits every city exactly once and returns to the starting point. Since the condition that one track must be passed only once is the same as the condition for determining the order of cities in TSP, the problem of selecting the track sequence was substituted was the TSP.

Determination of track sequence with minimum non-working distance

In this study, the method of determining the optimal track sequence was devised to satisfy the condition that odd and even-indexed tracks were navigated sequentially. To solve this problem where the tractor visits each track exactly once with a special condition, i.e., divided odd and even tracks, TSP, which is the challenge of finding the most efficient route for a salesperson to visit every city

exactly once, was modified. To determinate possible track sequences separated by odd and even-indexes, a bijective function was defined: $s(\cdot): H \rightarrow H$, such that for every field track, $i \in H$, the function value s(i) returns the order in which the tractor covers the i^{th} inner-work track (Bochtis & Vougioukas, 2008). The inverse function: $s^{-1}(j): H \rightarrow H$ provides the specific sequence number of the tracks covered by the tractor entering the inner-work area's j^{th} selection.

The selection of a certain sequence of the tracks proposed in modeling of the puddling and leveling path, was performed separately for odd and even sets of tracks based on the headland turning distances. The definitions of the travel distance and the function $s^{-1}(\cdot)$ were computed based on the minimum turning radius of the tractor (R), exit and two angles of the intersection of an inner-work track and the field boundary, i.e., θ_{exit} and $\theta_{re-enter}$, and the swath (w) using Eq. 3.9. In addition, the travel distances of turning in odd and even sets respectively were defined using Eqs. 4.2–4.4 Given the optimal sequence of the odd-indexed tracks, the turning distance between the last track of an odd track set and the first track of an even set were defined and used in the calculation of the even track cost (J_{even}). To consider the non-holonomic characteristic of the tractor in the equations, the cost functions include the $p(i)$ term given by Eq. 4.5, which represents a penalty for a problem solver to find an impossible sequence covered consecutively by the tractor at steps from i to $i+1$.

$$J_{odd} = \sum_{i=1}^{\lceil 0.5\|H\| \rceil} p(i) \times d_{turning}((s^{-1}(i+1), (s^{-1}(i))$$

$$s^{-1}(i) \in \{1, 3, \ldots, 2\lceil 0.5\|H\| \rceil - 1\} \quad (4.2)$$

$$J_{\text{even}} = d_{odd\ to\ even} + \sum_{j=1}^{\lfloor 0.5\|H\| \rfloor} p(j) \times d_{turning}((s^{-1}(j+1), (s^{-1}(j)) \qquad s^{-1}(j) \in \{2, 4, \ldots, 2\lfloor 0.5\|H\| \rfloor\} \tag{4.3}$$

$$d_{odd\ to\ even} = p(\lceil 0.5(\|H\| - 1) \rceil) \times d_{turning}\left(s^{-1}\left(\lceil 0.5(\|H\| - 1) \rceil + 1\right), s^{-1}(\lceil 0.5(\|H\| - 1) \rceil)\right) \tag{4.4}$$

$$p(\text{i}) = \begin{cases} M & (w \times \left|s^{-1}(i+1) - \left(s^{-1}(i)\right)\right| \leq 2R) \\ 1 & (w \times \left|s^{-1}(i+1) - \left(s^{-1}(i)\right)\right| > 2R) \end{cases} \qquad s^{-1}(i) \in \{1, 2, , \ldots, \|H\|\} \tag{4.5}$$

To solve the problem, the GA was applied to determine a sequence to minimize the sum of the travel distances of turning, while considering the non-holonomic characteristic of the tractor (Figure 34). Although the GA, which is a random heuristics method, could not guarantee the best solution in all conditions by getting stuck with a local maximum, it can find a good-enough solution without a global analysis description of the problem (I. Hameed et al., 2010). In this study, the location of the entrance of the paddy field was also considered by adding the two Euclidean distances ($\mathrm{d_{start}}$, $\mathrm{d_{end}}$) calculated from the entrance to the start of the operational path and from the end of the operational path to the entrance. To generate the agricultural path suitable to the paddy field, weight values ($\mathrm{w_1}, w_2$) were assigned to $\mathrm{d_{start}}$ and $\mathrm{d_{end}}$ to create various situations, so that the optimal work sequence could be generated in consideration of the importance of operational start and end. Given the traversal sequence $\sigma = [s^{-1}(1), s^{-1}(2), \ldots, s^{-1}(\|H\|)]$, the total cost was written as Eq. 4.6, and the optimal sequence ($\sigma *$) given by Eq. 4.7, would be found by reclusively performing the evolutionary search process consisting of four different genetic operators:

evaluation, the elitist preserving selection (De Jong, 1975), the order crossover (Davis, 1985), the random uniform mutation (Goldberg & Holland, 1988), and replacement.

$$J(\sigma) = \mathrm{J_{odd}} + \mathrm{J_{even}} + \mathrm{w_1 d_{start}} + \mathrm{w_2 d_{end}} \quad (4.6)$$

$$\sigma * = argmin_{\sigma}\ J(\sigma) \quad (4.7)$$

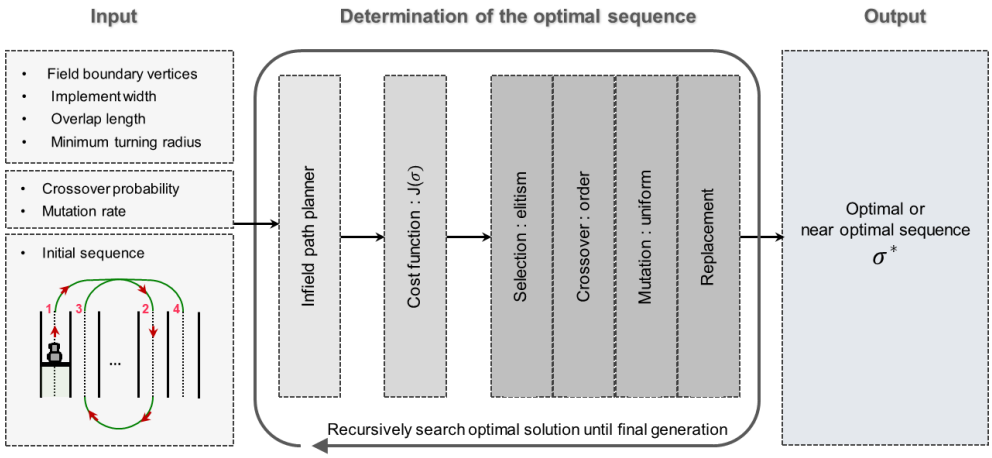

Figure 34. Framework of optimal path planning algorithm

Path planner program

Figure 35 illustrates the graphical user interface of the developed path planner, which was programmed using the LabVIEW software (ver. 15.0, National Instruments Co., USA) for operation and observation of results. The input data include a set of coordinates of the points on the field boundary, the width of the implement, the number of headland passes, the overlap length, the headland turning pattern (C-, X-, Ω-, R-types) (Han et al., 2013), the driving direction defined as the angle between the driving direction, limits of the boundary offset (LBO), agricultural tasks (tillage and puddlin· leveling) and the horizontal axis of the TM coordinate system. The field coordinates formatted at TM coordinates were imported into the

path planning program with the sequentially clockwise or counterclockwise direction in a text field. The import of parameters related to the optimal path planning, including weight values (w_1, w_2) and position of entrance, enabled the obtainment of an optimal track sequence using GA. Given the field and tractor information, the developed planner generated the path and allowed the user to observe the geometrical representation of the reference path via a display. In addition, the predicted time, travel distance, and field efficiency on the path when the tractor ideally navigated the proposed path was also provided as useful information.

Two diagnostic algorithms were designed to investigate whether the waypoints generated on the outer-work path are located within the field boundary and whether they can cause an impossibly sharp turning maneuver for the autonomous tractor to follow because of the narrow outer-work area. The first diagnostic algorithm was implemented by inwardly moving the field boundary by half of the implement width to limit the area where the waypoints can be generated to allow the autonomous tractor to perform agricultural tasks without colliding with the field boundary. The second algorithm calculated the direction change of sequential three vectors consisting of consecutive four waypoints. When errors were detected, the number of headland passes was increased to obtain a wider headland area.

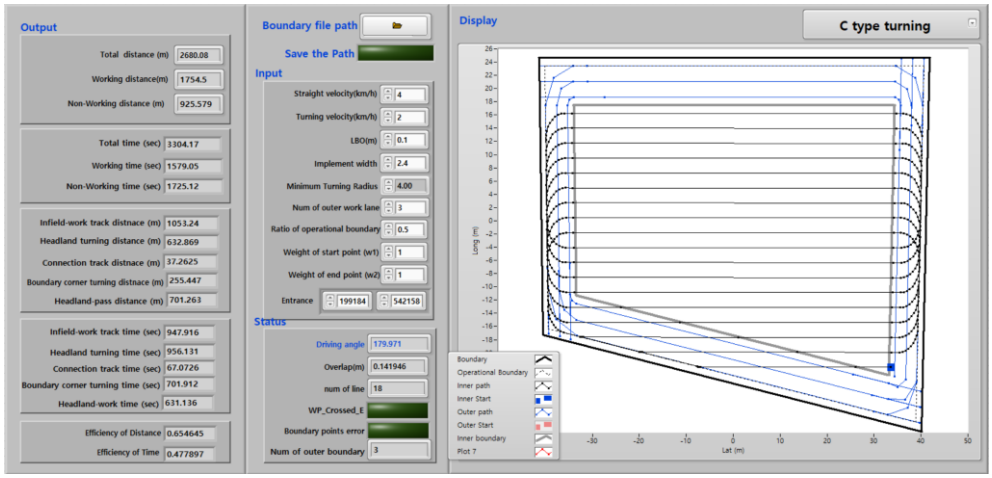

Figure 35. User interface of the full-coverage path planner

The path was then imposed to waypoint data in a Route Data Definition File (RDDF) form that includes the latitude and longitude coordinates of a target waypoint, the LBO, traveling velocities, and implement control values including rotary cultivator up (0)/down (1) and wing harrows folding (0)/unfolding (1) commands (Figure 35). This RDDF file is the input reference path and control strategies for a tracking method: the tractor searches for the next waypoint when it reaches a waypoint within the offset distance, which is predefined in terms of LBO (X. Z. Han et al., 2015). A navigation controller running a slip estimation-based path-tracking algorithm proposed in our previous study (X. Han, Kim, Jeon, Moon, et al., 2019) was used to recursively calculate the steering angle, tractor velocity, implement up/down, and wing harrows folding/unfolding commands by comparing the position and heading angle obtained from GNSS aided Inertial Navigation System (INS) sensor was mounted on the autonomous tractor system and the reference, and then transferred those control values to the test platform to follow the path until it reaches the final waypoint.

Table 13. An example of RDDF generated as the reference information for path tracking and agricultural task.

Index	Northing (m)	Easting (m)	LBO (m)	Velocity (km/h)	Rotary cultivator up/down	Wing harrows folding/unfolding
1	410296.5	212973.3	0.1	4	1	0
2	410206.1	212965.2	0.1	2	1	0
…						
n-1	410290.5	212985.7	0.1	2	1	1
n	410289.5	212984.9	0.1	4	1	1

Performance testing of autonomous puddling and leveling path planner

Simulation study of the tracking and covering performance

Prior to the path-tracking simulation, to investigate the feasibility of using the puddling and leveling path planner with an optimal sequence to effectively cover the whole area, three simulation tests were performed in the three different polygonal paddy fields located at Chungnam, South Korea: pentagonal (Field 1, 4361.3 m^2, +36°18’01.73’’ E, +127°09’34.85’’ N), trapezoidal (Field 2, 3451.3 m^2, +36°17’58.36’’ E, +127°09’34.78’’ N), and rectangular (Field 3, 3167.3 m^2, +36°16’50.90’’ E, +127°08’35.37’’ N) fields (Figure 36). In the first test, the feasibility of using the puddling and leveling model to perform wetland preparation task in the paddy fields were investigated. To do this, the path was generated using the planner that was developed based on the proposed model in the trapezoidal field (field 1 in Figure 36) and separately observed according to the wing harrows control commands required for the autonomous tractor: folding and unfolding. In the second test, to study the effectiveness of the method for determining the optimal sequence using GA, two different track sequences, i.e., the optimal

sequence derived by the GA and the gathering sequence pattern (Jeon et al., 2021), which lead the tractor to recursively navigate tracks that were located parallel to each other at around half the width of the field, and were applied on the path planner to compare operational parameters such as distance (ε_d) and time (ε_t) efficiencies in three different polygonal paddy fields (field 1, 2, and 3 in Figure 36). The values for path generation parameters used in this study were 0.1 m, 4 m, 2.2 m, 100, 0.5, 0.2, 100 for the minimum turning radius of the tractor, the overlap length, the working swath, population size, mutation rate, crossover probability, and total number of generations, respectively. To generate the paths, the algorithm programmed in LabVIEW, 2015 was simulated on an i7-5500U CPU in a 2.4-GHz Intel Centrino Mobile Workstation with an 8 GB RAM.

Figure 36. View of Google map image showing the three different paddy fields used for simulation test: trapezoidal (green), pentagonal (blue), and rectangular (white) fields, respectively.

As one scenario for evaluating the tracking and covering performance, we assumed that the tractor-driving simulator developed in previous studies (Han, Kim, Jeon, Moon, et al., 2019; Han et al., 2015) followed those paths while operating puddling and leveling implements (Figure 37 (a)), such that the two traffic intensity maps of puddling and leveling operations performed by the autonomous tractor simulator were generated. The traffic intensity was measured

as the number of passes by the puddling and leveling implements over a field area where gridding was performed with the grids of size 5 x 5 cm^2 using Bresenham's line algorithm (Bresenham, 1965) that determines the points of a raster that should be selected to form a close approximation to a straight line between both endpoints of the implements as presented in Figure 37 (b). A navigation controller developed by (Han, Kim, Jeon, Moon, et al., 2019) was used to calculate the steering angle. Consistent with the velocity control method used in a previous study (Jeon et al., 2021), the working and turning velocities to follow the waypoints were set to 4 km/h and 1 km/h, respectively. Navigational parameters such as the look-ahead distance, LBO, and the PD control gains for the path-tracking algorithm were the same as those used in our previous studies (Han, Kim, Jeon, Moon, et al., 2019).

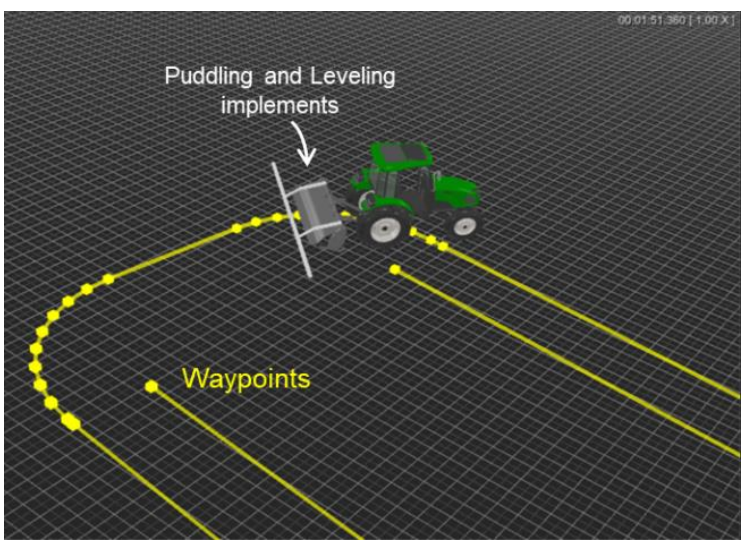

(a)

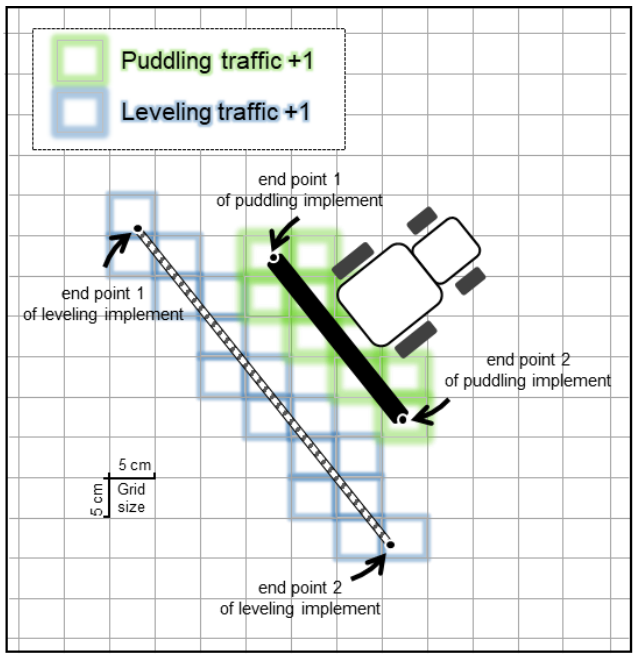

(b)

Figure 37. (a) Simulator (b) Generation of traffic map of the implement using Bresenham's line algorithm

Field testing on autonomous puddling and leveling operation in paddy field

Consistent with Chapter 3, the platform for the field tests built using a 63.4-kW tractor (TX853, TYM., Seoul, Republic of Korea; Figure 38 (a)) was used. The TX853 tractor, which weighs 3421 kg, is a four-wheeled tractor with front-wheel steering, 24-level forward and reverse speeds. The wheelbase, the length between the front and rear axles, and the height of the tractor are 2.2 m, 2.24 m, and 2.71 m, respectively. A GNSS/INS (Ellipse-D, SBG SYSTEMS., France) was mounted on the roof canopy of the tractor. Differential correction data provided by a network-RTK device (MRD-1000T, SYNEREX., Republic of Korea) based on the long-term evolution LTE wireless network, were then transmitted to the rover via networked transport of Radio Technical Commission for Maritime Services using

Internet protocol (NTRIP) to achieve 2 cm positioning and to observe the heading angle within ±0.1^{o} accuracy during 60 s outage at a sampling frequency of 20 Hz. An integrated navigation controller for high- and low-level controller (MXE-5500, ADLINK, Taiwan) for the path-tracking algorithm was used to control the autonomous tractor of the steering angle, traveling velocity, and implement up/down status. Consistent with the simulation, the steering angle for path-tracking was calculated based on the slip-estimation method (Han et al., 2019), programmed in LabVIEW 2018 on the navigation controller. An electrical power steering system (Unmanned Solution Co., Seoul, Republic of Korea) consisting of motor and control units was installed on the tractor to change the orientation of the tractor during the autonomous navigation. An angle sensor (Steer sensor, ComeSys, Republic of Korea) was installed at the center of the front kingpin. The tractor tilt compensation method for correcting GNSS (Global Navigation Satellite System) positioning errors caused by the difference in height between the vehicle tires and the transceivers was applied using the roll-pitch-yaw obtained from the IMU (Inertial Measurement Unit) mounted on the tractor. As presented in Figure 38 (b), a rotary-type cultivator with a width of 2.2 m (SW220BPX, Sungwoo Industrial Co. Ltd., Republic of Korea) and a paddy drive harrow with a width of 2.4 m and 5.64 m when folding and unfolding wings, respectively (BHB240, Buhueng Agricultural Machinery., Republic of Korea) were attached to the three-point hitch of the tractor. The implement control algorithm (X. Han, Kim, Jeon, & Kim, 2019), which reduced the not-covered or over-covered areas by enabling a three-point hitch to be raised or lowered with appropriate delay times, was implemented in the tracking algorithm.

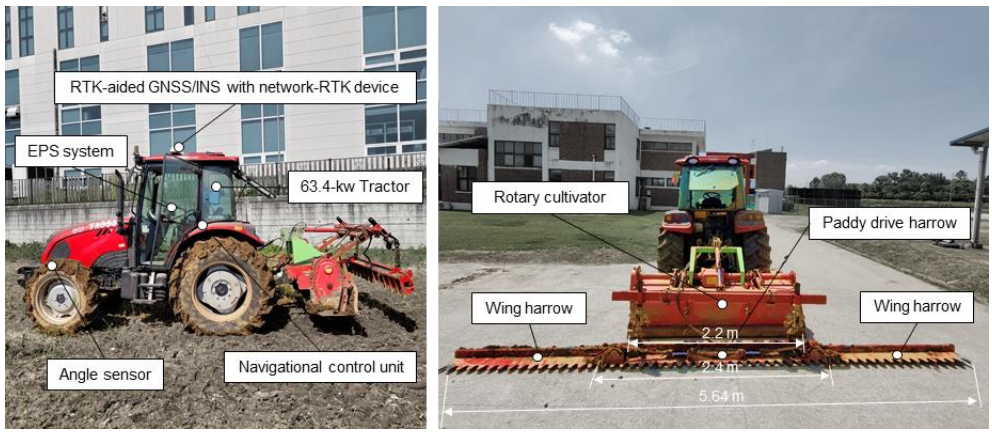

(a) (b)

Figure 38. The puddling and leveling tractor equipped with (a) autonomous navigation components and (b) implements: a rotary cultivator and an attached paddy drive harrow with foldable wings.

A full-scale puddling and leveling experiment for covering the paddy field was conducted by comparing the tracking and leveling performance obtained with two different navigational strategies: autonomous and manual navigation using the same 63.4 kW test planform described in Chapter 3 and the target field with a size of 57.3 m x 55.3 m (Figure 39 (a)), where the entrance for the tractor to enter and exit the field was located at one of the corners of the field boundary. Before the autonomous system and the skilled farmers performed the puddling and leveling operations, the pre-land leveling work for spreading the soil evenly in the high places to adjust the height of the rice paddies evenly was conducted by the same skilled workers to create a similar paddy environment. The autonomous puddling and leveling operations were performed using an RTK-GNSS/INS in an open sky condition after initializing the positioning module to determine and predict its velocity, heading, and position accurately.

To investigate the tracking performance following the path generated by the proposed path planner in this study, the performance was evaluated by comparing

the trajectory, time consumed, traveled distance, fuel consumption of the tractor, and puddling & leveling traffic maps obtained using the autonomous system and the manual operation. In addition, for evaluating the leveling performance of the proposed path planner, the elevation maps generated by Pix4Dmapper Pro software package (Pix4D SA, Lausanne, Switzerland) using megapixel images were acquired using UAV (Mavic 3, DJI., China) after autonomous and manual operations were performed and, were compared. As presented in Figure 39 (b), to effectively increase the absolute accuracy of the map, 9 ground control points (GCP) represented by white circles in Figure 39 (a), were evenly installed and the 3D position data of those were measured using the RTK-GNSS device (TDR-3000, Synerex, Republic of Korea) after all the water was drained from the ground.

(a) (b)

Figure 39 View of (a) the test field and the sub-location of installing the GCPs, and (b) measuring the 3D position data of the GCPs after all the water was drained from the target field.

RESULTS AND DISCUSSION

Simulation studies of puddling and leveling path planner

Figure 40 presents the inner-work path consisting of odd and even-indexed inner-work tracks with two different sequences, i.e., the optimal sequence derived by the GA and the gathering sequence patterns in the full area of the two test fields (rectangular and pentagonal paddy fields in Figure 36 (a) and Figure 36 (b), respectively). The inner-work tracks which were generated in the same direction as the longest segment of the field boundary filled the inner-work area at regular intervals with a difference of the track index ranging from 5 to 11. Even though the processing times for generating the path (T) were increased from 0.01 sec to approximately 30 sec, it is noticeable that the average intervals of the index between consecutive track sequences (n_{avg}) were decreased from 10.5 to 5.4, 5.6, and 5.7 in the pentagonal, trapezoidal, and rectangular fields when using the optimal sequence derived by GA, thereby resulting in decreases in the predicted travel distance and time consumed to perform headland turning maneuver, compared to those obtained with gathering patterns (Table 14). The efficiency of the predicted travel distance (ε_d) and time (ε_t) was increased when using the proposed method to determine the track sequence.

For example, as presented in Figure 36 (a), the reference path generated with optimal and gathering pattern lead the tractor to navigate the 19^{th} indexed track to the 15^{th} and the 9^{th} track respect, which resulted in a 55% increase of the turning distance from 17.6 m to 32.0 m. In addition, as presented in Figure 36 (b), it is apparent that the optimization method could be more effective to increase ε_d and ε_t when applied to the polygonal paddy field, which could cause the turning

maneuver performed at the different segments of the field boundary and increase the travel distance and time because of an arc path at the corner for the tractor to follow the next track.

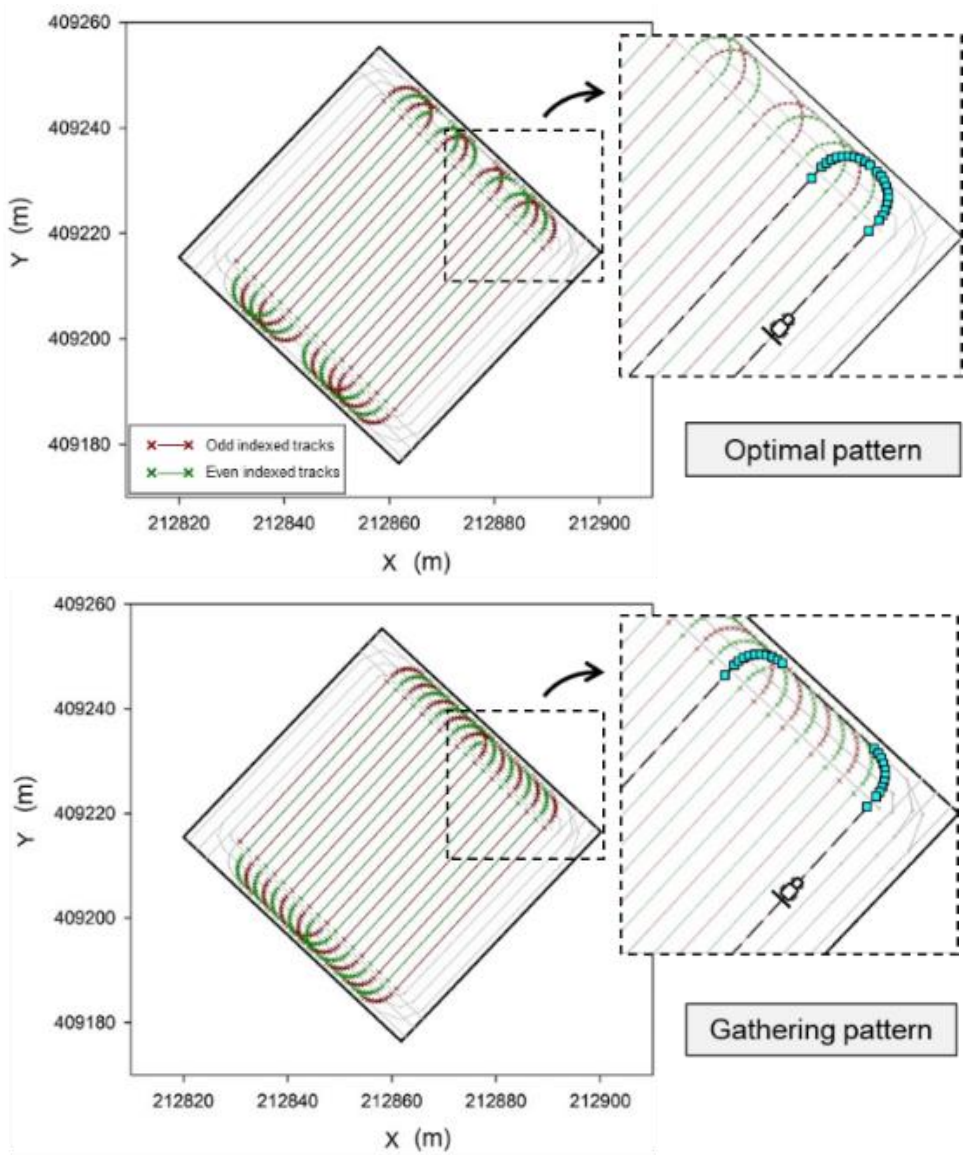

(a)

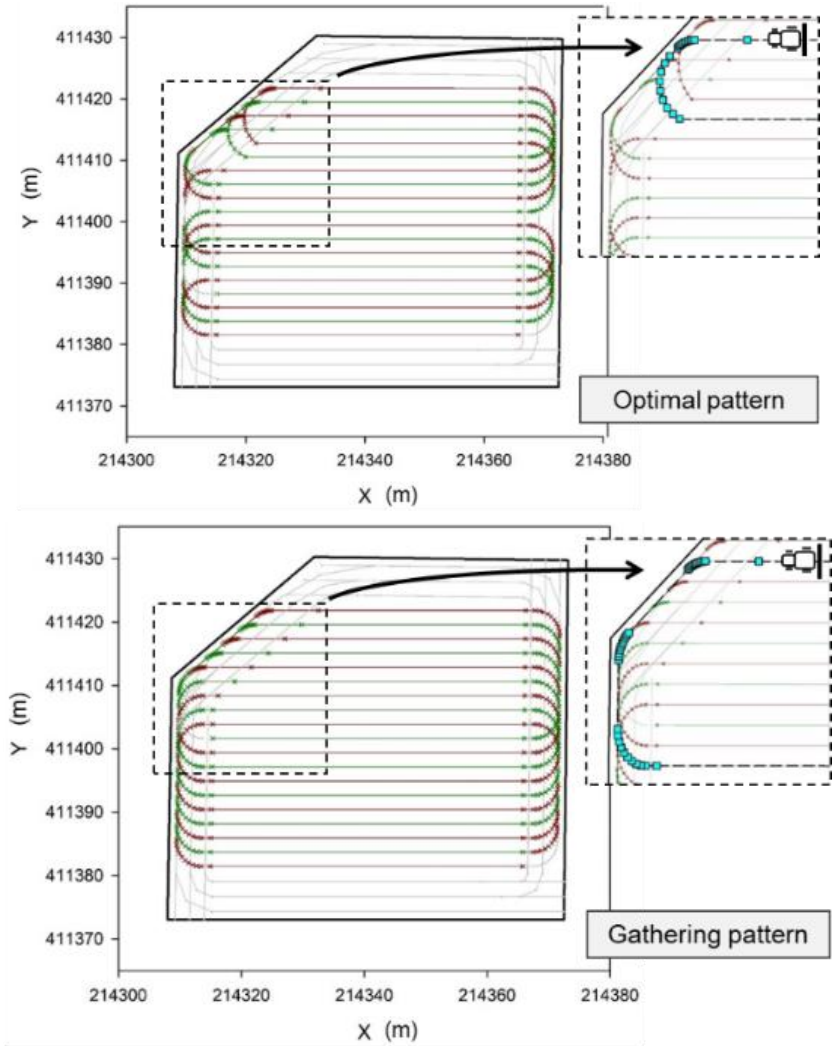

(b)

Figure 40. Comparison of the reference path generated using two different track sequences, i.e., the optimal sequence derived by the GA and the gathering sequence pattern in (a) rectangular and (b) pentagonal paddy fields.

Table 14. Comparison of the operational parameters for the three puddling and leveling paths with optimal and gathering sequence.

Field Shape	Track sequence pattern	Predicted Travel Distance (m)				Predicted Time (s)				n_{avg}	ε_d (%)	ε_t (%)	T (s)
		Inner-work	Headland turning	Outer-work (connection paths)	Total	Inner-work	Headland turning	Outer-work (connection paths)	Total				
Pentagon	Optimal	1199.9	522.0	942.6 (53.2)	2664.5	628.5	833.8	1752.5 (95.8)	3214.9	5.4	70.6	52.7	30.2
	Gathering	1199.9	729.9	928.7 (63.2)	2858.5	628.5	1032.4	1727.5 (113.8)	3388.5	10.5	65.8	50.0	0.01
Trapezoid	Optimal	923.3	402.7	903.8 (36.2)	2229.7	822.2	674.3	1399.2 (65.2)	2895.7	5.6	66.9	46.4	2895.7
	Gathering	923.3	600.2	890.2 (22.6)	2413.7	822.2	887.8	1374.6 (40.7)	3084.6	10.5	61.8	43.5	3084.6
Rectangle	Optimal	661.1	379.7	779.5 (75.1)	1820.3	595.0	586.7	1173.8 (135.18)	2355.5	5.7	64.3	44.7	2355.5
	Gathering	661.1	689.9	779.5 (75.1)	1935.0	595.0	788.1	1173.8 (135.18)	2689.3	10.5	61.8	45.5	2689.3

Puddling and leveling path generation and tracking simulation studies

Figure 41 illustrates the predefined maps of reference paths based on the proposed model so that autonomous puddling and leveling tasks could be performed in the full area of the trapezoidal paddy field with a size of 3451.3 m^2: 19 inner tracks and 3 headland passes on the inside and outside working areas, respectively. The maps were automatically generated using the proposed path planner based on information about the coordinates of the corners of the test field, the swath of the implement, and the minimum turning radius of the tractor. As presented in Figure. 10 (a), the path could lead the autonomous tractor located in a corner of the paddy field to start agricultural tasks along the outmost headland passes (brown circle) and enter the 1^{st} inner-work track (green x mark) via the connection path (blue circle) adaptive to the field shape. After traversing the odd-indexed tracks (e.g. 1, 3, …, 19) with the C-type headland turning pattern to perform churning and pre-leveling on the field, the wing harrows were unfolded and the remaining area was covered by the even-indexed inner-tracks (e.g. 2, 4, …, 18) and two subsequent headland passes.

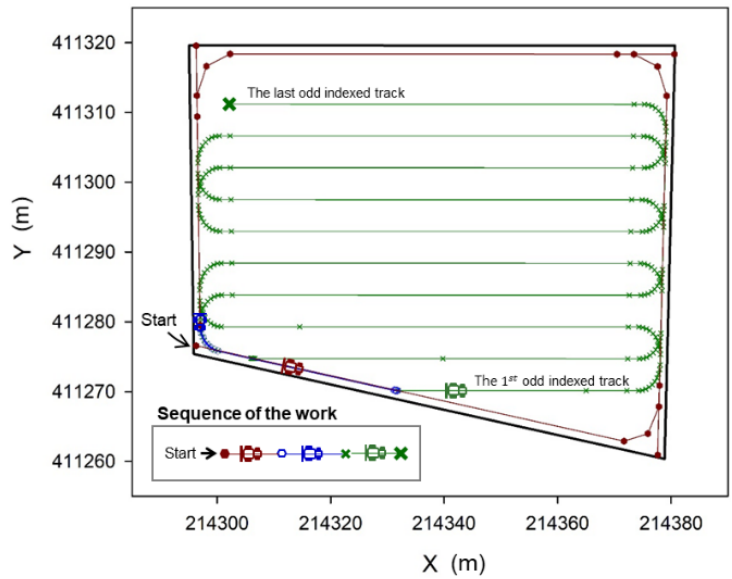

(a)

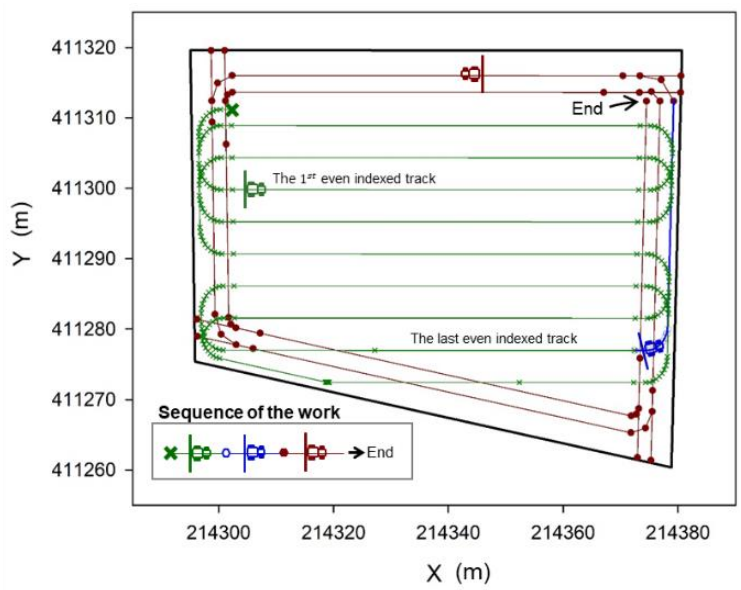

(b)

Figure 41. Views of the operational path in the trapezoidal field shape for autonomous puddling and leveling tractor equipped with a rotary cultivator and an attached paddy drive harrow with (a) folding and (b) unfolding wings.

Figure 42 presents the grid maps of the puddling and leveling traffic intensities measured by counting the number of passes of the implements over a field area during the autonomous pudding and leveling tractor in the simulation test. As

designed by the model, given that the RMESs of lateral deviation and heading error obtained along the working path were 4.3 cm and 1.7 deg, 98.7 % of the arable area was covered with the traffic intensity 1 during the puddling operation (Figure 42 (a)) except boundary corner zones labeled A and overlapping zones of the inner tracks labeled B, indicating that the developed path planner would be effective in covering the whole area with minimum traffic.

Figure 42 (b), Figure 42 (c), and Figure 42 (d) present the traffic maps of leveling processes obtained when the virtual tractor equipped with the paddy drive harrow with foldable wings, navigates the even-indexed inner track (stage 3 in the proposed model), the subsequent headland passes (stage 4), and the final waypoint, respectively. As presented in Figure 42 (b), even though the tractor across most of the arable area is with traffic 1, it was noticeable that the areas chunked in advance were re-leveled by the tractor following the odd-indexed tracks and the traffic intensity, ranging from 1 to 4, and were measured (Figure 42 (d)) due to usage of the unfolded wings. In addition, when the tractor returns to the outer-work area to finish the agricultural task following subsequent headland passes (Figure 42 (c)), the outer-work areas including the headland area damaged by the machine when performing the headland turning maneuver while the implement was raised, were leveled or re-levelled by the paddy drive harrow with foldable wings.

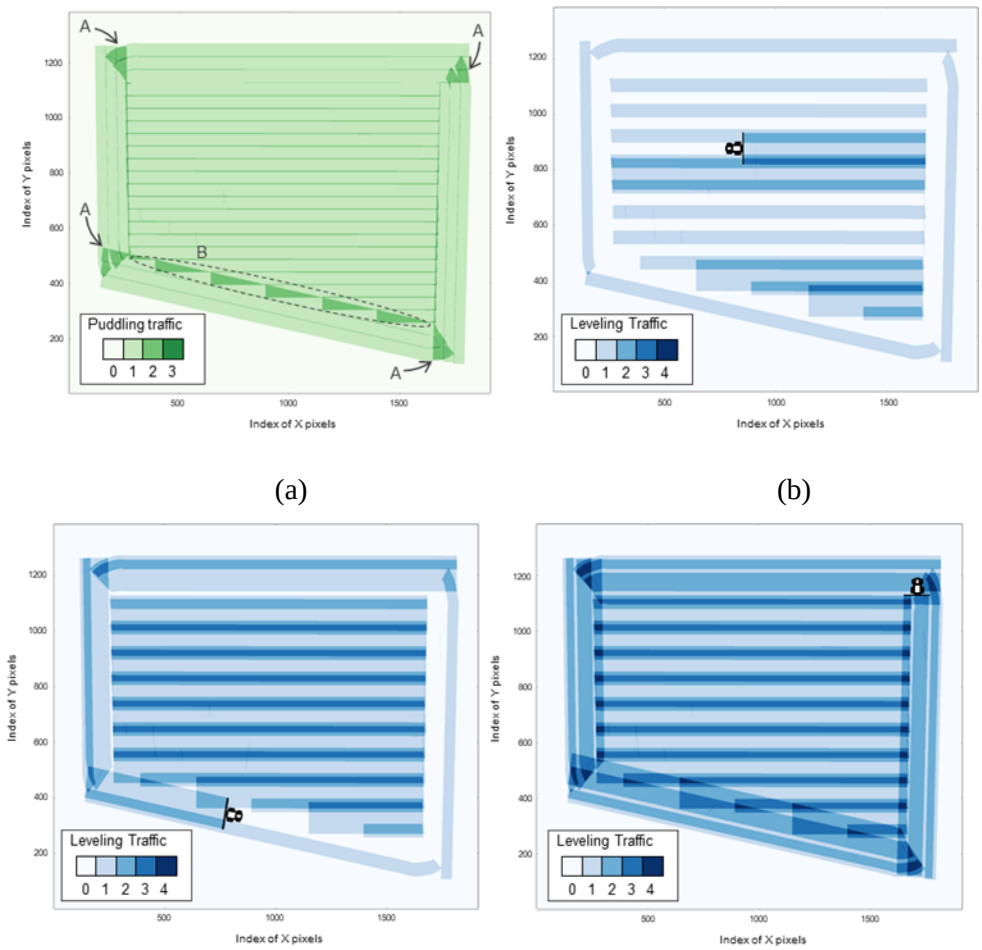

Figure 42. Results of traffic map obtained with the virtual simulation tractor equipped with the puddling and leveling implements after (a) puddling operation and in the three process of leveling operation, navigating (b) the even-indexed inner work tracks, (c) the subsequent headland passes, and (c) the final waypoint.

Field tests of autonomous puddling and leveling operation

Tracking performance of the autonomous puddling and leveling tractor

Figure 43 shows the trajectories of the full-scale tractor performing the puddling and leveling operation in the field test, obtained from the two different tracking methods, i.e., autonomous and manual operations when more than 99.1 % of

position and heading data were obtained in RTK status by using an average of 8.17 satellite signals status (Figure 44). When the autonomous puddling and leveling task was performed in the field test, the complete coverage operation was successfully achieved without any stops or collisions with the field boundary (Figure 43 (a)). Even though the tractor equipped with the paddy drive harrow with unfolded wings covered the wider area, which could cause the larger traction force to the tractor navigating in the wet paddy field, as compared when the wings were folded into 17 (9 odd- and 8 even-indexed tracks) and 12 (4 outmost and 8 subsequent headland passes) straight working paths on the inner- and outer- work area, respectively, and were followed with acceptable path-tracking performance (< overlap length, 15.2 cm): lateral deviation ranging from -11.3 cm to 13.7 cm and a heading error ranging from -2.7 deg to 1.8 deg (Figure 45).

In contrast, a total number of 38 and 16 passes on the inner- and outer- work area, respectively were traversed by the manually driven tractor, thus showing an increased travel distance of 3039.6 m compared to that of 1940.1 m obtained using the autonomous system to cover the whole area (Table 15). As presented in Figure 43 (b), it was notable that the increased travel distance caused an additional trajectory in which multiple puddling and leveling operations could be performed on the same area labeled A. In addition, there was also a section that was expected to occur in the non-work areas labeled B in Figure 43 (b). A cause for the overlapped and skipped zone can be inferred that it is difficult for the driver to identify those areas only using visual information because of the water filled in the paddy field. The autonomous tractor exhibited the performance of covering fields of the same size at a shorter distance, but it was confirmed that it took

approximately 20 more time because it traveled at a slower average velocity (1.35 km/h) than the manual-driven tractor (2.75 km/h) to ensure the stability of the system. However, the fuel consumption, which is closely related to the travel distance and driving velocity, was reduced by 5% when using an autonomous driving system. The results indicated that the speed control algorithm should be improved to increase the time and distance efficiencies of the autonomous puddling and leveling system.

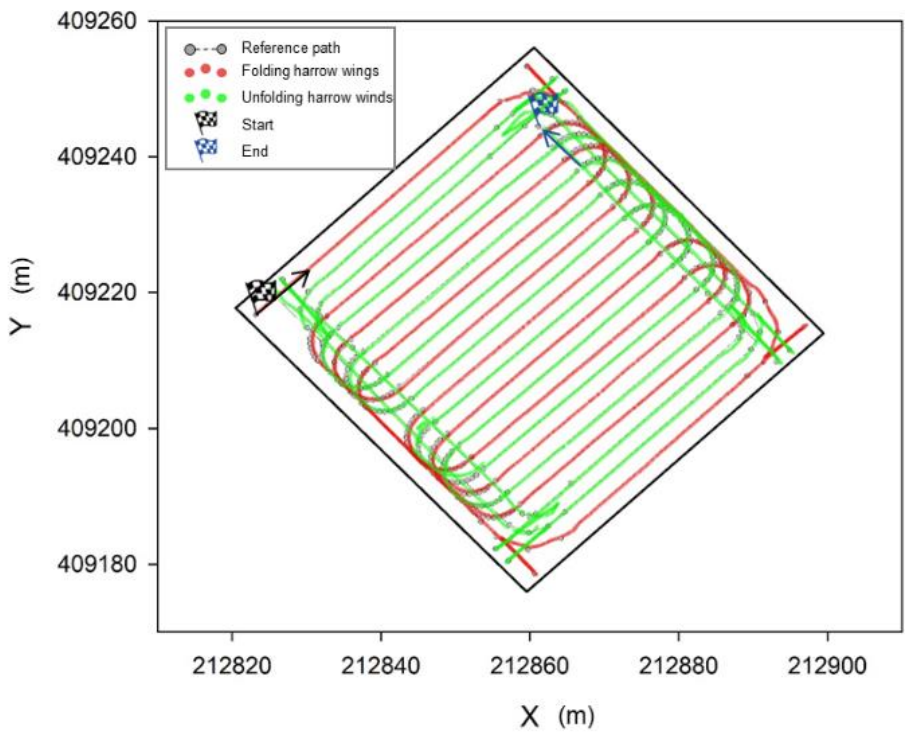

(a)

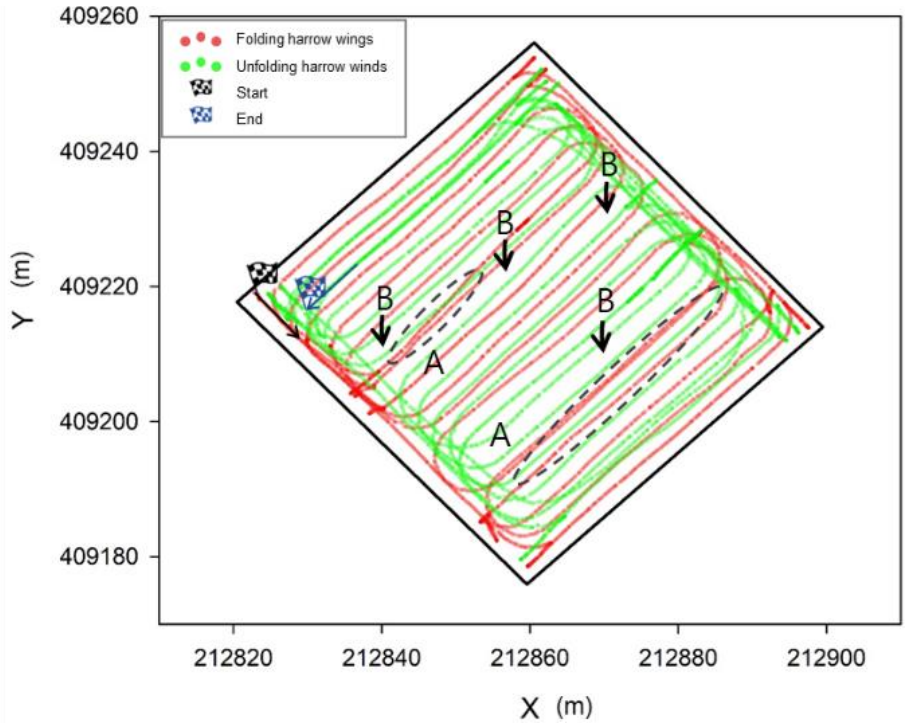

(b)

Figure 43. Trajectories of the full-scale (a) autonomous and (b) manual-driven tractor performing puddling and leveling operation in an arable area of 57.3 m x 55.3 m.

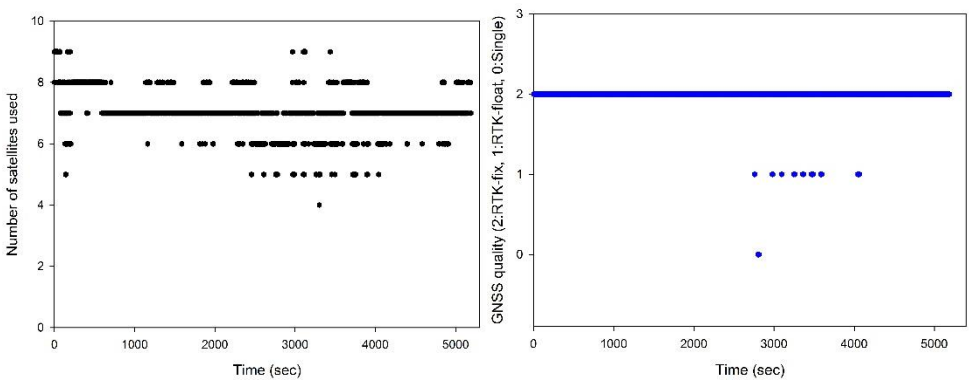

Figure 44. Results of GNSS status obtained when performing the autonomous puddling and leveling operation.

(a) (b)

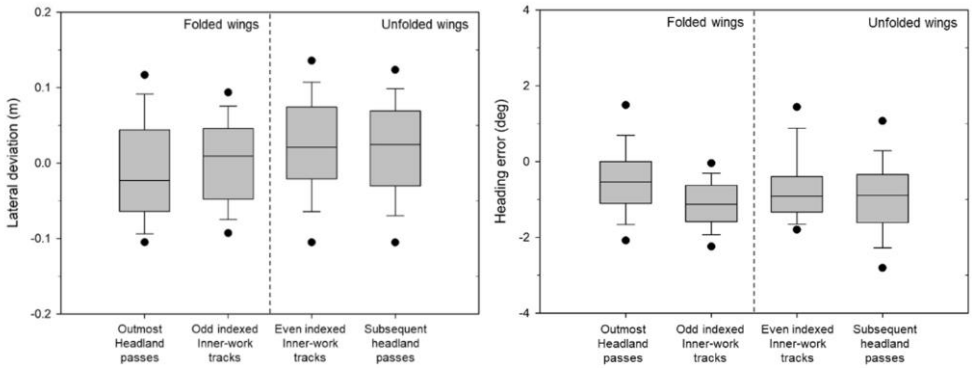

(a) (b)

Figure 45. Results of (a) lateral deviations and (b) heading errors of the autonomous tractor conducting puddling and leveling operation at outmost & subsequent headland passes and odd and even-indexed inner work tracks.

Table 15. Tracking performance of autonomous and manual-driven tractor

	Time consumed (min)	Travel distance (m)	Average velocity (km/h)	Fuel consumption (L)
Autonomous	86.5	1940.1	1.35	16.3
Manual	66.4	3039.6	2.75	17.1

Comparison of covering and leveling performance between autonomous and manual-driven tractor

Figure 46 presents the puddling and leveling traffic maps of autonomous and manual operations measured by applying Bresenham's line algorithm based on the trajectories of the rotary cultivator (puddling) and the leveler (leveling) obtained when each implement performed the agricultural task. Using the traffic intensity map, a coverage rate was measured as the number of grids with more than 1 traffic intensity in total grids inside the field boundary. Overall, complete coverage performance was successfully achieved in both the autonomous and manual

operation with a coverage rate of 97.8 % and 98.0 % in puddling and 99.8 % and 99.9 % in leveling, respectively.

When the manual operation was used to puddle the field (Figure 46 (a)), the uncovered areas (labeled A in Figure 46 (a)) were found in the inner-work area, accounting for 2.0 % of the total area of 3167.3 m^2. As presented in Figure 46 (b), the uncovered area of full-scale autonomous puddling operation (labeled A in Figure 46 (b)), was calculated to be 66.5 m^2, thereby accounting for 2.1% of the total area. A possible cause for the skipped area could be because of a difference in the rounding direction required for the tractor during navigating outer-work path along the outmost and subsequent headland passes, which leads the autonomous tractor to cover the same zone labeled B in Figure 46 (b) and un-puddled zones occurred at the boundary corner area. The uncovered zone of the leveling operation was reduced to 19.3 m^2, compared to that of the puddling operation because those un-puddled zones were leveled by the unfolded wings when the autonomous tractor navigating the subsequent headland passes.

Compared with the traffic map of autonomous operation (Figure 46 (b)), it was apparent that an increase in the total number of 38 and 16 traversal passes performed by a manual-driven tractor on inner- and outer-work area caused an increase in the traffic intensity of puddling and leveling operation in the range from 0-3 to 0-6 and from 0-3 to 0-9, respectively. Especially in the headland turning area, multiple-covered zone with more than 4 traffic intensities, which were bigger than the maximum traffic of autonomous operation, occurred because an implement control strategy that always descends during the navigation was different from autonomous tractor system. In addition, when the human-driven

tractor traversed across the inner-work area, reversing (labeled B in Figure 46 (a)) was conducted to improve the leveling performance and a traffic intensity was increased.

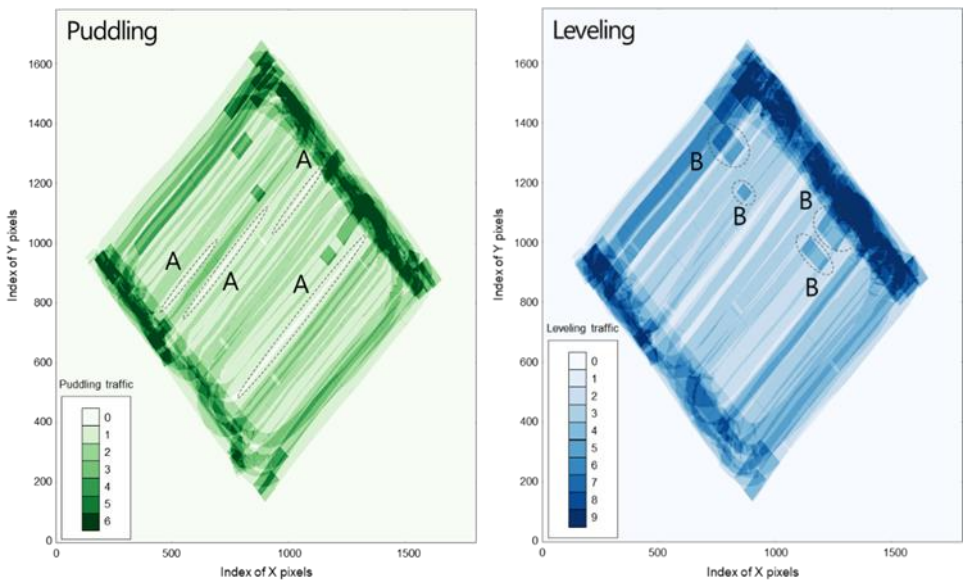

(a) Puddling and leveling traffic map of manual-driven tractor

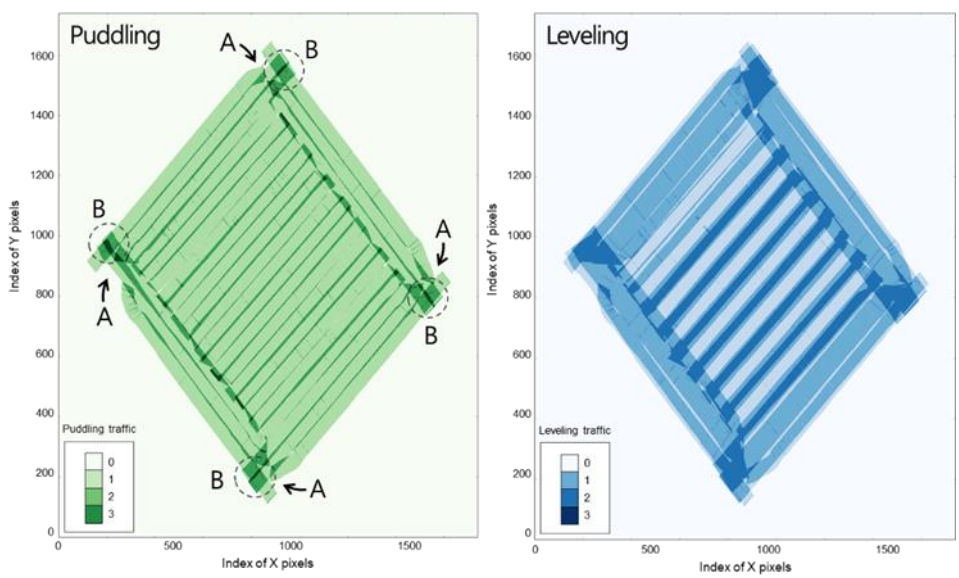

(b) Puddling and leveling traffic map of autonomous tractor

Figure 46. Traffic maps of puddling and leveling operations obtained using the trajectory of the implements attached to (a) the manual-driven and (b) the autonomous tractor.

Figure 47 presents the results for the height maps of the manual-drive and the autonomous tractor using the digital elevation model function in Pix4D on the rectangular paddy field. The relatively high and low altitude value was measured in several places and displayed in blue and red, respectively. Even though it was difficult to determine an exact relationship between the topographic characteristics of the heightmap and the trajectory of the tractor, it was apparent that the trajectory affected the distribution of soil. For example, as presented in Figure 47 (a), when the field was flattened by the autonomous tractor with less than 4 traffic intensities, the height map in the form of a bowl with high corners was generated. In contrast, when the field was covered by the manual-driven tractor with the traffic ranging from 0 to 9, which navigated the full-coverage path including the headland turning while always descending the implements, the height map in the form of an inverted bowl with low corners was generated. The distribution of altitude values exhibited a similar variability ranging from 39.61 m to 39.85 m (autonomous) and from 39.62 m to 39.81 m (manual) with a mean and standard deviation of 39.73 m and 1.89 cm (autonomous) and 39.71 m and 1.81 cm (manual), respectively. Overall, the comparison results of autonomous and manual leveling performance via the height maps indicated the capability of the autonomous tractor equipped with the developed path planner to perform fully automated puddling and leveling operations in an arable field.

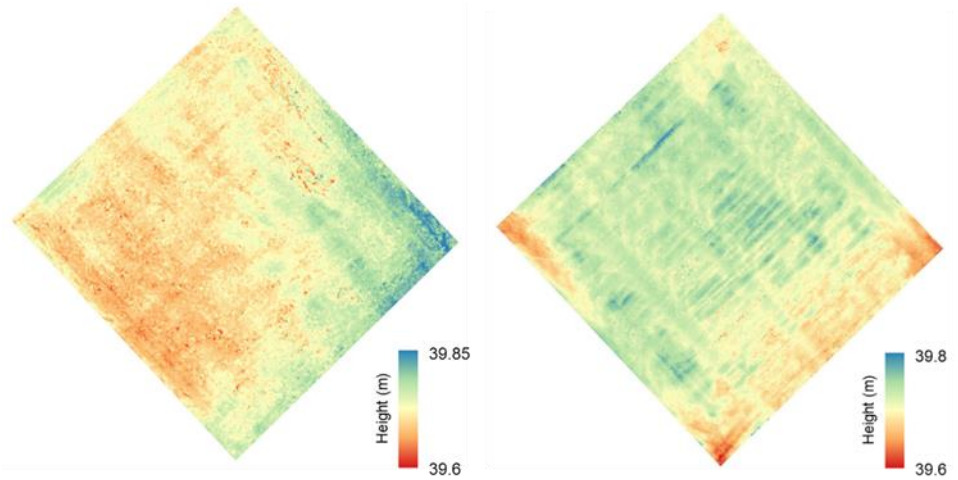

(a) (b)

Figure 47. Height maps of the autonomous (a) and manual-driven (b) puddling and leveling operation based on altitude values measured by applying digital elevation model function in Pix4D in the rectangular paddy field of 57.3 m x 55.3 m.

CONCLUSIONS

In this study, a complete paddy field-CPP with an optimal sequence for an autonomous puddling and leveling tractor were developed by modifying our previously developed path planner (C.-W. Jeon et al., 2021) and its performance was investigated via simulation and field tests. The main contribution of this study was designing the full-CPP based on the proposed model for the autonomous puddling and leveling tractor and validating it by comparing the covering and leveling performance of the autonomous tractor with a skilled worker using the same tractor in the same paddy field where the pre-land leveling work for spreading the soil evenly in the high places, was conducted by the same worker. Its practicality was investigated using a 3D driving tractor simulator developed in our previous studies (X. Han, Kim, Jeon, Moon, et al., 2019; X. Z. Han et al., 2015).

The test platform for the field test was built using a 63-kW tractor equipped with an autonomous system based on a GNSS/INS sensor and a paddy drive harrow with foldable wings attached to a rotary cultivator to puddle and level the field. The following conclusions can be drawn from the tests. Future studies include a validation test in the various paddy fields to investigate the leveling performance of autonomous tractor system. We will also develop an improved path-tracking method by taking into account various velocity conditions to enhance the tracking performance by increasing the time efficiency.

- A puddling and leveling path model consist of four stages, 1) collecting soil from the edge of the field inwardly, 2) chunking and pre-leveling in an inner-work area covered by odd-indexed tracks, 3) puddling and leveling the remaining inner-tracks, while leveling the softened area in the second stage once more, and 4) covering the remaining areas including the headland area damaged by the machine when performing headland turning, were proposed. A geometrical representation applicable to irregular paddy fields was derived based on the proposed model. In addition, to increase the field efficiency, a method that algorithmically determined sequences of field-work tracks to completely cover an arable field with a decreased distance of a headland turning, compared to that obtained when applying the gathering pattern used in our previous study (C.-W. Jeon et al., 2021).

- The results of a simulation study indicated that the designed puddling and leveling path planner could derive a feasible path with an optimal sequence to reduce the predicted travel distance obtained along headland

turning maneuver of 28.5% (pentagon, 4361.3 m^2), 33.9% (trapezoid, 3451.3 m^2), and 45.0% (rectangle, 3167.3 m^2). In tracking and covering performance in one of irregular field (trapezoid), given that the RMESs of lateral deviation and heading error obtained along the working path were 4.3 cm and 1.7 deg, 98.7 % of the arable area was covered with the traffic intensity 1 during the puddling operation. However, because of the use of foldable wing leveler, 99.2 % of the whole field was covered with intensity 2 and 3 when performing the leveling operation.

- In a field test conducted in a rectangular paddy field, the autonomous tractor successfully followed without any stops or collisions with the field boundary (lateral deviation ranging from -11.3 cm to 13.7 cm and heading error ranging from -2.7 deg to 1.8 deg) and performed puddling and leveling operation with an efficiency of 97.8 % and 99.8 %, respectively. Compared to manual operation that navigate the whole area with 38 and 16 passes on the inner- and outer- work areas, The autonomous tractor showed the performance of covering fields of the same size at a shorter distance from 3096.6 to 1940.1 m because of a refined track sequence with 17 and 12 passed on those areas. However, it was confirmed that it took approximately 20 minutes more time because it traveled at a slower average velocity (1.35 km/h) than the manual-driven tractor (2.75 km/h) to ensure stability of the system, but the fuel consumption, which is closely related to travel distance and driving velocity, was reduced by 5% when using an autonomous driving system.

- The results of the height maps of manual-driven and autonomous tractor

measured using digital elevation model function in Pix4D confirmed that the distribution of altitude values showed a similar variability ranging from 39.61 m to 39.85 m (autonomous) and from 39.62 m to 39.81 m (manual) with the mean and standard deviation of 39.73 m & 1.89 cm (autonomous) and 39.71 m and 1.81 cm (manual), respectively. Therefore, the comparison results of autonomous and manual leveling performance via the height maps exhibited the potential of the autonomous tractor for fully automated puddling and leveling operation in an arable field.

CHAPTER 5

ENTRY-EXIT PATH PLANNER FOR AN AUTONOMOUS TRACTOR

ABSTRACT

A field boundary with a single entrance as well as the entry and exit paths of the tractor based on the entrance location are key design requirements that must be considered when planning an effective path for an autonomous tractor operating in a paddy field to avoid collisions with the embankments that hold floodwater. In creating a complete in-field coverage path, an entry-exit path planner that generates paths to/from the start/end points of the auto-traveled path is needed to achieve effective field operations for an autonomous tractor. In this study, a novel path planner for the entry and exit operations of an autonomous tractor was developed using the A* algorithm to enable the tractor located at the entrance to automatically go to the start point of an agricultural task and return to the entrance after completing the agricultural task. An occupancy grid map with virtual obstacles was designed and the A* algorithm was applied to it to create a path for the tractor to reach its destination via the entry-exit path accurately in terms of positioning and heading. Two path-smoothing processes, a line-of-sight path smoother (LOPS) and a collinear-node path smoother (CNS), were performed to reduce redundant turning and control waypoints derived by the A* algorithm. The feasibility of using the developed algorithms was investigated via computer simulations followed by field tests with a 60-kW autonomous tractor. The simulation results confirm that the entry and exit paths generated by the proposed planner effectively guided the

tractor to reach the given target points in terms of location and direction under the various entry, start, and end conditions by reducing the lateral and heading errors compared with those obtained without using the proposed search space and smoothers. For validation testing in two real paddy fields, the entry-exit paths were successfully generated in response to different entrance locations and the tractor followed the entry path and started the operation at the start point of the work path with a lateral deviation of $\leq$ 8.5 cm. In addition, the tractor navigated the exit path automatically and reached the destination with a lateral deviation of < 12 cm and a heading error of < 22° to the entrance and the operator was then able to drive the tractor to exit the field easily without backward navigation.

Keywords: Path planning; A* algorithm; Entry-exit path; Paddy field; Autonomous tractor

INTRODUCTION

The agricultural sector, including the industrial and academic fields (e.g., agronomy, geology, genetics, and engineering), is increasingly facing challenges in terms of farm management related to increasing agricultural production with fewer resources (Tilman et al., 2002). Agricultural routing planning (ARP) is one of the integral tasks of farm management to optimize resource utilization (i.e., water, fuel, and fertilizer) and the time needed to manage farm logistics with less land degradation (Utamima et al., 2019).

Advanced technologies for solving ARP problems by substituting ARP with coverage path planning (CPP) (Galceran & Carreras, 2013) to generate routes that

traverse all waypoints in a region have been widely studied. The CPP approach involves increasing the field efficiency (E_f), which is defined as the ratio of productivity of a machine under field conditions to its theoretical maximum at the full rate (ASAE, 2005). In many cases, solving ARP problems involves minimizing the distances traveled by machines to cover all of the requisite tracks (Bochtis et al., 2009; Bochtis & Vougioukas, 2008; Utamima et al., 2018). This fundamental approach has been modified and extended to fulfill the objectives (e.g., optimization of time, multiple machines, minimization of input costs, among others) (Conesa-Muñoz et al., 2016; Seyyedhasani & Dvorak, 2017; Spekken & de Bruin, 2012), dealing with constraints (e.g., limited machine capacity and multiple fields or obstacles) (Ibrahim A Hameed et al., 2013; Jensen et al., 2015), and saving energy (e.g., reducing fuel consumption) (Hameed, 2013; Rodias et al., 2017).

In general, since a paddy field is commonly segmented by embankments of around 30 cm to hold flood water for supplying nutrients evenly to the rice and a dedicated entrance is built near a farming road so that the agricultural machines does not destroy the field boundary when entering and exiting it, two major conditions, a field boundary and a single entrance, should be considered when attempting ARP for an autonomous tractor system in a paddy field. Therefore, when planning the coverage path for autonomous machines in the paddy field, the planner should propose the operational and entry-exit paths with strategies to avoid collisions with the field borders, even in irregular-shaped fields. Given the above challenges and with the aim of providing in-field path planning methods, many researchers have proposed the coverage path planners for various applications

(Edwards et al., 2017; I. A. Hameed et al., 2013; I. A. Hameed et al., 2010; Han et al., 2013; Jeon et al., 2021; Matsuo et al., 2012; Zhou et al., 2014). In a previous study (Jeon et al., 2021), we developed the complete paddy field coverage path planner and validated the algorithm via field tests in three irregular-shaped fields using an autonomous tillage tractor. However, constructing an in-field coverage path for autonomous agricultural operations is limited because the driver must navigate to the start point of agricultural tasks in the field with a single entrance and return to the entrance manually before and after performing autonomous operations, respectively. Moreover, such a manual traveling between the entrance and the start point can cause fatigue to the driver because it might be difficult to position the tractor accurately at the start point.

The commonly known method to generate the curved path between two arbitrary points was to use the Dubins curve method (Dubins, 1957) that concatenates line segments with circular arcs of minimal turning radius using prescribed initial and terminal tangents to the path and a constraint on the curvature has been. Several researchers have worked to automatically generate the path using the Dubins curve method for ARP applications (Backman et al., 2015; Bochtis et al., 2015; Hameed, 2017; Liu et al., 2018; Sabelhaus et al., 2013; Yu, 2015; Zhang et al., 2020). For example, Backman et al. (2015) proposed a Dubins curve-based approach to provide an automatic headland turning path with a limited steering rate and acceleration profile for non-holonomic agricultural vehicles. Hameed (2017) designed an optimal path planning planner using the Dubins curve method to connect field tracks over the headland area in an optimal sequence for an autonomous robotic lawnmower. Although this method is a useful strategy for

finding the curved path by considering the initial and final states (position, heading) of the vehicle, there is a limitation when generating the path in the paddy field because the field boundary condition was not taken into the algorithm.

As a heuristic search method, the A* algorithm (Hart et al., 1968) has been widely used in pathfinding in various applications, such as mobile robots, unmanned aerial vehicles (UAVs), and unmanned surface vehicles (USVs), because it can be efficiently utilized for finding the optimal path with minimal cost when the search space is fully known without the need for complex equations to account for conditions such as an irregular field shape, randomly determined start and end points for the operational path, and tractor dimensions (Fernandes et al., 2015; Song et al., 2019). However, when employing the A* algorithm only, it may be difficult to ensure that the tractor can reach the target points (i.e., the start and end points) in the entry-exit path. Although the A* algorithm guarantees the shortest path, its ability to generate piecewise-linear paths without considering the direction of the vehicle in each cell (i.e., a non-holonomic constraint) is limited. In previous studies, researchers have modified the A* algorithm to address the heading problem (Dolgov et al., 2010; Li et al., 2014; Sedighi et al., 2019. For example, {Dolgov, 2010 #220). For example, Dolgov et al. (2010) developed a hybrid-state A* search algorithm that uses the state of the vehicle, including its heading information, and has a modified heuristic function for each node to overcome the non-holonomic constraint.

In this study, to enhance the performance of fully automated navigation of the autonomous tractor system developed in previous study (Jeon et al., 2021), an entry-exit planner for an autonomous tractor operating in a paddy field was

developed using the A* algorithm to design a reasonable solution capable of decision-making based on the kinematic characteristics of the tractor and field conditions, considering the location of the entrance, an irregular field shape, and a dynamically determined operational path. For handling the non-holonomic constraints on the tractor, a method for generating a search space with virtual obstacles to induce the A* algorithm to determine a curved path was proposed to enable the autonomous tractor to reach the destination accurately in terms of both position and heading.

The specific objectives of this work were

- 1) to develop an entry-exit path planning algorithm that enables the tractor located at the entrance to automatically go to the start point of an operational path and return to the entrance after completing agricultural tasks
- 2) to investigate the feasibility of the developed path planner by analyzing its tracking performance via simulations
- 3) to validate the entry-exit path planner in two real paddy fields.

MATERIALS AND METHODS

Design of entry and exit path

For guiding the autonomous tractor in a paddy field to cover the entire area systematically, a complete navigation pattern is generated within the field border to enable the tractor to go to the start point of the operational path, perform the agricultural task, and return to the entrance. The pattern for the entry-exit path

planning can be described using a set of waypoints representing the path from the entrance to the start point and the exit route from the end point to the entrance, as shown in Figure 48. The approach provides entry and exit paths using the field boundary, the entrance position, the locations of the start and end points of the in-field coverage path, and the mechanical characteristics of the tractor (such as the minimum turning radius, implement width, and look-ahead distance for path-tracking). In this study, the basic idea for generating the entry-exit path was to reach the destination of the autonomous tractor accurately in terms of both the position and heading by taking into account the limitations due to the non-holonomic constraint of the tractor.

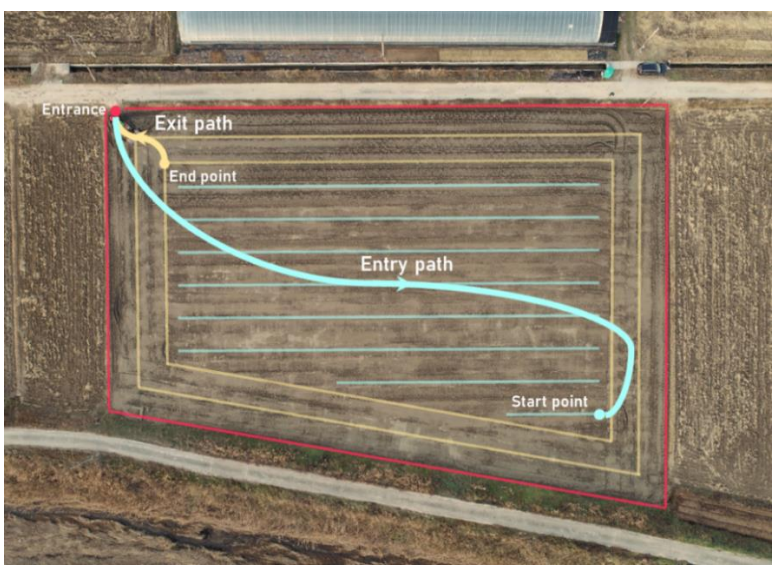

Figure 48. Examples of entry and exit paths generated for an in-field coverage path in a paddy field.

The developed approach includes three stages (Figure 49). In the first stage, the search space is defined as a collection of nodes that can be used to find the shortest path from the start node to the goal node using the A* algorithm. These were obtained by moving inward with the field boundary coordinates imported from a

text file. Points specified as Transverse Mercator (TM) coordinates, which are widely used in national and international mapping systems around the world, were then translated into grid coordinates to build a 2D grid map of the search space. In the second stage, the entrance, start point, and end point were used as the start and goal nodes in each space to create the entry and exit search spaces. To control the position and heading of the autonomous tractor, U-shaped virtual obstacles were geometrically designed based on information about the turning radius of the tractor and look-ahead distance and were then located at the start and end nodes generated using the information for the start and end points of the in-field coverage path. In the third stage, the A* algorithm was applied to the entry and exit search spaces to generate the entry-exit path. After creating the paths for a sequence of line segments connected by nodes with sharp turns, two path smoothers, namely the line-of-sight path smoother (LOPS) and the collinear-node smoother (CNS), were applied to improve the continuity and efficiency of the path. By changing the coordinate system from a grid to TM, the smoothed path was imposed on the waypoint data in Route Data Definition File (RDDF) form that included the latitude and longitude coordinates, the limit of the boundary offset (LBO), target travel velocities, and implement up/down commands. This file contains the input reference path and control strategies for the tracking method. In principle, the tractor searches for the next waypoint when it reaches the current waypoint within

the offset distance, which is predefined in terms of the LBO (Han et al., 2015).

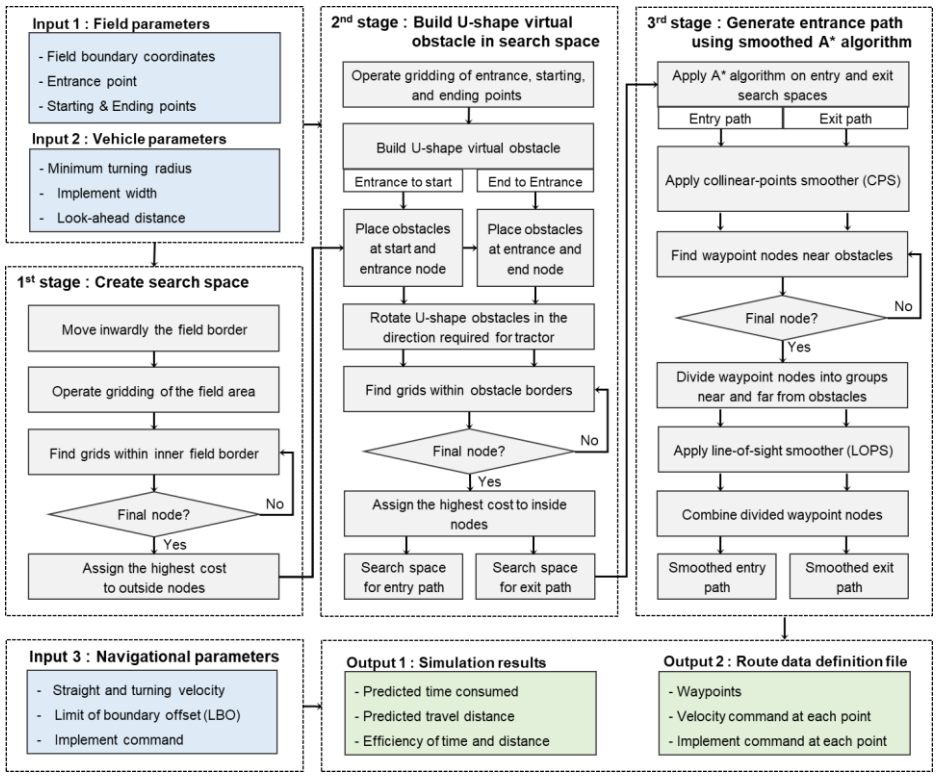

Figure 49. A flowchart of the entry-exit path planning approach.

Representation of the search space with U-shaped virtual obstacles

Coordinate transformation of the search space

As shown in Figure 50, to avoid generating a path where the autonomous tractor route and field border are likely to collide, the search space was set by moving the field boundary inward by half of the implement width except for one side of the field boundary where the entry point was located to generate the collision boundary. The vertices of the collision boundary (determined from GPS data) were converted from Earth coordinates (latitude and longitude) to grid coordinates to generate a search space. The approach for coordinate transformation is based on

the minimum bounding box (MBB) method (I. A. Hameed et al., 2010; O'Rourke, 1985), which refers to the rectangle of the minimum area enclosing the vertices of the field boundary to concisely express a complex shape. Gridding was then performed on the bounding rectangle oriented in the same direction as the eastward axis of the TM coordinate system represented with a north-eastern vertex. By defining the width (w) and height (h) of the MBB, as well as the square-grid size (r), the vertices of the search space boundary and entrance, start, and end points were projected onto the nearest grid using eq. 4.1:

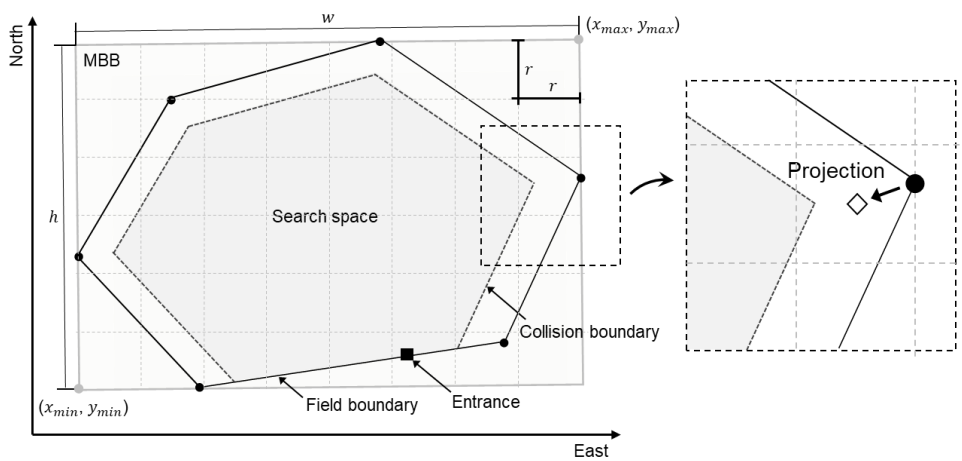

Figure 50. Search space generation

$$\begin{bmatrix} x_{grid} \\ y_{grid} \end{bmatrix} = \begin{bmatrix} \lceil w(x - x_{min})/r(x_{max} - x_{min}) \rceil \\ \lceil h(y - y_{min})/r(y_{max} - y_{min}) \rceil \end{bmatrix}, \quad (4.1)$$

where x_{grid} and y_{grid} are the spatial indexes of the latitude and longitude values in the grid map, respectively; x and y are the latitude and longitude in the TM coordinate system, respectively; x_{min} and y_{min} are the minimum values of the latitude and longitude in the Earth coordinate system, respectively; and x_{max} and y_{max} are the maximum latitude and longitude in the Earth coordinate system, respectively.

The nodes in the MBB are recursively examined to identify those that can be used to generate the entry-exit path depending on whether they are inside or outside the search space. Nodes outside the space incur the highest cost, while the others are indexed as the grid map of the search space.

Generation of U-shaped virtual obstacles

To provide a curved path from the start point with an initial state (position, heading) to the goal point with a final state using prescribed initial and terminal tangents to the path and considering the kinematic limitation of the tractor, virtual obstacles (dark gray grids) were designed based on the minimum turning radius of the tractor (R), the look-ahead distance ($l_{look-ahead}$), and the grid size (r), as shown in Figure 51 (a). To derive the A* algorithm for generating the entry-exit path for the autonomous tractor to arrive at the goal node or start from the node without sharp turns, the arc points were arranged in a U-shape in which the points were arranged at 45° intervals with minimum turning radii. By adding straight lines of the look-ahead length between the arc and goal node, the U-shaped obstacle provided the space for generating the buffer track so that the tractor could align its direction and position for the next pass. The parts of the nodes contained within the obstacle boundary were transformed at the nearest nodes using the aforementioned method to find the search space. In addition, the turning zone nodes (light gray grids in Figure 51 (a)) were created as grids adjacent to the boundary of the obstacle to guide the autonomous tractor at its turning speed.

The U-shaped virtual obstacles were located at the start and goal nodes of the entry and exit search spaces (Figure 51 (b) and Figure 51 (c)), while the direction

was determined based on whether the departure and arrival angles were at the start or goal, respectively. When an obstacle is placed on the goal node, the direction of the entrance along the buffer track is consistent with the direction that the tractor will traverse, while the opposite is true for an obstacle placed at the start node. For example, when generating the path from the entrance (start) to the goal node in the entry search space, the direction from the entry node is opposite to the heading of the tractor leaving the field, which is perpendicular to the segment of the field boundary where the entrance is located.

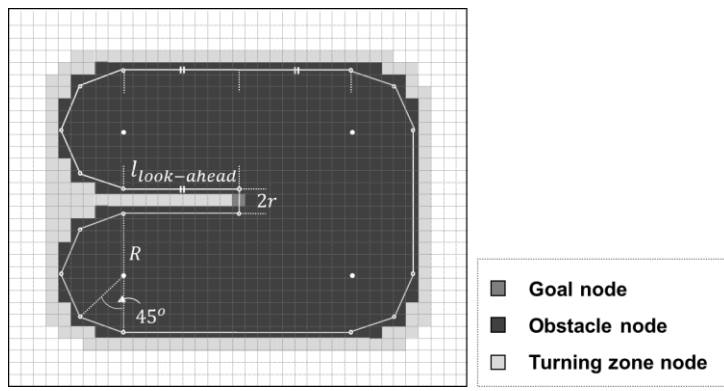

(a)

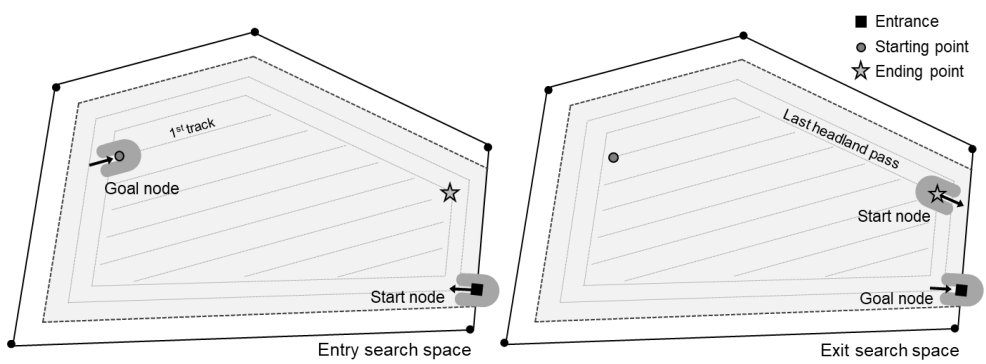

(b) (c)

Figure 51. An example of a U-shaped virtual obstacle placed on (a) the grid map, (b) the entry search space, and (c) the exit search space.

The A* algorithm with a path smoother

Implementation of the A algorithm for the search space*

The A* algorithm (Chabini & Lan, 2002) was implemented for the search space to find the shortest path. In principle, the algorithm examines the costs of the neighboring nodes around the node n as follows (eq. 4.2):

$$f(n) = g(n) + h(n) + o(n), \quad (4.2)$$

where, $f(n)$ is the total cost of the path, $g(n)$ is the cost of the path from the start node to the node *n*, $h(n)$ is the heuristic cost to move from that given node *n* to the goal node, and $o(n)$ is the obstacle cost imposed on each node by the virtual U-shaped obstacle when generating the search space.

The obstacle cost for node n (i.e., $o(n)$) was simply added to the conventional terms consisting of the exact distance cost calculated from the start node to node *n* ($g(n)$) and the heuristic distance cost estimated from the goal node to node *n* ($h(n)$), as shown in Figure 52. Hence, when the cost of an adjacent node (including the node of a virtual U-shaped obstacle) was relatively high, it was excluded from being used to update the next node (Figure 52 (b)). After selecting new current node *n* that has the lowest $f(n)$, both the exact and heuristic distance costs were computed based on the diagonal distance for allowable horizontal, vertical, and diagonal movements until the goal of identifying the next candidate nodes was achieved (Figure 52 (c)). The costs of the neighboring nodes were assigned according to the direction: horizontal and vertical nodes with a cost of 10 and diagonal nodes with a cost of 14, which are roughly proportional to the exact

distance (Figure 52 (a)). The optimal path consisting of a sequence of path-nodes (a sequence at the center of the nodes) was determined as the lowest-cost path by comparing the sum of costs including the obstacle cost among the multiple candidate nodes with the same cost (the squares in Figure 52 (c)). Subsequently, the curved path along the virtual obstacle was derived automatically, as shown in Figure 52 (d).

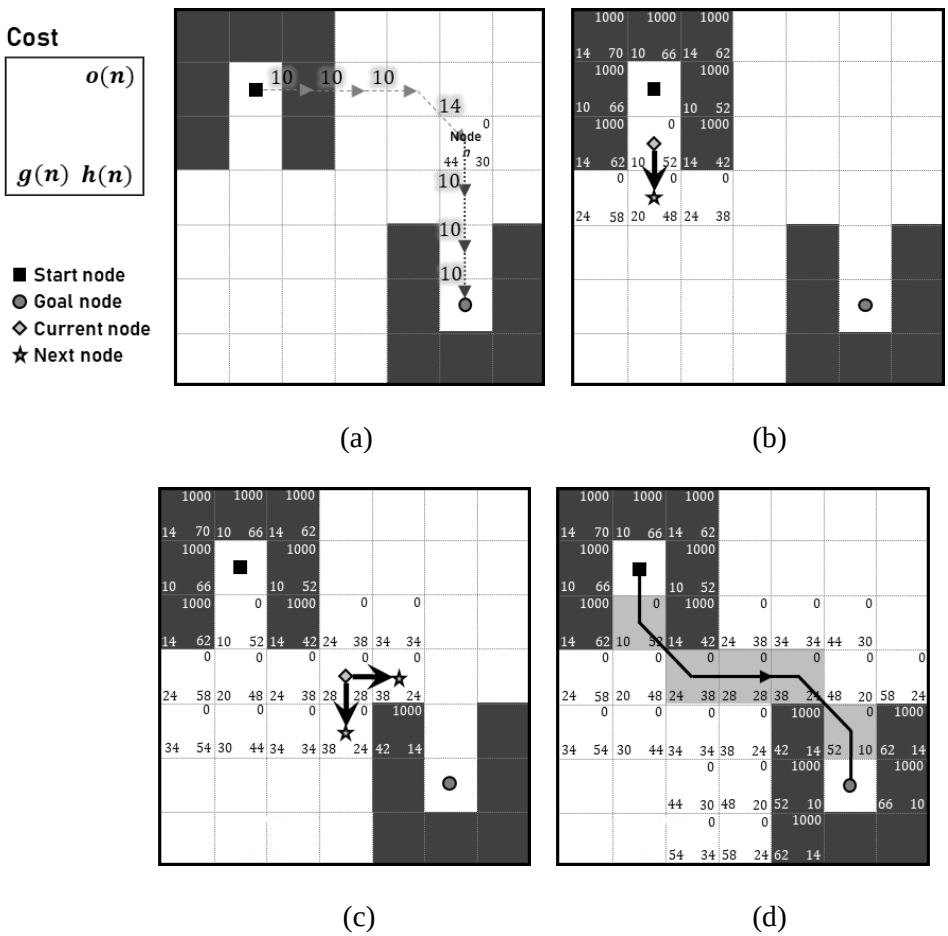

Figure 52. An example of the implementation of the A* algorithm (a) to represent how to calculate the cost, (b) to update the node *n*, (c) to calculate the cost of each grid, and (d) to determine the optimal path.

The path-smoothing approach

In principle, the entry-exit path provided by the A* algorithm consists of several short line segments that connect a series of adjacent nodes (Figure 52 (d)) that the autonomous tractor can follow. Even though the theoretical distance of the path can be minimized based on the connections between the closest possible grids, this can cause 1) frequent turning and 2) redundant nodes along the same straight segment, thereby degrading the path-tracking performance with redundant control points (Song et al., 2019). To compensate for the limitations of the A* algorithm, two path-smoothing approaches, LOPS and CNS (Koyuncu & Inalhan, 2008), were designed and implemented on the entry-exit path because of their ability to refine the turning and collinear waypoints, respectively.

Figure 53 shows the procedure of applying the two path smoothers on the trajectory provided by the A* algorithm. The nodes obtained with the A* algorithm in the search space were divided into two groups depending on whether the nodes were within the turning zone or not. The LOPS was then applied to reduce the number of turning maneuvers on the path by comparing two distances: from point A to point C ($d(A,C)$) and from point A to point B to point C ($d(A,B,C)$) calculated using three consecutive path-node groups and eliminating node B when $d(A,C) \leq d(A,B,C)$ until node C is the final path-node (Figure 54 (a) and Figure 54 (b)). In addition, CNS was additionally applied to a combined node-set consisting of smoothed nodes generated using LOPS and nodes located inside the

turning zone (Figure 53) by checking if the consecutive three nodes were collinear by the calculating slopes (Figure 54 (b) and Figure 54 (c)).

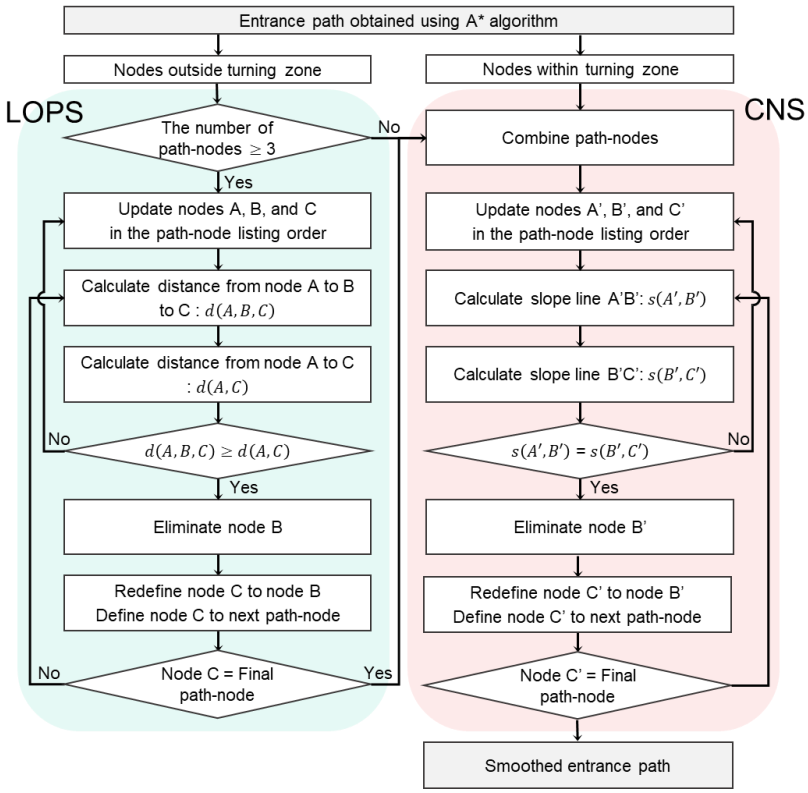

Figure 53. A flowchart of the path-smoothing approach with the two path smoothers, LOPS and CNS.

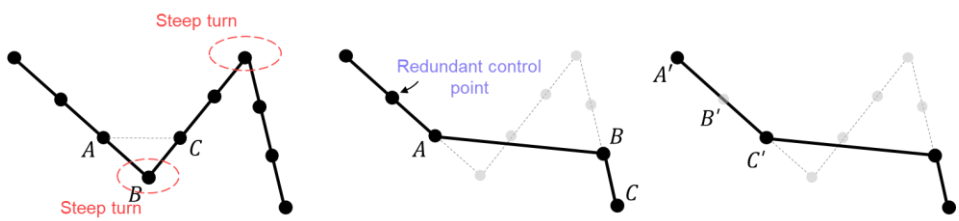

(a) (b) (c)

Figure 54. An example of the path-smoothing process: (a) the original path and the paths (b) after applying LOPS and (c) LOPS with CNS.

Simulation studies of the effects of U-shaped virtual obstacles and path-smoothing

Prior to field testing, two simulation studies were conducted to investigate the effects of using the search space with the U-shaped virtual obstacles and the smoothing methods to generate an entry-exit path in an irregular paddy field. For the entry and exit search spaces as a case study, the start point was located 15 m horizontally and 10 m vertically, and the end was placed 20 m horizontally and 15 m vertically from the entry point placed in one of the segments of the pentagonal field boundary (Figure 55 (a)) to generate the entry and exit paths, respectively. In the first test, the feasibility of using the search space with the U-shaped virtual obstacles to derive the entry-exit paths within the field boundary and control the position and direction of the autonomous tractor at start and goal points was investigated. To do this, the exit paths were generated from the end to the entrance under various conditions of the start-goal directional difference angles (SGDDAs) defined as the included angle measured counter-clockwise from the departure vector at the start point to the arrival vector at the goal node (Figure 55 (b)). In addition, for evaluating the tracking performance, we assumed that the virtual tractor developed in previous studies (Han et al., 2015; Han, Kim, Jeon, & Kim, 2019a) (Figure 56) followed those paths (from the entrance to the start point) generated with and without U-shaped obstacles at 8 different SGDDA levels from 0° to 315° at 45° intervals.

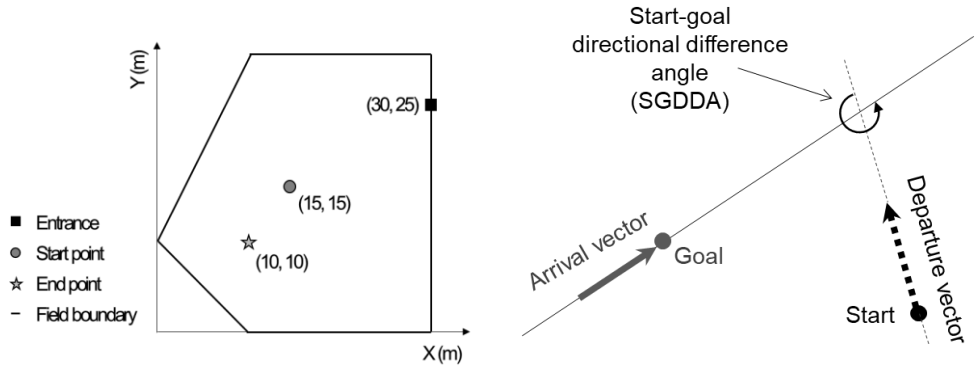

(a) (b)

Figure 55. Setup for the simulation test: (a) the search space environment and (b) the arrival/departure vectors and the SGGDA.

In the second test, to sequentially verify the effectiveness of using the path-smoothing approaches (LOPS and CNS), three entry paths (original, LOPS-smoothed and LOPS with CNS-smoothed paths) combined with the 10 m straight path at the last waypoint of the path (Figure 56 (a)), which represents the first working track, were generated at an SGDDA of 90°, and to compare the trajectories, the virtual tractor followed these paths.

To investigate the tracking performance following the exit paths generated by the proposed algorithm in this study, the performance was evaluated by measuring the maximum and root-mean-squared error (RMSE) values for the lateral deviation when the tractor followed the straight path of 10 m after arriving at the start point in the entry path (Figure 56 (a)) and calculating the distance (l_{exit}) from an end point where the tractor finished the operation to the entrance. In addition, the difference (θ_{exit}) between the heading angle of the tractor at the end point and the direction required for the tractor to exit the field was measured to determine whether the tractor could easily exit the field via a single steering operation in the exit path (Figure 56 (b)). Consistent with the velocity strategy shown in a previous

study for navigating straight working lines and headland turns (Han, Kim, Jeon, Moon, et al., 2019), the travel velocities to follow the waypoints inside and outside the turning zone were set to 1 and 4 km/h, respectively. To generate the paths, the algorithm programmed in Labview 2015 was run on an i7-5500U CPU in a 2.4-GHz Intel Centrino Mobile Workstation with 8 GB RAM.

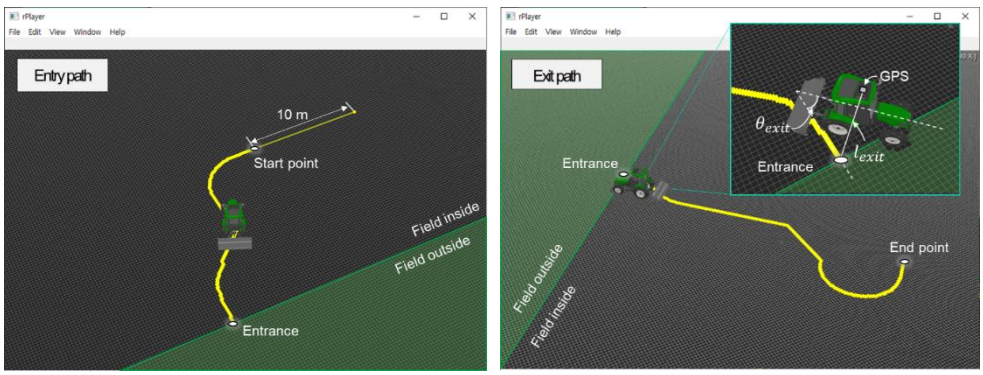

(a) (b)

Figure 56. A schematic of the 3D virtual tractor following (a) the entry path and (b) the exit path generated by using the entry-exit path planner and the evaluation criteria for each path.

Field testing of entry-exit path planner

Consistent with the Chapter 3, The platform for the field tests was built using a 63-kW tractor (TX853, Tongyang Moolsan Co., Seoul, Korea) equipped with a global positioning system/ inertial navigation system (GPS/INS) as the rover. Differential correction data provided by a network-RTK device (MRD-1000T, SYNEREX., Republic of Korea) based on the long-term evolution (LTE) wireless network, were then transmitted to the rover via networked transport of Radio Technical Commission for Maritime Services (RTCM) using Internet protocol (NTRIP) to achieve 2 cm positioning and to observe the heading angle within ±0.1o accuracy during 60 s outage at a sampling frequency of 20 Hz.

To validate whether the autonomous tractor would follow the entry-exit path at an acceptable level with the maximum lateral deviation < overlap length (defined as 10 cm in this study), a field test was conducted by applying the algorithm to two rectangular-shaped paddy fields with different entrance locations: the center and corner of the short segment of the field boundary, as shown in Figure 57. The operational path except for the entry-exit path for providing the start and end points was generated using a program developed in a previous study (Han, Kim, Jeon, Moon, et al., 2019) based on the coordinates of the corners of the target field, the width of the implement, and the minimum turning radius of the tractor. The entry point was defined as the first acquired point after the tractor had entered the field boundary. The first tracks connected to the start point and the last headland pass connected to the end point were also provided in both fields to give the entry-exit path planner the arrival and departure headings when generating the entry and exit paths, respectively. The travel velocities to follow the waypoints inside and outside the turning zone were set to 1 and 4 km/h, respectively. Consistent with the method for evaluating the performance in the simulation test, the lateral deviation obtained by the tractor navigating while operating the implement along the first track after following the entry path, and the values of l_{exit} and θ_{exit} were measured. In addition, to validate the feasibility of the exit path, the trajectories of the tractor were also obtained when leaving the field by manual operation through the entrance.

Figure 57. Google map and the field test images showing the two target fields and entrance locations in Chungnam, South Korea.

RESULTS AND DISCUSSION

The entry-exit path generation and tracking simulation with and without the U-shaped obstacles

Figure 58 and Figure 59 show the results of the entry and exit paths generated using the A* algorithm in the search spaces with and without the U-shaped obstacles. Because of the MBB and the representation of the search space, an entire rectangular grid map enclosing the field boundary was built and divided into three areas: outside the field boundary space (dark gray), the search space (white), and the collision space (gray) between the field and the collision boundaries. A high cost was imposed on the grids outside the field boundary to prevent the A* algorithm from generating paths that invade or cross over it. In addition, it was apparent that the method of allocating a high cost to the grid outside of the field

boundary and the collision area allowed the A* algorithm to generate the path within the search space in an irregular paddy field.

When generating the paths in the search space without U-shape obstacle, even though the entry and exit paths (black) were successfully generated in the search space from the entrance to the start point in Figure 58 (a) and the end point to the entrance in Figure 59 (a), the algorithm calculated the shortest path consisting of straight segments only to connect the points without considering the arrival and departure heading angles of the tractor. For example, as shown in Figure 59 (a), the exit path required the tractor located at the end point to rotate in place to be able to follow the reference and return to the entrance because there was a difference in the initial angle between the ideal attitude of the tractor and the reference. In addition, even after the tractor had accurately navigated the exit path and reached the entrance, there was a difference between the direction to exit the field and the direction to follow the path that caused the tractor to rotate in place or move backward to realign its direction.

Figure 58 (b) and Figure 59 (b) show the entry and exit search spaces with the U-shaped obstacles automatically placed at SGDDAs of 90° and 135°, respectively, and the paths generated under each condition. Compared to the results obtained in the spaces without the virtual obstacle shown in Figure 58 (a) and Figure 59 (a), the paths were generated with controlled arrival and departure heading angles due to following the curvature of the U-shaped obstacles. A buffer track, which was the straight lines of the look-ahead length between the arc created by the U-shaped obstacle and the start, end, and entrance points was provided when leaving and

approaching the points to enable the tractor to align its direction and position to follow the path more precisely.

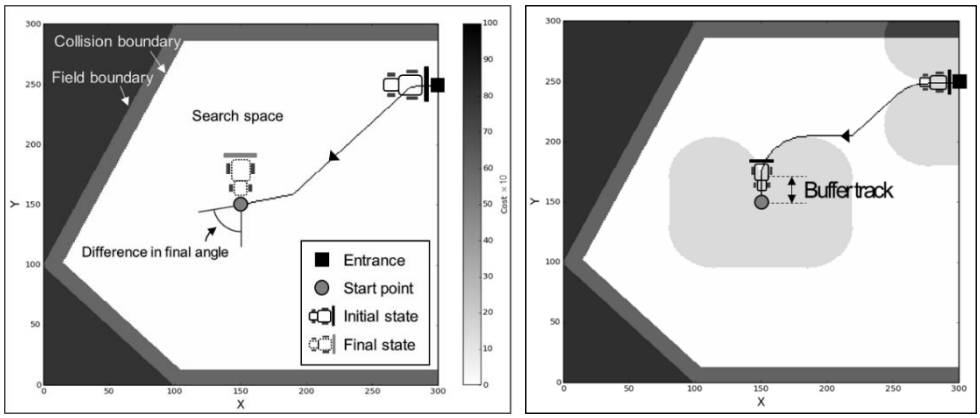

(a) (b)

Figure 58. Entry path and search space generation (a) without and (b) with U-shaped obstacles for an SGDDA of 90°.

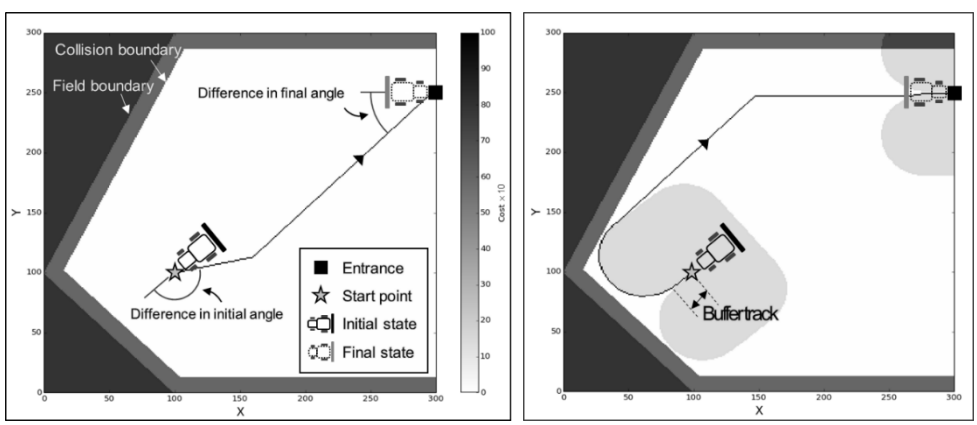

(a) (b)

Figure 59. Exit path and search space generation (a) without and (b) with U-shaped obstacles for an SGDDA of 135°.

Figure 60 shows the simulated trajectories of the tractor following the exit paths generated in the previous path generation test (Figure 59) to investigate the effect of the U-shaped obstacles on tracking performance. Overall, given that the trajectory points were acquired within the collision boundary, all waypoints on the

path were navigated by the tractor without any collisions with the field boundary. However, when the exit path generated in the search space without the U-shaped obstacles was used, overshooting on the trajectory was noted after starting at the end point while performing a turning maneuver deviated from the generated path in the opposite direction, which caused a significant error due to oscillations. In contrast, when using the proposed search space with U-shaped obstacles, the performance of the exit path following was improved while the oscillations were almost diminished, thereby reaching the entrance location with an acceptable level of heading angle. As a result, when using the U-shaped obstacles in the generation of the exit path, the tractor showed superior tracking performance with l_{exit} and θ_{exit} of 6.2 cm and 0.6° as compared with those obtained without the U-shaped obstacles 63.2 cm and 40.1°, respectively. This indicates that the exit path induced by the search space with the U-shape obstacles would be effective in improving the path-tracking performance of the tractor to reach the entrance, such that the operator would more easily drive the tractor to exit the field.

.

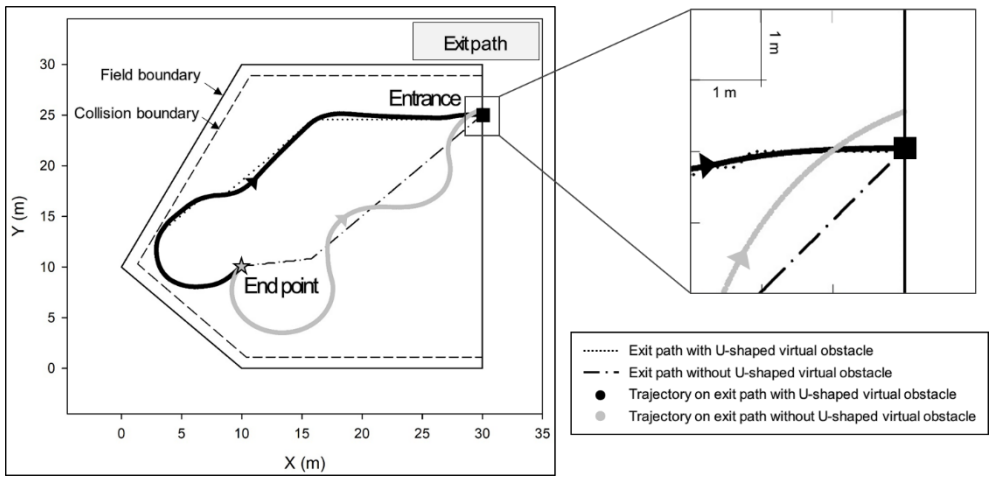

Figure 60. Trajectories of the tractor simulator following exit paths generated with and without U-shaped obstacles for an SGDDA of 135°.

Figure 61 shows a comparison of l_{exit} and θ_{exit} measured when the tractor reached the entrance with and without U-shaped obstacles under varying SGDDA conditions. It is apparent that the curved path induced by the U-shaped obstacle affected the tracking performance of the tractor in the simulation study. In addition, as shown in Figure 61 (a), when the SGDDAs were 135°, 180°, and 225°, which required the tractor to rotate in place at a larger angle, the values of l_{exit} obtained within the search spaces with U-shape obstacles were considerably reduced as compared with those obtained without the obstacles (Figure 60) because an SGDDAs $\geq$135° might cause an overshoot on its trajectory. Moreover, as shown in Figure 61 (b), using the U-shaped obstacle was effective in improving the values of θ_{exit}, which is an indicator of describing how well the direction of the tractor is aligned by reducing almost 40° to 2°. This implies that using the U-shaped obstacles when building the search space to generate the entry-exit path guides the

tractor accurately in terms of both the position and heading with the consideration of the tractor's steering limitation (i.e., a non-holonomic constraint).

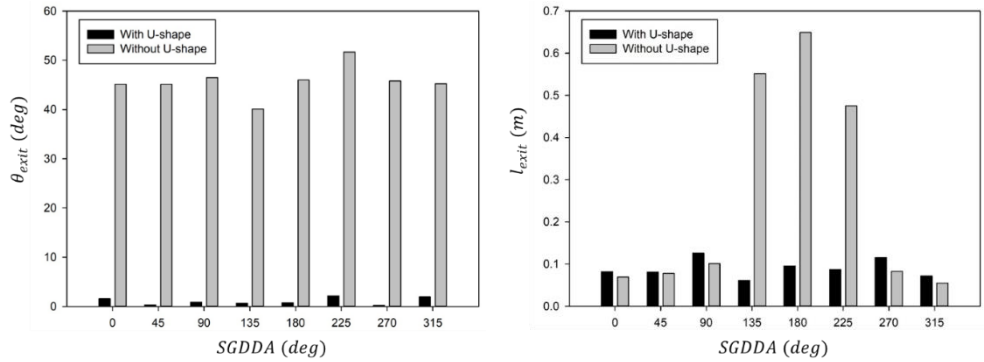

(a) (b)

Figure 61. Tracking performance parameters (a) l_exit and (b) θ_exit measured when the tractor reached the final waypoint on the exit path (entrance) for various SGDDAs.

Feasibility testing of the path-smoothing methods

Figure 62 shows the results for tracking accuracy for the original entry path compared to the LOPS- and LOPS with CNS-applied paths generated using the same entrance and start point as those used in the previous simulation study (Figure 56). Figure 62 (a) and Figure 62 (b) show the effect of the LOPS smoother on the lateral deviation obtained when following the straight path after navigating the entry path. When using the LOPS smoothing method, the maximum lateral deviation obtained when following the 10 m straight path was decreased from 26.2 cm to 14.6 cm (Table 16) because the redundant turn induced by the waypoints generated using the A* algorithm, which locally calculated the cost of the route based on the adjacent grid, was eliminated and replaced with a straight segment. However, even when following the curved path to enter the 10-m straight line, the

trajectory of the tractor deviated from the straight path beyond the acceptable level of < 10 cm (the blue zone in Figure 62). A possible cause for this increase in lateral deviation could be because the waypoint update process synchronization with the GPS sampling rate of 20 Hz, which is the same as the global navigation satellite system (GNSS) module specification used in an autonomous tractor platform, was delayed due to the waypoints being closely placed within a grid size of 10 or 14 cm. For example, as shown in Figure 62 (b), there was a difference between when the tractor entered the straight path and when the waypoint was updated and the straight path was recognized in the algorithm (the black circle in Figure 62 (b)). Hence, the steering and velocity commands to follow the straight path were executed when the tractor passed the waypoint.

On the other hand, when the CNS filter was applied on the entry path (Figure 62 (c)) to reduce the redundant points by eliminating the collinear nodes, the waypoint was updated exactly on time after entering the straight path (the black circle in Figure 62 (c)) and achieved an acceptable tracking trajectory with a maximum lateral deviation of 4.5 cm (Table 16). Consistent with the effect of the LOPS filter refining the turning maneuver, the number of the waypoints was reduced from 179 to 34 by eliminating the redundant control points (especially on the curved path) using the CNS filters. In addition, the travel distance and time consumption were also decreased from 30.3 m and 23.7 sec to 29.9 m and 22.9 sec obtained when the simulator following the paths. This indicates that the CNS filter improved the tracking performance in terms of reducing latency to recognize the present state of the autonomous tractor system and increasing the time tracking efficiency. As shown in Table 16, the computation time to generate the original path was

measured at 7.8 s, and the calculation time for the smoothing processes using LOPS and CNS was 0.1 s.

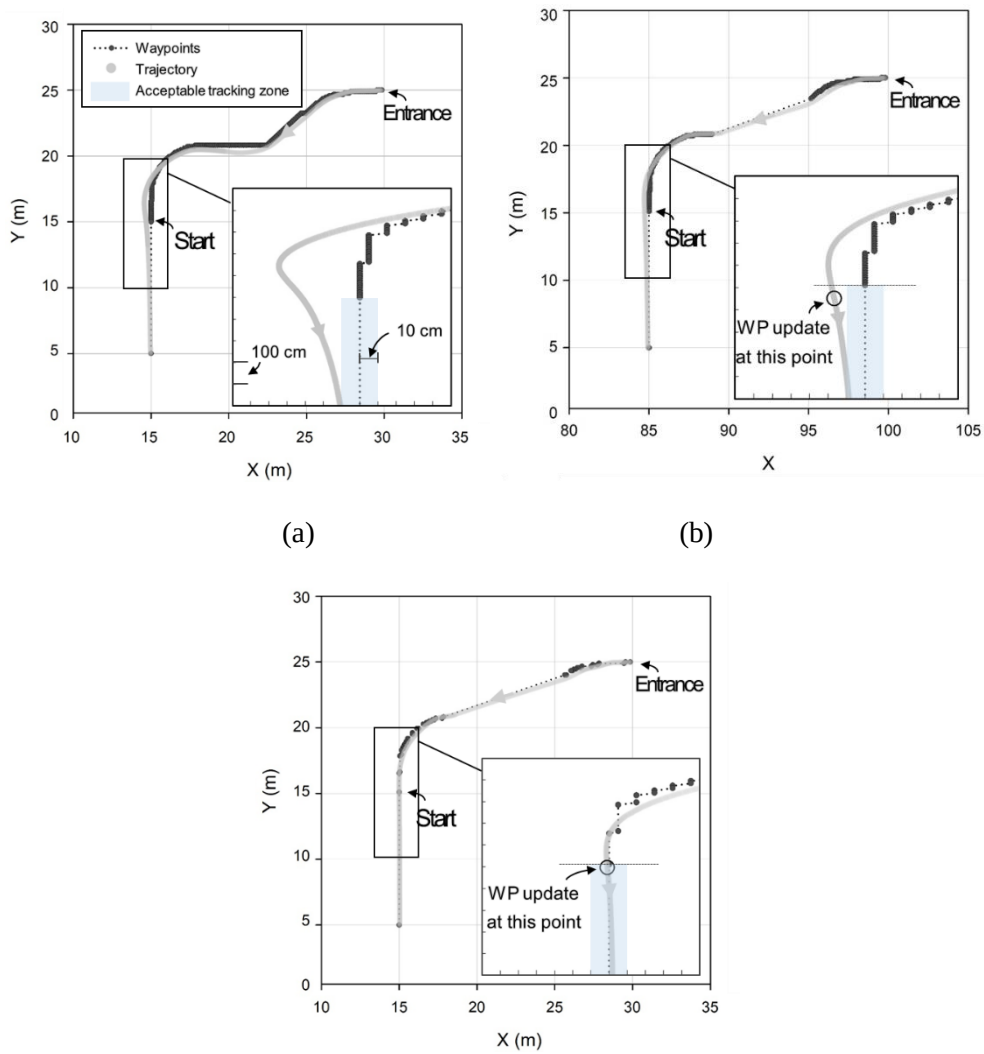

Figure 62. Tracking trajectories of the tractor following the (a) original, (b) LOPS-smoothed, and (c) LOPS with CNS-smoothed entry paths generated in the search space with U-shaped obstacles.

Table 16. Simulation results for the original, LOPS-smoothed, and LOPS with CNS-smoothed entry paths.

Path type	Num of WPs	Travel distance (m)	Time consumed (sec)	Maximum deviation (cm)	Computation time (sec)
Original	214	30.8	25.1	26.2	7.81
LOPS-smoothed	179	30.3	23.7	14.6	7.92
LOPS & CNS-smoothed	34	29.9	22.9	4.5	7.96

Field tests in real paddy fields

Figure 63 shows the trajectories of the autonomous tractor that followed the paths generated using the developed entry-exit path planner operating in two arable fields with different entry positions (the middle and corner of the short segment of the field boundary). In both fields, given that the first track and the last headland pass provided the arrival heading for the entry path and departure heading for the exit path, respectively, the proposed path planner successfully generated the entry (gray circle) and exit paths (white circle) for the tractor to reach the destination of the autonomous tractor accurately in terms of both the position and heading from the entrance to the start and from the end point to the entrance. In addition, all waypoints were located within the field boundary. Therefore, as can be seen in the trajectory obtained following the entry path (the green points in Figure 63), the autonomous tractor could follow the entry path, reach the start point, and navigate the first straight track corresponding to the working line while performing tillage

operation with an acceptable error level (< 10 cm, which is the same as the overlap length) of the maximum lateral deviation of 8.4 cm (field 1) and 7.9 cm (field 2) in both target fields without any collisions with the field border. This indicates that using the entry path generated by the proposed planner could effectively provide the in-field path and guide the autonomous tractor from the entrance location to the start point and cover the work area without leaving any of it untilled.

For the trajectories obtained along the exit paths (including the last lines of the operational maps in both fields), the tractor successfully reached and finished the automated navigation paths with the distance (l_{exit}) from the entrance and the point at which the tractor completed the task of 11.6 and 9.7 cm in fields 1 and 2, respectively. In addition, the angles (θ_{exit}) between the heading angle at the end point when the tractor completed the agricultural task and the direction required for the tractor to exit the field were measured as 15° and 12° in fields 1 and 2, respectively. Given that the maximum steering angle of the tractor used in this study is $\pm$35°, these results imply that the operator can drive the tractor to exit the field without backward navigation, as indicated by the trajectories for the manual

exit (the red scattered points) in Fig. 16.

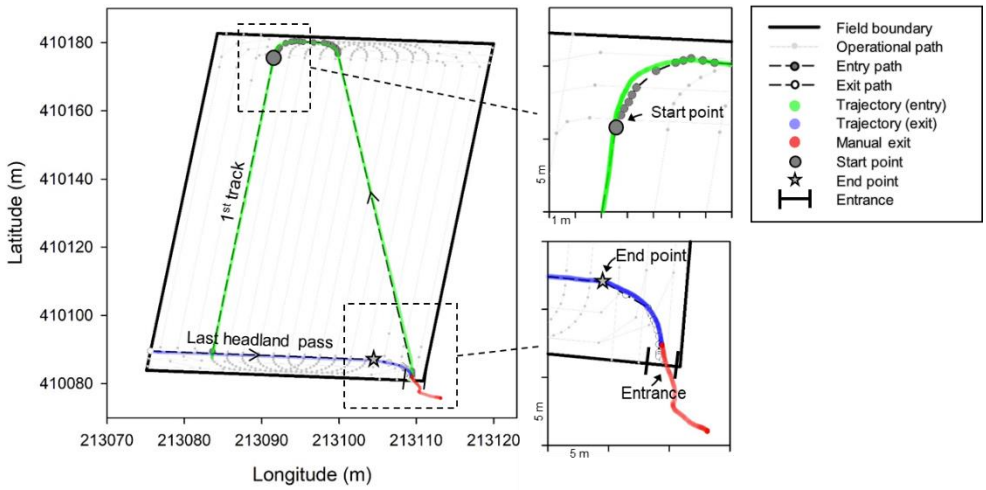

(a)

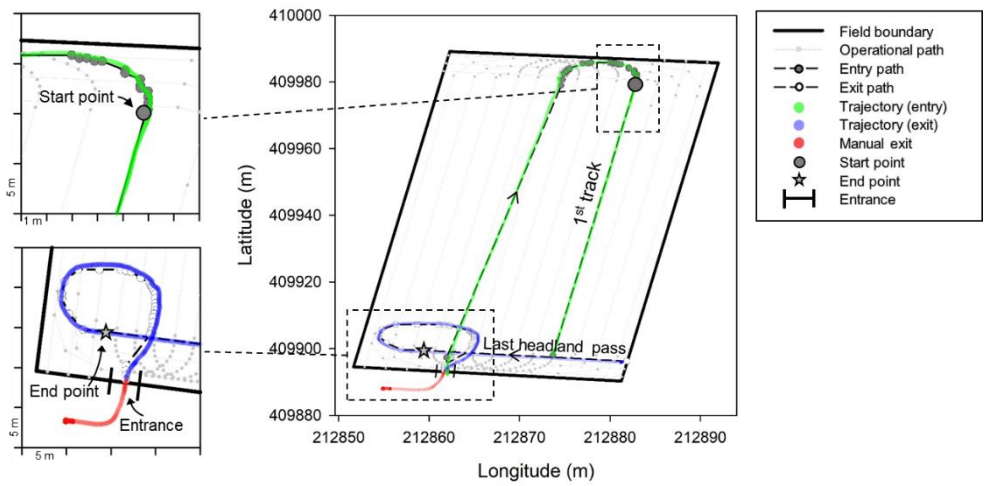

(b)

Figure 63. Trajectories of the autonomous tractor following the entry and exit paths in two paddy fields with different entrance positions: (a) field 1 and (b) field 2.

CONCLUSIONS

In this study, an entry-exit path planner was developed to generate a path for a tractor in a paddy field by applying the A* algorithm. A path is created in a search space with U-shaped obstacles designed in this study to guide the autonomous

tractor to automatically maneuver from the start point of the path and return to the entrance after completing the agricultural task. The key contribution of this study is enhancing the path generation algorithm for a completely automated tractor operation in an arable field by providing a feasible method to generate the entry-exit path. Its practicality was investigated using a 3D virtual simulator developed in our previous studies (Han, Kim, Jeon, & Kim, 2019; Han et al., 2015). Consistent with our previous study for generating operational maps (Han et al., 2013), the platform for the field tests was built using a 60 kW tractor equipped with a GPS/INS system. Field tests were conducted to validate the potential for the proposed path planner with acceptable tracking performance in two paddy fields with different entrance locations. The following conclusions can be drawn from the results of our experiments. Future studies include a validation test in the various paddy fields to investigate the effect of the field shape and the location of the entrance when generating and following the entry and exit paths. We will also develop a complete path planner which could provide the autonomous tractor the whole tillage path by automatically combining the field-coverage path with entry-exit path to enhance the performance of the autonomous tractor system.

- An entry-exit path planner consisting of three processes, search space construction, path generation using the A* algorithm, while path-smoothing was conducted to generate feasible routes with turning maneuvers to enable an autonomous tractor to arrive at the start point by controlling its position and direction. To induce the A* algorithm to find the turning path with the consideration of the non-holonomic constraint of the tractor, U-shaped virtual obstacles were designed based on the

minimum turning radius and look-ahead distance of the tractor and located in the search spaces at the start, end, and entry points. A path-smoothing process comprising CNS with LOPS was applied to reduce redundant turning and control waypoints to improve the tracking performance.

- The results of a simulation study show that the designed entry-exit path planner could derive a feasible path for the autonomous tractor to reach its destination accurately in terms of position and heading by taking the steering characteristics of the vehicle, such as the minimum turning radius and look-ahead distance, into account when designing the search space with the U-shaped obstacles. In the tracking performance, the lateral deviation and heading angle error of 6.2 cm and 0.6°, respectively, decreased compared to those obtained with the search space generated without the U-shaped obstacles (63.2 cm and 40.1°, respectively) owing to the curved path derived by avoiding them to induce the tractor to follow a path causing fewer oscillations and lower error. In addition, as compared to when creating a path using the A* algorithm only, two path-smoothing processes (LOPS and CNS) reduced the maximum lateral deviation from 26.2 to 4.5 cm due to their capability of removing redundant waypoints that caused steep turning and control latency.

- In a real environment test conducted in two rectangular paddy fields with different entrance positions, the autonomous tractor could reach and follow the first inner track, corresponding to the first working line, with a maximum lateral deviation of < 8.5 cm (entry path) in both target fields. In

addition, the tractor successfully reached the entrance along the exit path and finished the automated navigation with l_{exit} < 12 cm and θ_{exit} < 15 ° such that the operator could drive the tractor to exit the field without backward navigation.

CHAPTER 6

INTELLIEGENT PATH-TRACKING CONTROLLER BASED ON REINFORCEMENT LEARNING

ABSTRACT

A robust path-tracking algorithm is integral for an autonomous agricultural vehicle to accurately follow a guidance line, including straight and curved paths with headland turning in an arable field. To enhance the performance of a path tracking method developed based on pre-determined look ahead distance variables, this article proposes a reinforcement learning (RL) based intelligent tracking controller for an autonomous tractor to keep the implement on the reference line at higher speeds. An architecture of an RL-network was designed using deep Q-network (DQN) model to adaptively provide look-ahead distances based on the navigational conditions represented by lateral deviations and heading errors. In this study, a path-tracking algorithm was self-developed with DQN trained by the computer simulator developed in our previous study while following the C-shaped headland turn with varing entry and exit angles. A field evaluation was conducted by comparing the performance of lateral deviation obtained with a 63-kW autonomous tractor equipped with the developed path tracking algorithm. The results of the computer simulation confirmed that the RL-based intelligent tracking controller guided the tractor to follow the path with smaller oscillations, as compared those obtained with the previously developed tracking controller. In the field test performened in an arable field, the autonomous tractor equipped with the RL-based intelligent path tracking controller provided improved path-tracking

accuracy (lateral and heading RMSEs of 12.9 cm and 3.8 deg), as compared with those (lateral and heading RMSEs of 30.1 cm and 8.6 deg) obtained using the system develeopd in previous study at 4 km/h.

Keywords: Path tracking; Reinforcement learning; Deep Q-Network; Autonomous tractor

INTRODUCTION

The increasing demand for farming products and environ- mental considerations has led to the agricultural industry seeking cost efficiency measures from diverse solutions involving various academic fields, e.g. agronomy, geology, genetics, and engineering (Tilman et al., 2002). To achieve higher productivity even with lower energy consumption and less terrestrial field degradation, engineering has been focused on the development of advanced technologies in terms of autonomous tractor systems and optimal fieldwork management (Gebbers & Adamchuk, 2010).

A robust path-tracking algorithm is integral for an autonomous agricultural vehicle to accurately follow a full-path, including straight and curved paths with headland turning in the off-load environment. Currently, Advanced technology for implanting path-tracking algorithms have been widely studied for different vehicle models using different principles such as model free controller (e.g., Fuzzy logic model, Proportional-Integral-Derivative (PID) control), Model based controller (e.g., Linear-Quadratic Regulator (LQR), Model Predictive Control (MPC), Nonlinear Model Predictive Control (NMPC)), and geometric controller (e.g., Stanley and Pure-Pursuit Control).

PID control is a widely used to develop auto-guidance controller due to its simplicity and robustness (Normey-Rico et al., 2001). (Dong et al., 2011) proposed a path-tracking controller based on a two-layer PID control structure to guide autonomous harvester on a desired path. Their path tracking results showed lateral deviations of less than 3 cm when tracking straight path at travelling speed of up to 0.8 m/s. Nevertheless, the method requires the parameter tunning process according to each condition, and is so sensitiveto direct feedback error that it is difficult to guarantee system. Fuzzy logic can be modelled to approximate non-linear motions by a set of If-Then rules without fully characterizing the non-linear systems (Precup & Hellendoorn, 2011). For example, (Cho & Lee, 2000) designed a fuzzy controller trained by genetic algorithm (GA) for autonomous speed sprayer system in an orchard using a differential global positioning system (DGPS). The results showed that the speedsprayercould be autonomously operated within 50 cm deviation. (Zhang & Qiu, 2004) designed an autonomous system with a pure-pursuit-based tracking controller for a robotic tractor to navigate a desired path including inner-work track with headland turning at the ends of a field, using geo-referenced information obtained with an RTK-GPS system, and the lateral deviations of less than 0.1 m at a travelling speed of up to 3.5 m/s. In previous study decribed in Chapter 4, the autonomous puddling and leveling tractor system equipped with a slip-estimation based tracking controller was developed and validated by comparing the tracking and covering results with the skilled operator in the same field and platform condition. Even though the autonomous system reduced 36 % of the travel distance and 5 % of the fuel consumption, it took about

20 minutes more time because it traveled at a slower average velocity (1.35 km/h) than the manual-driven tractor (2.75 km/h).

Recently, methods based on optimization theory and dynamic models, such as LQR (Vougioukas, 2012), MPC (Lenain et al., 2006; Wu & Hung, 2017), and NMPC (Kayacan et al., 2014; Vougioukas, 2012), have been widely stidued for the path-tracking control algorithm of autonomous agricultural vehicle. However, these methods require the repeated solution of an optimization problem at each control step, which may increase the computational burden and challenge their real-time application (Zhang et al., 2019).

During agricultural task, the autonomous vehicle navigated the desired path with nonlinear behavior due to the complex interrelationship between the off-road environment and the mechanical and hydraulic operations inside the tractor. Therefore, in order to calculate appropriate steering and speed commands based on the difference in tractor position and posture compared to the reference route for the driving environment, real-time environment response path tracking technology is required. Many existing researches have proposed a path follower using and applying a vehicle-centered method (Fang et al., 2011; Han et al., 2015; Lenain et al., 2005). Compared to automobiles, a tractor requires a high following accuracy (within 10 cm) and an agricultural task which was aimed for implemtent where agricultural task was really performed.

Recently, many automated agricultural applications, such as passive & active implement control (e.g. John Deere AutoTrac, Trimble Agriculture TrueGuide, Agleader SmartSTEER, ProTrakker Implement guidance) and tractor implement management (TIM) with the concept where the implement can control certain

tractor functions based on the ISOBUS protocol. In addition, advanced techonology for solving a motion control problem (MCP) of the agricultural vehicle operated in an off-load environment by substuting MCP with data-driven modelling problem using an artificial intelligent have been widely studied to handle constraints, process nonlinearity, uncertainty, complexity or time-delay (Ding et al., 2018; Luckow et al., 2016; Wasala et al., 2020).

Among various artificial intelligent technologies (e.g., supervised learning (Convolutional Neural Network (CNN), Recurrent Neural Network (RNN)), Reinforcement Learning (RL), and Generative adversarial network (GAN)), RL that can self-recognize the current driving situation and modify behavioral strategies based on the reference path planned by the path generation algorithm and the location and heading angle information acquired from the GNSS sensor, has been gaining significant traction in autonomous driving for a range of scenarios. Because, unlike automobiles operated on roads that can be recognized as reference routes (Forbes, 2002; Kendall et al., 2019; Li et al., 2019; Riedmiller et al., 2007; Veres et al., 2011), agricultural vehicle does not have reference paths that humans can recognize. Such that it is difficult to use supervised learning or GAN that must be preceded by data acquisition and human classification for developing path-tracking controller in an agricultural sector. For example, Zhang et al. (2019) designed a modified structure that developed an unmanned ground vehicle (UGV) tracking controller for an agricultural observer system using the Double DQN structure and how agricultural autonomous driving can be posed as a Markov Decision Process (MDP) and present RL-based approaches for waypoint following. The results showed that the Double DQN-based control dramatically reduced

thesettling time and the overshoot at the corner at higher forward speeds at a minor expense of slightly increased rise time and steady state error compared to pure-pursuit based controller.

In this study, to enhance the tracking performance of a fully automated navigational controller of the autonomous tractor system developed in previous study (Han, Kim, Jeon, Moon, et al., 2019; Jeon et al., 2021) in terms of improving the field effciency with a less oscillation by increasing the travel velocity, RL-based intelligent tracking controller with an adaptive look-ahead calculator, which provides control point by determining how far along the path the robot should look from the current location to compute the steering commands based on the navigational environment in real-time, was developed. For handling the non-linear constraint of the kinmatic chatacteristic of the tractor and implement-centered navigation, an architecture of the DQN network structure including 2 inputs based on the position and posture of the tractor and 1 output of the look-ahead distance was designed to induce the proposed RL based controller to determine the driving environment and calculate steering angle in real-time.

The specific objectives of this study were

- 1) to design the network architecture for training and controlling the path tracking controller.
- 2) to train the model of the adaptive look-ahead calculator and investigate the feasilbility of the developed controller by analyzing its tracking performance by a comparison to the previously developed controller (Han, Kim, Jeon, Moon, et al., 2019) via simulation tests.
- 3) to validate the RL based tracking controller in field test.

MATERIALS AND METHODS

Path-tracking controller

Navigational controller

To provide an autonomous tractor a steering control robust to slippage, while performing puddling operation in paddy fields, slip-estimation based navigational controller developed in our previous study (Han, Kim, Jeon, Moon, et al., 2019) was used. As shown in Figure 64, the navigational controller used in this study was based on the extended kinematic bicycle model (EKBM) combined with the pure pursuit method, which considers sliding effects to the original kinematic bicycle model with an assumption that the sliding phenomenon is entirely described by the introduction of the front (β_f) and rear (β_r) sliding parameters. In addition, by assuming the tractor was virtually located on the look-ahead point to calculate the path tracking variables, i.e., lateral deviation (y) and heading error ($\tilde{\theta}$), in advance, a dynamic motion such as delay cause by overshoots and rise time induced by the steering actuator, could be accounted and compensated. In this study, reinforcement learning-based look-ahead generator was designed and used to provide an appropriate control point to calculate navigational variable, i.e., lateral deviation and heading error for steering command. Given those navigational variables, derivatives of the kinematic state variables (y and $\tilde{\theta}$) with respect to the reference trajectory can be written as eq. 5.1 (Lenain et al., 2007). The curvature of the path is regarded as zero because the path-tracking task is performed based on waypoints which build segmented lines. The EKBM was transformed into a chained form with one input, i.e., steering angle (δ), to allow the design of nonlinear control system a controllability, such that two state variable (y and $\tilde{\theta}$)

was ensured to converge from any initial value to any final value. Therefore, eq. 5.2 yields the calculation of the steering angle to be sent to the actuator.

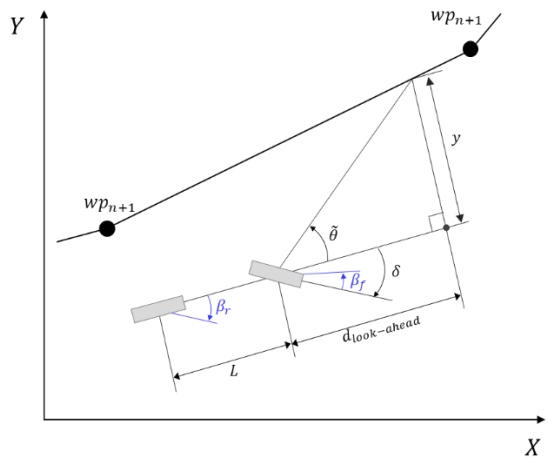

Figure 64. Notation of extended kinematic bicycle model combined with pure-pursuit method and path tracking parameters.

$$f(y, \tilde{\theta}, \delta, \beta_f, \beta_r) = \begin{cases} \dot{y} = v \sin(\tilde{\theta} + \beta_r) \\ \dot{\tilde{\theta}} = v cos\beta_r \frac{\tan(\delta+\beta_f) - tan\beta_r}{L} \end{cases} \quad (5.1)$$

$$\delta(y, \tilde{\theta}, \beta_f, \beta_r) = \tan^{-1}\left\{L \frac{(-K_P y - K_D \tan(\tilde{\theta}+\beta_r))\cos^3(\tilde{\theta}+\beta_r)}{\cos\beta_r} + \tan\beta_r\right\} - \beta_f \quad (5.2)$$

where y is the lateral deviation of the tractor with respect to the reference path (m), $\tilde{\theta}$ is the heading error of the tractor with respect to reference path (rad), v is the forward velocity of the tractor (m s^{-1}), δ is the steering angle of the front wheel (rad), L is the wheelbase of the tractor (m), K_P is the proportional gain and K_D is the derivative gain, and β_f and β_r are the sideslip angles of the front and rear wheels (rad), respectively.

Observer-based estimation of sideslip angles

Figure 65 shows the architecture of calculating the steering angle of the tractor (δ). Given a navigational variable calculated based on the look-ahead distance (D) derived by the RL-based look-ahead generator, $X = \left(y, \tilde{\theta}\right)$, obtained from the tracking algorithm based on the position and heading data measured from GNSS/INS system, the estimated state variable, $\hat{X} = \left(\hat{y}, \hat{\tilde{\theta}}\right)$, converges to it for observer controller to change the variables of the sideslip angles (β_f, β_r), which are then fed into the steering model formula (eq. 5.2) to calculate a steering angle. The steering angle of the tractor can be calculated when the sideslip angles of the front and rear wheels are known, such that it was estimated on-line using the observer theory proposed by (Lenain et al., 2007). To apply the observer to the EKBM system, the formula was linearize with respect to the sliding parameters, u = (β_f, β_r), around zero with assumption that slip angles are generated within a few degrees (eq. 5.3). As described in eq. 5.4, $B\left(\hat{y}, \hat{\tilde{\theta}}, \delta\right)$ denotes the derivative of $f\left(\hat{y}, \hat{\tilde{\theta}}, \delta, 0,0\right)$ with respect to control u. Introducing the equation of error dynamics defined using H Hurwitz matrix, the observer model was derived to ensure that the estimated output converges to the corresponding measured values by the variables of the sideslip angles (β_f, β_r) changed by an observer controller. As a result, the sideslip angles of the front and rear wheels can be determined as eq. 5.5 based on theoretical vehicle motion model, i.e., EKBM, using consecutively measured lateral deviation and heading error and steering angle sent to the autonomous tractor system.

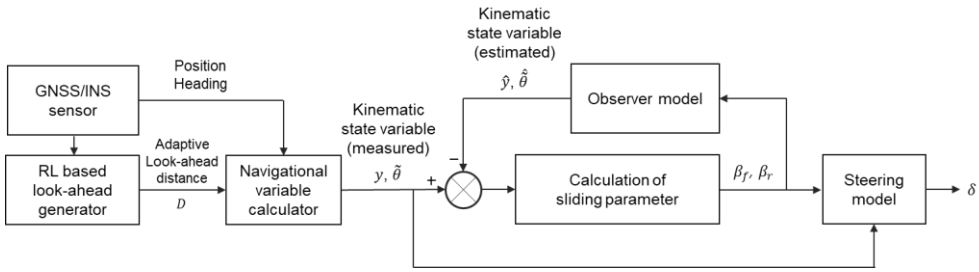

Figure 65. Architecture of path-tracking algorithm with slip estimation observer.

$$\dot{\hat{X}} = f(\hat{X}, \delta, 0,0) + B(\hat{X}, \delta)u \tag{5.3}$$

$$B\left(\hat{y}, \hat{\tilde{\theta}}, \delta\right) = \frac{\partial f\left(\hat{y}, \hat{\tilde{\theta}}, \delta, 0,0\right)}{\partial u} = \begin{bmatrix} 0 & v\cos\hat{\tilde{\theta}} \\ \frac{v}{L}(1 + tan^2\delta) & -\frac{v}{L} \end{bmatrix} \tag{5.4}$$

$$u = \begin{pmatrix} \beta_f \\ \beta_r \end{pmatrix} = B\left(\hat{y}, \hat{\tilde{\theta}}, \delta\right)^{-1}\left(H\left(\dot{\hat{X}} - \dot{X}\right) + \dot{X} - f\left(\hat{y}, \hat{\tilde{\theta}}, \delta, 0,0\right)\right) \tag{5.5}$$

where H is the Hurwitz matrix, $\hat{X}$ is the estimated state variable, X is the measured state variable, B is the derivative of vehicle motion model with respect to sideslip values, $\hat{y}$ is the estimated lateral deviation of the tractor with respect to reference path (m), $\hat{\tilde{\theta}}$ is the estimated heading error of the tractor with respect to reference path (rad).

Framework of RL based intelligent tracking controller

Environment of the RL framework

Figure 66 shows a learning framework of RL based intelligent tracking controller. In the environment part of the architecture, the autonomous tractor system eqqiuped with the path-tracking controller that produced steering angles, velocity values, and implement control commands and transmit those to the autonomous tractor system based on the position and heading data obtained from the RTK-GNSS/INS system. In addition, to improve an ability to interpret a driving condition in detail compared to the method used in the previous study (Han, Kim,

Jeon, Moon, et al., 2019), which calculated the steering angles using the leteral deivation and heading error measured at the look-ahead point, a driving-status predictor was designed as shown in Figure 67. The predictor sequentially calculated the lateral deviations and heading errors at 5 cm intervals from the position of the implement to the point 7.5 m ahead, generate the two driving-status arrays including 151 data, resepectively, and transmit those driving-status arrays to the agent of the RL based intelligent tracking controller using TCP/IP protocol.

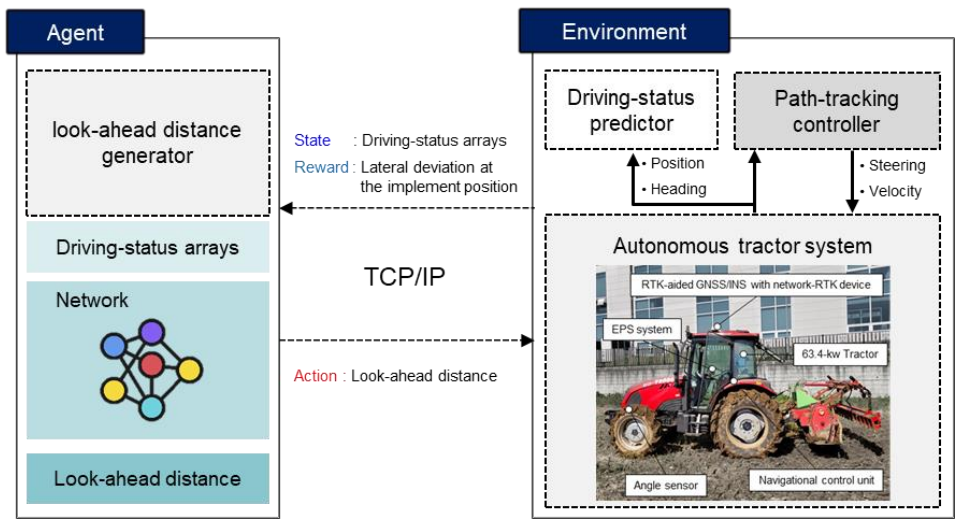

Figure 66. Learning framework of the RL based intelligent tracking controller

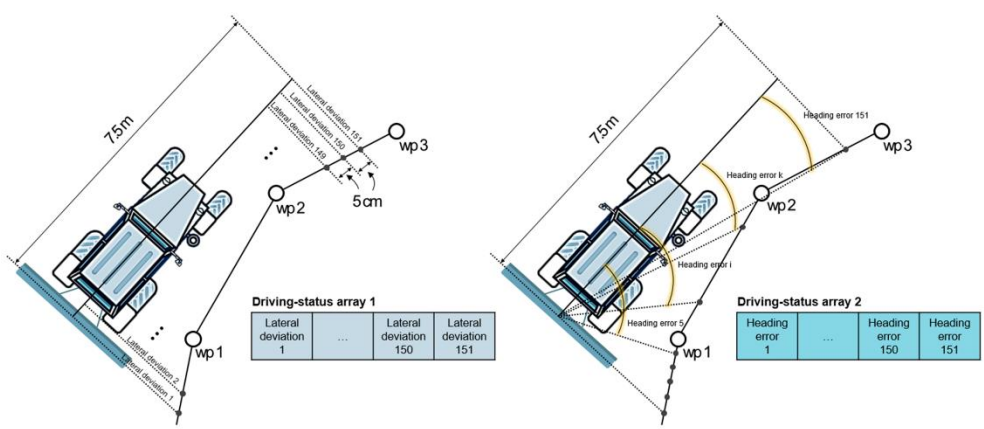

Figure 67. Maneuvering of Driving-status predictor

Agent for adaptive look-ahead generator

In an agent environment, the look-ahead distance, which is intrgral parameter to calculate the tracking errors was calculated using an adaptive look-ahead generator using DQN network. We used an architecture in which there is a separate output unit for each action, i.e., the look-ahead distance, and the state representation is the input to the neural network. The main advantage of this type of architecture is the ability to compute Q-values for all actions in a given state S with only a single forward pass through the network (Mnih et al., 2015). As shown in Figure 68, the network architecture for training and controlling had 7 layers, an input layer, 5 fully-connected hidden layers, and an output layer. The activation function between hidden layers was relu function. Each hidden fully connected layer had 128 neurons. TensorFlow library was used in python 3.7.0 version to build and train the agent.

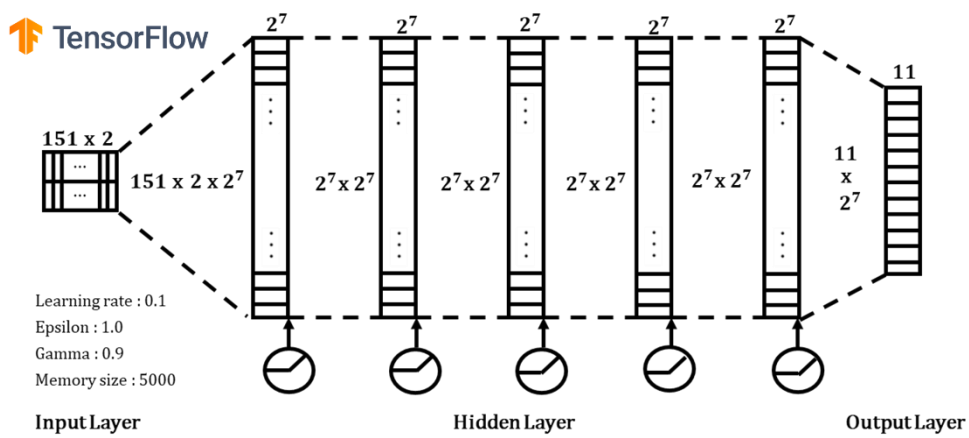

Figure 68. Schematic illustration of the DQN network of the RL based intelligent

Input and output of the network

The input layer received the driving status arrays of lateral deviation and heading error and the output layer had 11 neurons corresponding to 11 pre-defined look-ahead distance from 0.5 to 3.0 at 0.25 intervals. For tracking control and training

network, elements of the status arraies were normalized before intput to the network using eq. 5.6 and 5.7 to avoid gradient vanishing and accerlerate training time by giving similar weights to the two status arrayies. The normalization ranges (d_{norm} and θ_{norm}) were set 3 m and 90 deg in this study.

$$S_d = \frac{1}{d_{norm}}\{e_{d,1}, e_{d,2}, e_{d,3} \ldots \ e_{d,151}\} \tag{5.6}$$

$$S_\theta = \frac{1}{\theta_{norm}}\{e_{\theta,1}, e_{\theta,2}, e_{\theta,3} \ldots \ e_{\theta,151}\} \tag{5.7}$$

where S_d and S_θ are the input state variables to the network, d_{norm} and θ_{norm}, are the normalization range for $e_{d,i}$ and $e_{\theta,i}$,respectively, i is the index of the status array ranging from 1 to 151.

Design of the reward of RL network

In this study, to induce the tracking cotroller to generate the steering angle for the purpose of allowing the position of the implement to be located on the desired path, not the center of the vehicle, a reward function ($r(d_{im}, \theta_{im})$) that encourage the agent to maintain the given trajectory of the implement by adaptively modifying look-ahead distance, was proposed using eq. 5.8. Lateral deviation (d_{im}) and heading error (θ_{im}) at the center of the implement were normalized and linearly combined with the reward gain of K, which was defiend as -5000 in this study.

$$r(d_{im}, \theta_{im}) = K(d_{im}/d_{norm} + \theta_{im}/\theta_{norm}) \tag{5.8}$$

Training of the RL model via stimulation

Reinforcement learning, an unsupervised learning, has the advantage of being able to encode complex behavior of the environment, so it can be used in areas that

are difficult or impossible to solve with existing algorithms, but numerous training courses are required to actually reach qualified performance. In order to learn, multiple driving tests must be performed in the real environment, but there are limitations such as safety and time consuming problems. Therefore, by utilizing the characteristic that the autonomous agricultural work driving environment is similar to the simulation environment, the training process for the intelligent path tracking algorithm was performed via the simulation.

Prior to the evaluation of the tracking performance, to learn RL model for calculating the look-ahead distance adaptive to the driving environment definced by the two driving-status arrays, the virtual tractor navigate the inner-work paths based on the C-type headland turning generated with varing exit (θ_{exit}) and re-enter ($\theta_{re-enter}$) angles, which formed two parallel inner-tracks with the length of 30 m before and after the heading turning path at a certain angle (Figure 69 (a)). The interval between the tracks was set as the minimum multiple of swaths capable of generating C-type headland turning (w_{minimum}) calculated by the optical path planning method based on the minimum turning radius of the tractor and the implement width, which was 4 in this study.

Figure 69 (b) shows the reference map consisting of 15 straight lines and 14 curved paths generated with varing exit (θ_{exit}) and re-enter ($\theta_{re-enter}$) angles ranging from from 30° to 150° at 10° intervals. To enable the controller to experience various turning conditions, the modelling path guided the virtual tractor to follow the curved path with the symmetric θ_{exit} and $\theta_{re-enter}$ as shown in Figure 69. In addition, to learn the left and right turning situations, we assumed that

the vehicle traveled on a path that reversed the starting and ending points of the modeling path.

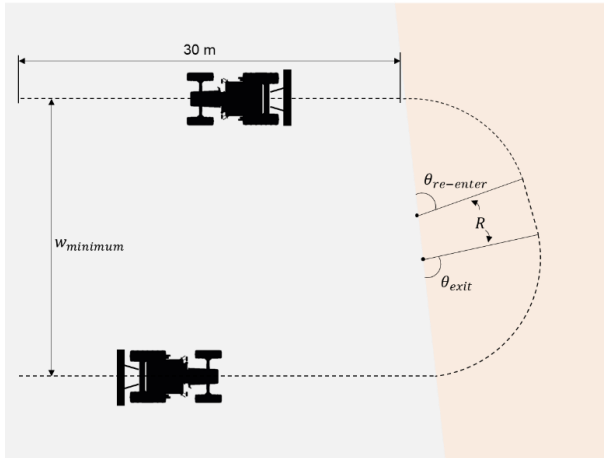

(a)

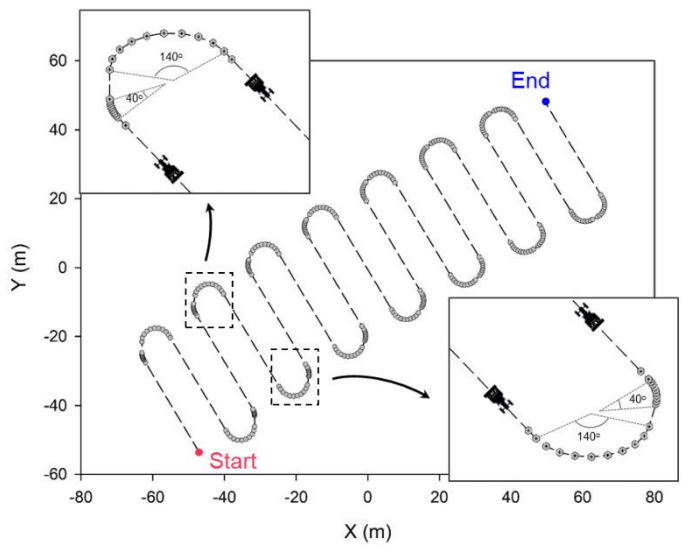

(b)

Figure 69. Illustration of mapping the reference path with exit (θ_{exit}) and re-enter ($\theta_{re-enter}$) angles (a) and the training path generated with varing θ_{exit} and $\theta_{re-enter}$ ranging from from 30° to 150° at 10° intervals (b)

The values of the navigational parameters used in this study were 0.1m, 4km/h, 2km/h, 3m, 1m, (0.8, 0.3), $\begin{bmatrix} -1 & 0 \\ 0 & -1 \end{bmatrix}$, and (6800, 7500 N/rad) for LBO, straight velocity, turning velocity, look-ahead distance, look-behind distance, The proportional-derivative control gains for calculating steering angle, Hurwitz matrix, and front and rear coefficients of cornering stiffness on tractor motion, respectively. The training velocities of straight and turning path were same as 4.5 km/h, which was faster than our previous parameter (1.3 km/h). The behavior policy during training was ε-greedy with ε annealed linearly from 0.99 to 0.01 and finally fixed at 0.01 to train the model with a sufficient exploration for obtaining various driving experiences. The Xavier initialization is to initialize the weights w of the network from a Gaussian distribution (Glorot & Bengio, 2010). A laptop with an Intel i7-10700F, 16GB RAM, and GeForce RTX 2060 SUPER with 2176 cores was used to train the model.

Evaluation of RL-based intelligent tracking controller via simulation and field testing

Three different simulation tests were conducted with the driving simulator described in Chapter 3. As one scenario for studying the feasibility of using two driving-status arrays of a lateral deviation and a heading error to learn the various situational environment such as travelling velocity and turning pattern and calculate a reasonable look-ahead distance based on the position of the implement, a simulation test was performed to guide the tractor located with a lateral displacement of 2 m and a heading error of 45^{o} compared to the 25 m straight reference path as show n in Figure 70 (a). Three models trained with 10, 30, 50

episodes were used to show the effect of the RL-based intelligent tracking controller to improve the tracking performance that converges to the target path quickly and stably. In addition, for evaluating the tracking performance to steers the tractor to keep the implement on the guidance line, the second test was performed by comparing the trajectories of the tractor and implement obtained along C-shaped headland turning with 25 m two straight lines (Figure 70 (b)) at 4.5 km/h.

In the third test, to investigate the effect of using the proposed path-tracking algorithm to improve path-tracking performance on high speed condition, we assumed that a virtual tractor followed a C-shaped headland turning pattern as shown in Figure 70 (b) at 2 km/h and 4.5 km/h, which was middle and the highest speed of the tillage and tge puddling·leveling operation proposed by the International Rice Research Institute (IRRI). Two different path-tracking algorithms, i.e., slip estimation-based navigation controller with the constant look-ahead distance tunned by trial and error method (1.3 m) and the intelligenet tracking controller, were applied to evaluate the effectiveness of the the proposed tracking controller.

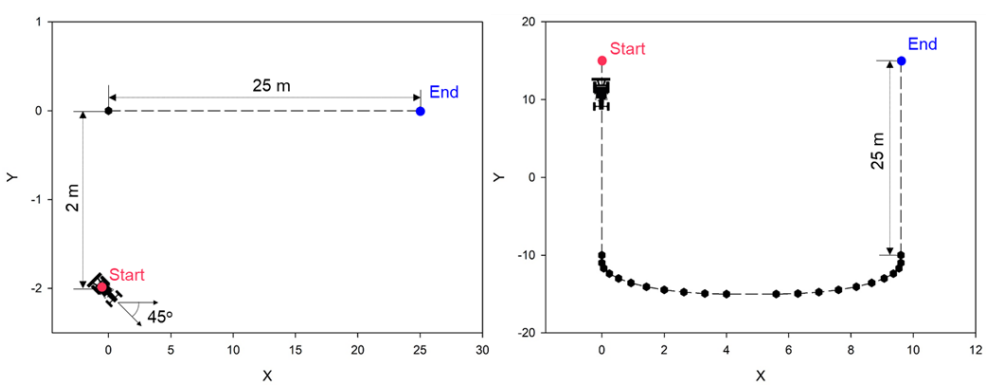

(a) (b)

Figure 70. Setup for the simulation tests: (a) the straight path for investigating the feasibility of using two driving-status arrays to learn the various situational environment and calculate the look-ahead distance and (b) the C-shaped path for studying the effect of using the proposed path-tracking algorithm to improve path-tracking performance on high speed condition.

The field test conducted with the autonomous tractor equipped with the RTK-GNSS/INS sensor described in Chapter 3 for navigating a reference path generated based on information about the coordinates of the corners of the experimental station of Seoul National Universirty (Figure 71), C-type headland turning method, implement width (2.4 m), and minimum turning radius of the tractor (4 m). To investigate the tracking proformance following the reference path Trajectories of the tractor obtained with two different path tracking controllers, i.e., the slip-estimation based steering control and RL-based intelligent tracking controller were compared with traveling speed of 4 km/h, which was the maximum speed that the autonomous tractor could achieve when driving on a second-stage forward gear of the transmission. The performance was evaluated by measuring the maximum and root-mean-squared error (RMSE) values for the lateral deviation of the implement position when the autonomous tractor navigated the inner straight tracks.

Figure 71. View of the field test for validating the proposed path tracking controller

RESULTS AND DISCUSSION

Feasiblity test of RL-based tracking controller

The tracking simulation using the models trained at various episodes

Figure 72 shows the simulated trajectories for the implement attached to the tractor equipped with an RL-based intelligent tracking controller trained at three levels (10, 30, 50 episodes) obtained when following the 25 m straight lines with the lateral displacement and heading error of 2 m and 45°. The colorbar shows the look-ahead distance calculated by the developed adaptive look-ahead generator based on the driving-status information, i.e., lateral deviation and heading error arrays. Overall, it was possible for the autonomous tractor to follow the guidance line without a divergence using the look-ahead distance provided by the proposed method. It was apparant that the tractor followed the path with a smaller oscillation and the position where the trajectory converges to the steady-state on the reference path was earlier when the model that was trained with a high number of episodes was used. For example, when the model trained at 10 episode was used, the less

change of the look-ahead distance occurred during the first entry into the straight line compared to that obtained using the model trained at 30 episode, showing a relatively small oscillation and following the guidance line, but it took a long time to converge. However, when the vehicle equipped with the model trained at 50 episode could follow the reference path with less oscillation and earlier point, compared to those using the less trained models. Even though it was difficult to determine an exact quatitative repationship between the two driving status arrays measured during the navigation and the look-ahead distance, possible cause for that improvement include the use of the adaptive look-ahead distance generator with highly trained model, which take a dynamic driving environment into account.

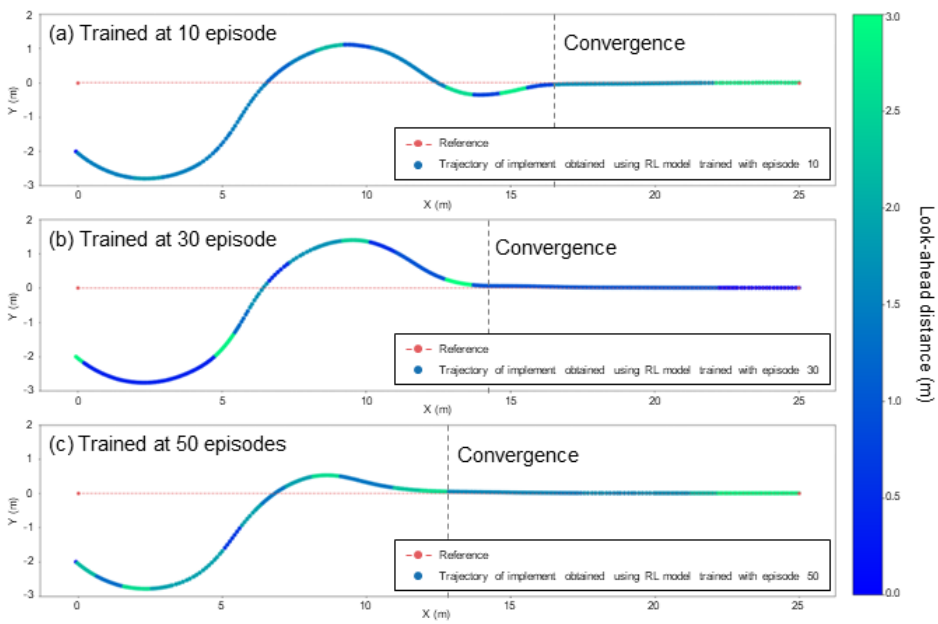

Figure 72. Trajectories of the implement attatched to the virtual tractor equipped with the RL-based tracking controller with the models trained at three levels (10 (a), 30 (b), 50 (c) episodes) followng 25 m straight reference line and the look-ahead distance values calculated by the controller .

Figure 73 compares the simulated trajectories of the tractor following a path of C-shaped headland curves and straight lines obtained from two different measurement

point, i.e., the center of the tractor and the implement, when the RL-based tracking controller trained at 50 episode was used. Given the reward designed to induce the tracking cotroller to calculate the steering angle for the purpose of keeping the position of the implement on the desired path, the trajectory of the implement showed better path-tracking performance on the straight path where the agricultural operations was performed with a maximum lateral deivation of 2.6 cm (root mean square error (RMSE) = 1.2 cm), compared to the maximum lateral deviation of 11 cm (root mean square error (RMSE) = 5.1 cm) obtained using the trajectory of the tractor. Because the autonomous tractor equipped with the developed tracking controller performed the turning maneuver in advance just before entering the headland turning path (labelled A) while the implement position was kept on the straight path. In addition, similar to the results of the simulation to follow the 20 m line, the tracking controller allowed the tracjectory of the tractor to rapidly converge to the reference path before the implement escaped the turning zone when the tractor entered the next straight path (labelled B), such that the implement could be located on the guidance line along the straight path. This indicated that the developed path tracking controller would be effective in improving the tracking performance of autonomous tractor by increasing accuracy at the implement.

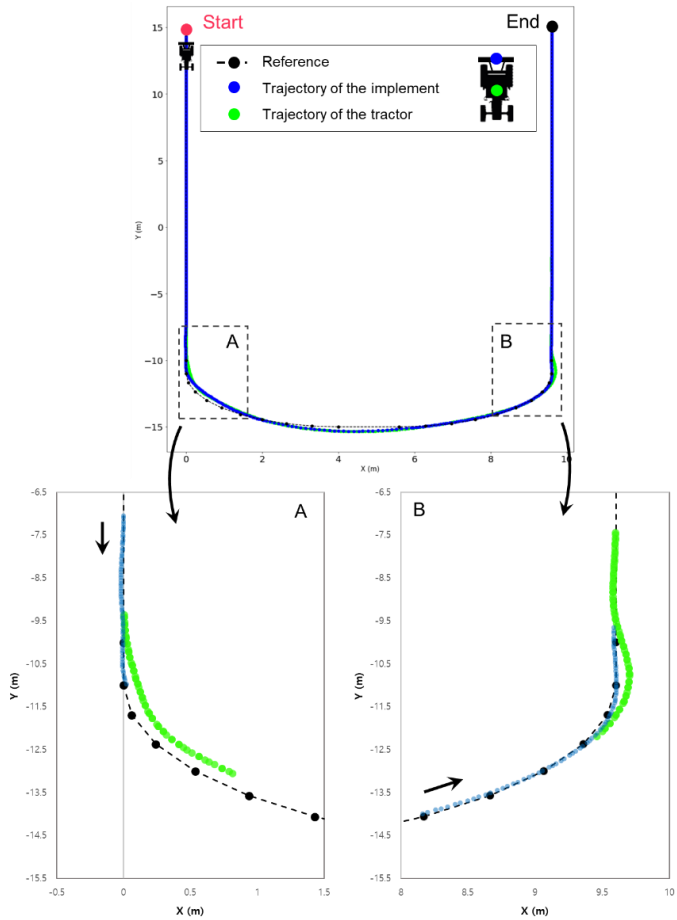

Figure 73. Comparison of trajectories obtained at the tractor and implement positions when the vehicle followed the C-shaped path.

Feasibility testing of the RL-based tracking controller at high-speed condition

Figure 74 shows the results for tracking accuracy of the implement attached to the autonomous tractor obtained using two different path tracking control methods, i.e., the slip-estimation based steering control and RL-based intelligent tracking controller, while following the C-shaped paths with different traveling speeds of 2 km/h and 4 km/h, which were middle and high velocity of tillage and puddling·leveling operations proposed by IRRI. As shown in Figure 74 (a), when

applying tracking controllers to guide the tractor to follow the C-shaped path at middle velocity, i.e., 2 km/h, there was little difference in the trajectory obtained with two different tracking algorithm on both straight and curved paths. This indicated that there would be no significant difference in tracking performance between two controllers at low or middle speed. In constrast, when the traveling velocity was increased to 4.5 km/h, the RL-based intelligent path tracking controller showed superior performance on curved path (Figure 74 (b)), with a maximum lateral deviation and heading error of 2.6 cm and 1.7 deg (root mean square error (RMSE) = 1.2 cm and 1.1 deg), compared to those of 13.5 cm and 8.2 deg (root mean square error (RMSE) = 7.6 cm and 2.4 deg) measured at the zone A in Figure 74 (b). Because when the tractor entered the second straight line along the headland turning path, the controller decreased the look-ahead distance from 1.8-2.2 to 0.5-0.8 to move quickly towards the path and increased it again after determining that the tractor has settled in the guidance line. This indicated that the adaptive look-ahead generator implemented in the path tracking controller would be effective in improving the path tracking performance of the autonomous tractor under high-speed conditions.

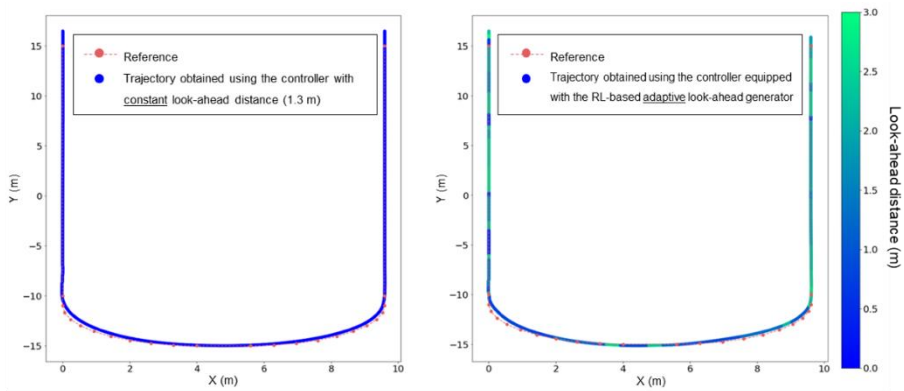

(a)

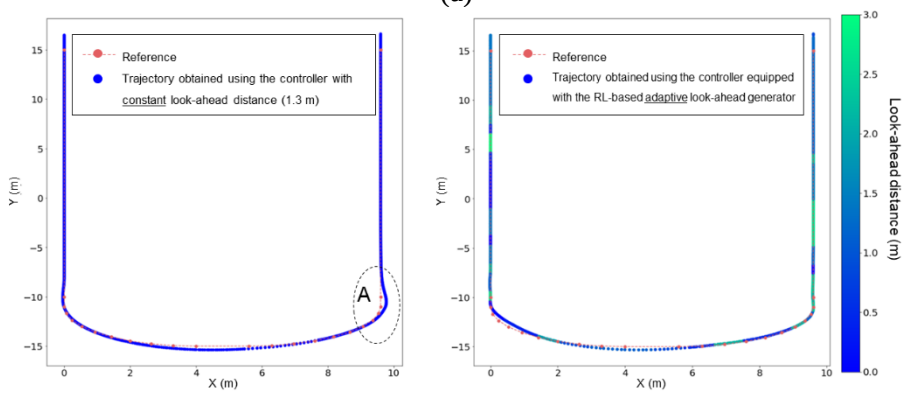

(b)

Figure 74. Trajectories of the implement attached to the tractor obtained with two different path tracking controllers, the slip-estimation based steering control and RL-based intelligent tracking controllerm following C-shaped paths with different traveling speeds: (a) 2 km/h and (b) 4.5 km/h.

Fied test using the autonomous tractor

Figure 75 shows the trajectories of the autonomous tractor operated using the slip-estimation based control logic and RL-based intelligent path tracking controller in arable field: 10 straight reference path with C-shaped headland turning pattern to connect those tracks. Similar to the results of the simulation study for C-shaped path tracking, both tracking controllers showed the fully automated navigation with any stops or divergence at 4km/h. However, larger lateral deviations and heading

errors, rainging from -0.91 m to 2.31 m and from -49.7 º to 26.7 º (lateral and heading RMSEs of 30.1 cm and 8.6 deg) were obtained along straight lines when relying on the slip-estimation based method, compared with those rainging from -0.32 m to 0.55 m and from -13 º to 17.7 º (lateral and heading RMSEs of 12.9 cm and 3.8 deg) obtained using the RL-based intelligent tracking controller as shown in Figure 76. The superior performance of the RL-based control method might be explained by the fact that the dynamic changes of the look-ahead distances calculated by the developed algorithm along the curved path were obvious to keep the implement on the guidance line, ranging from 0.5 m to 2.8 m. In addition, even when the tractor navigated the straight path, it was apparent that the propose tracking controller effectively guide the vehicle to quickly and stablely converge to the reference at a velocity of 4km/h, compared to the trajectories obtained at zone A in Figure 75 (a). This indicated that the developed RL-based intelligent path tracking controller was a better candidate for use in an autonomous tractor to increase the field efficiency by accerlating the traveling velocity.

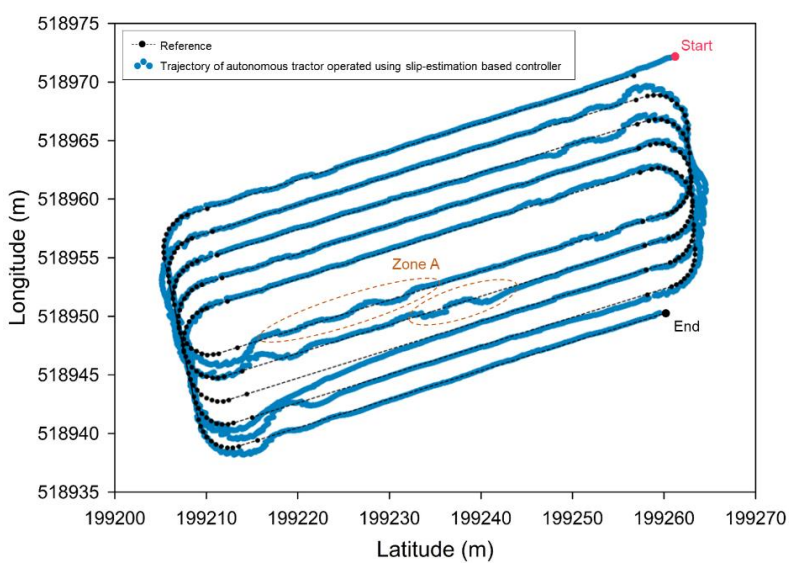

(a)

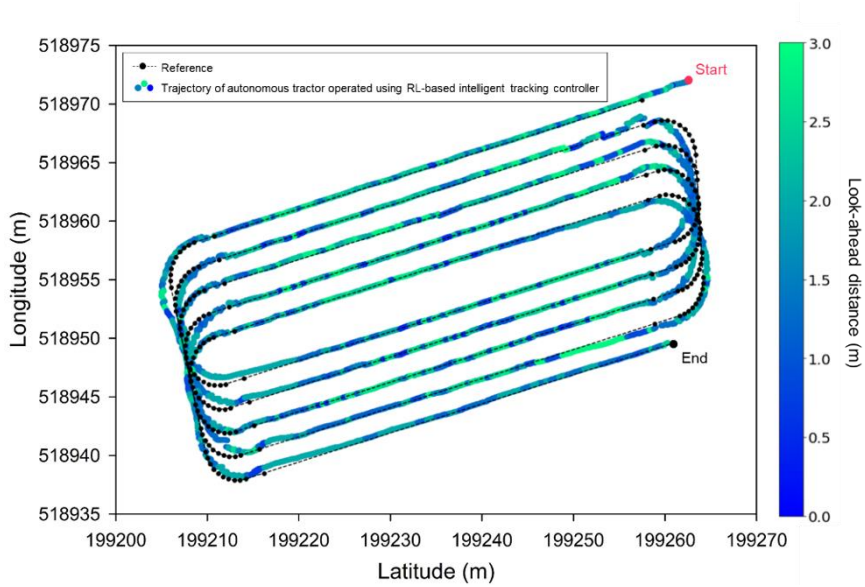

(b)

Figure 75. Results of the tracking trajectories of the implement attached to the full-scale autonomous tractor following the 8 straight guidance lines with C-shapes headladn turning using (a) the slip-estimation based and (b) RL-based intelligent tracking controllers.

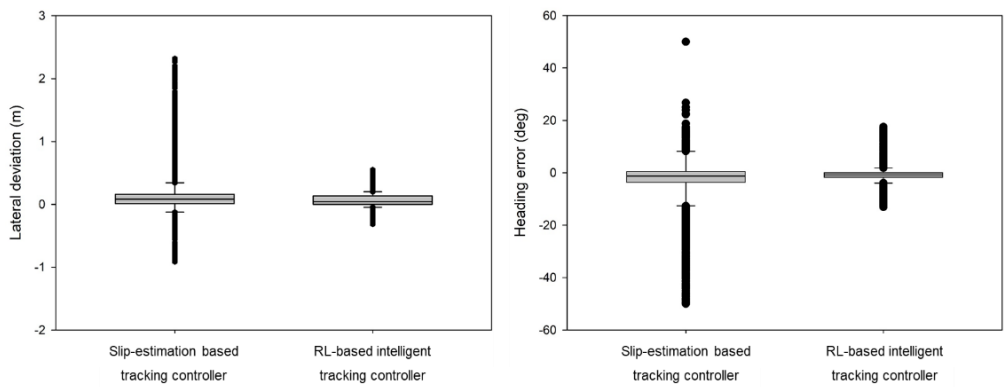

(a) (b)

Figure 76. Results of (a) lateral deviation and (b) heading error of the implement attached to the autonomous tractor obtained using two different tracking controller: the slip-estimation based tracking logic and RL-based intelligent tracking method.

CONCLUSIONS

In this study, an RL-based intelligent tracking controller was designed and its performance was investigated via both simulation and field testings. The main contribution of this research was to enhance the performance of the tracking controller for an autonomous tractor by taking into account the navigational condition represented by lateral deviations and heading errors to keep the implement on the reference line even at high speed. A Framework of an RL-based intelligent tracking controller was designed to provide a look-ahead distance, which is integral parameter to calculate the steering angle, adaptive to various driving conditions in real-time. To improve an ability of interpreting the driving condition compared to the method used in the previous study (Han, Kim, Jeon, Moon, et al., 2019), which calculated the steering angles using the leteral deivation and heading error measured at the look-ahead point, a driving-status predictor that could recognize the curved shape of the guidance line the was proposed. The feasibility of using the proposed path tracking controller for the autonomous tractor was investigated via a 3D graphic computer simulator. Field test was conducted to validate the potential of the proposed tracking method to increace the field efficiency with acceptable tracking performance in a paddy field. The following conclusions can be drawn form the results of the test

- The computer simulation study showed that the RL-based intelligent tracking controller guided the tractor to follow the path with a smaller oscillation and the position where the trajectory converges to the steady-state on the reference path was earlier, compared to the previously developed tracking controller (Han, Kim, Jeon, Moon, et al., 2019) due

to the use of the adaptive look-ahead distance generator. When applying the proposed tracking controllers to guide the tractor to follow the C-shaped path at two-level of the travelling velocity, i.e., 2 and 4.5 km/h, even though there was little difference in the trajectory obtained with two different tracking algorithm on both straight and curved paths, the RL-based intelligent path tracking controller showed superior performance on curved path with a maximum lateral deviation and heading error of 2.6 cm and 1.7 deg (root mean square error (RMSE) = 1.2 cm and 1.1 deg), compared to those of 13.5 cm and 3.19 deg (root mean square error (RMSE) = 7.6 cm and 2.4 deg).

- In the paddy field test, the autonomous tractor equipped with the RL-based intelligent path tracking controller navigated the reference without any stops or divergence with increased path-tracking accuracy compared with previous study (Han, Kim, Jeon, Moon, et al., 2019) even under high speed condition (4km/h). This indicated that the developed RL-based intelligent path tracking controller was a better candidate for use in an autonomous tractor to increase the field efficiency by accerlating the traveling velocity.

CHAPTER 7

CONCLUSIONS

CONCLUSIONS OF THE STUDY

In this study, a full coverage-path planner (CPP) with an optimal sequence and an intelligent path tracking controller were developed. to cover a whole area with the high field efficiency for autonomous tillage and puddling·leveling tractor operating in a polygonal paddy field. Conclusions drawn up based on the results are:

- A full-CPP for an autonomous tillage and puddling·leveling tractor that provides automatic generation of both inner and outer-work paths, and boundary corner turning methods applicable to polygonal-shaped paddy fields with various corner angles was developed and demonstrated that it could guide the autonomous tractor with tracking accuracy with lateral and heading root-mean-squared errors (RMSEs) of < 10.1 cm and 2.2° and tillage performance with the skipped areas of < 1.7% of the total area in three different polygonal paddy fields: triangle, (3020.3 m^2), quadrilateral (3451.3 m^2), and pentagon (4361.3 m^2). In addition, when the autonomous puddling·leveling tractor equipped with the developed CPP, navigated the paddy field where the water was flooded, the results showed lateral deviation ranging from -11.3 cm to 13.7 cm and heading error ranging from -2.7 deg to 1.8 deg, respectively, and the system showed superior tracking performance in terms of travel distance and fuel consumption by reducing from 3039.6 m to 1940.1 m and 17.1 L to 16.3 L as compared with those of the manual operation. However, it was

confirmed that it took about 20 minutes more time because it traveled at a slower average velocity (1.35 km/h) than the manual-driven tractor (2.75 km/h).

- A novel path planner for the entry and exit operations of an autonomous tractor was developed using the A* algorithm to enable the tractor located at the entrance to automatically go to the start point of an operational path and return to the entrance after completing the agricultural task. For validation testing in two paddy fields, the entry-exit paths were successfully generated in response to different entrance locations and the tractor followed the entry path and started the operation at the start point of the work path with a lateral deviation of < 8.5 cm. In addition, the tractor navigated the exit path automatically and reached the destination with a lateral deviation of < 12 cm and a heading error of < 22° to the entrance and the operator was then able to drive the tractor to exit the field easily without backward navigation.
- An intelligent path tracking controller designed using reinforcement lerarning (RL) to adaptively provide a tracking parameter (look-ahead distance) based on a navigational condition represented by lateral deviations and heading errors in real-time to keep the implement on the reference line at various speed conditions, was developed and validated. the autonomous tractor equipped with the RL-based intelligent path tracking controller without any stops or divergence with increased path-tracking accuracy (lateral and heading RMSEs of 12.9 cm and 3.8 deg) compared with those (lateral and heading RMSEs of 30.1 cm and 8.6

deg) obtained using the system with slip-estimation based tracking method developed in previous study (Han, Kim, Jeon, Moon, et al., 2019) at 4 km/h.

SUGGESTIONS FO FUTURE STUDY

Based on the results obtained from this study, future studies area recommended as follows:

- The shape of the fields is varied according to the local environment including infield obstacles (i.e., electrical utility pole, rock, tree, etc), natural contours, irrigation facility, and a road. In addition, since the developed CPP is insufficient to provide the path where the field is non-convex or contains obstacles, further studies on path planning strategies applicable to various conditions of the paddy fields are needed.
- The implementation of an optimization method of the CPP used in this study was limited to the determination of an optimal sequence of the inner tracks to minimize a non-working distance that mainly occurs during a headland turning maneuver. Therefore, further investigations about optimal field work pattern for autonomous tractor in terms of field efficiency are required by considering the geometric characteristics of the paddy field such as a field boundary and a single entrance.
- In this study, only look-ahead distance was considered as an action of the framework of reinforcement leraning (RL) implemented in an intelligent path tracking controller. Further studies on the tracking controller based on the RL are needed to achive improved tracking accuracy by considering additional tracking parameters. A possible approach might be

to modify the framework of RL to provide the tracking parameters such as proportional-integral-derivative parameters (Kp, Ki, Kd) of the control logic, traveling velocity, and steering angle.

LIST OF REFERENCES

Adhikari, S. P., Kim, G., & Kim, H. (2020). Deep neural network-based system for autonomous navigation in paddy field. *IEEE Access*, *8*, 71272-71278.

Alexandratos, N., & Bruinsma, J. (2012). World agriculture towards 2030/2050: the 2012 revision.

ASAE, A. (2005). Manure production and characteristics. *ASABE Standard D384. 2. American Society of Agricultural and Biological Engineers. St. Joseph, MI*.

Backman, J., Piirainen, P., & Oksanen, T. (2015). Smooth turning path generation for agricultural vehicles in headlands. *Biosystems Engineering*, *139*, 76-86.

Bergerman, M., Van Henten, E., Billingsley, J., Reid, J., & Mingcong, D. (2013). IEEE robotics and automation society technical committee on agricultural robotics and automation. *IEEE Robotics & Automation Magazine*, *20*(2), 20-23.

Bochtis, D., Griepentrog, H. W., Vougioukas, S., Busato, P., Berruto, R., & Zhou, K. (2015). Route planning for orchard operations. *Computers and electronics in agriculture*, *113*, 51-60.

Bochtis, D., & Sørensen, C. G. (2009). The vehicle routing problem in field logistics part I. *Biosystems engineering*, *104*(4), 447-457.

Bochtis, D., Vougioukas, S., & Griepentrog, H. W. (2009). A mission planner for an autonomous tractor. *Transactions of the ASABE*, *52*(5), 1429-1440.

Bochtis, D. D., & Sørensen, C. G. (2009). The vehicle routing problem in field logistics part I. *Biosystems Engineering*, *104*(4), 447-457. https://doi.org/10.1016/j.biosystemseng.2009.09.003

Bochtis, D. D., & Sørensen, C. G. (2010). The vehicle routing problem in field logistics: Part II. *Biosystems Engineering*, *105*(2), 180-188. https://doi.org/10.1016/j.biosystemseng.2009.10.006

Bochtis, D. D., & Vougioukas, S. G. (2008). Minimising the non-working distance travelled by machines operating in a headland field pattern. *Biosystems Engineering*, *101*(1), 1-12. https://doi.org/10.1016/j.biosystemseng.2008.06.008

Bresenham, J. E. (1965). Algorithm for computer control of a digital plotter. *IBM Systems journal*, *4*(1), 25-30.

CASTRO, D. C. (1970). *Rice Production Manual. Los Banos: University of Philippines/IRRI, 1970*. University of philippines/IRRI.

Chabini, I., & Lan, S. (2002). Adaptations of the A* algorithm for the computation of fastest paths in deterministic discrete-time dynamic networks. *IEEE Transactions on intelligent transportation systems*, *3*(1), 60-74.

Chatterjee, S., Carrera, C., & Lynch, L. A. (1996). Genetic algorithms and traveling salesman problems. *European journal of operational research*, *93*(3), 490-510.

Chauhan, B. S. (2013). Strategies to manage weedy rice in Asia. *Crop Protection*, *48*, 51-56.

Chen, I.-M., & Chan, C.-Y. (2020). Deep reinforcement learning based path tracking controller for autonomous vehicle. *Proceedings of the Institution of Mechanical Engineers, Part D: Journal of Automobile Engineering*, 0954407020954591.

Cho Seung In, C. N. J., Kang In Sueng. (2000). Autonomous Tractor for Tillage Operation Using Machine Vision and Fuzzy Logic Control. *Transactions of the ASAE*, *25*(1), 55-62.

Cho, S. I., & Lee, J. H. (2000). Autonomous speedsprayer using differential global positioning system, genetic algorithm and fuzzy control. *Journal of Agricultural Engineering Research*, *76*(2), 111-119.

Choi, K. H., Han, S. K., Han, S. H., Park, K.-H., Kim, K.-S., & Kim, S. (2015). Morphology-based guidance line extraction for an autonomous weeding robot in paddy fields. *Computers and Electronics in Agriculture*, *113*, 266-274.

Chung, S., Park, W., Chang, Y., & Yeo, W. (1999). Optimal path planning of a tractor-implement for precision farming. *Journal of the Korean Society for Agricultural Machinery*, *24*(4), 301-308.

Conesa-Muñoz, J., Pajares, G., & Ribeiro, A. (2016). Mix-opt: A new route operator for optimal coverage path planning for a fleet in an agricultural environment. *Expert Systems with Applications*, *54*, 364-378. https://doi.org/10.1016/j.eswa.2015.12.047

Davis, L. (1985). Applying adaptive algorithms to epistatic domains. IJCAI,

De Jong, K. A. (1975). *An analysis of the behavior of a class of genetic adaptive systems*. University of Michigan.

Decker Walker, T. K., Jonathan Van Wyck, and Melissa Tilney. (2016). Lessons from the Frotilines of the Agtech Revolution.

Ding, Y., Wang, L., Li, Y., & Li, D. (2018). Model predictive control and its application in agriculture: A review. *Computers and Electronics in Agriculture*, *151*, 104-117.

Dolgov, D., Thrun, S., Montemerlo, M., & Diebel, J. (2010). Path planning for autonomous vehicles in unknown semi-structured environments. *The international journal of robotics research*, *29*(5), 485-501.

Dong, F., Heinemann, W., & Kasper, R. (2011). Development of a row guidance system for an autonomous robot for white asparagus harvesting. *Computers and Electronics in Agriculture*, *79*(2), 216-225.

Dubins, L. E. (1957). On curves of minimal length with a constraint on average curvature, and with prescribed initial and terminal positions and tangents. *American Journal of mathematics*, *79*(3), 497-516.

Edwards, G. T. C., Hinge, J., Skou-Nielsen, N., Villa-Henriksen, A., Sørensen, C. A. G., & Green, O. (2017). Route planning evaluation of a prototype optimised infield route planner for neutral material flow agricultural operations. *Biosystems Engineering*, *153*, 149-157. https://doi.org/10.1016/j.biosystemseng.2016.10.007

Fang, H., Dou, L., Chen, J., Lenain, R., Thuilot, B., & Martinet, P. (2011). Robust anti-sliding control of autonomous vehicles in presence of lateral disturbances. *Control Engineering Practice*, *19*(5), 468-478.

FAOSTAT, 2021. Land use statistics and indicators statistics. Global, reginal and country trends 1990-2019. FAOSTAT Analytical Brief Series No 28. Rome. Italy.

Fernandes, E., Costa, P., Lima, J., & Veiga, G. (2015). Towards an orientation enhanced astar algorithm for robotic navigation. 2015 IEEE International Conference on Industrial Technology (ICIT),

Forbes, J. R. N. (2002). *Reinforcement learning for autonomous vehicles*. University of California, Berkeley.

Galceran, E., & Carreras, M. (2013). A survey on coverage path planning for robotics. *Robotics and Autonomous Systems*, *61*(12), 1258-1276. https://doi.org/10.1016/j.robot.2013.09.004

Gebbers, R., & Adamchuk, V. I. (2010). Precision agriculture and food security. *Science*, *327*(5967), 828-831.

Glorot, X., & Bengio, Y. (2010). Understanding the difficulty of training deep feedforward neural networks. Proceedings of the thirteenth international conference on artificial intelligence and statistics,

Goldberg, D. E., & Holland, J. H. (1988). Genetic algorithms and machine learning.

Groover, G. E., & Grisso, R. D. (2009). Investing in GPS guidance systems?

GuideConnect, F. (2012). Two Tractors—One Driver. 2012. In.

Hameed, I., Bochtis, D., Sørensen, C., & Nøremark, M. (2010). Automated generation of guidance lines for operational field planning. *Biosystems engineering*, *107*(4), 294-306.

Hameed, I. A. (2013). Intelligent Coverage Path Planning for Agricultural Robots and Autonomous Machines on Three-Dimensional Terrain. *Journal of Intelligent & Robotic Systems*, *74*(3-4), 965-983. https://doi.org/10.1007/s10846-013-9834-6

Hameed, I. A. (2017). Coverage path planning software for autonomous robotic lawn mower using Dubins' curve. 2017 IEEE International Conference on Real-time Computing and Robotics (RCAR),

Hameed, I. A., Bochtis, D., & Sorensen, C. (2011). Driving angle and track sequence optimization for operational path planning using genetic algorithms. *Applied Engineering in Agriculture*, *27*(6), 1077-1086.

Hameed, I. A., Bochtis, D., & Sørensen, C. A. (2013). An optimized field coverage planning approach for navigation of agricultural robots in fields involving obstacle areas. *International journal of advanced robotic systems*, *10*(5), 231.

Hameed, I. A., Bochtis, D. D., Sørensen, C. G., Jensen, A. L., & Larsen, R. (2013). Optimized driving direction based on a three-dimensional field representation. *Computers and Electronics in Agriculture*, *91*, 145-153. https://doi.org/10.1016/j.compag.2012.12.009

Hameed, I. A., Bochtis, D. D., Sørensen, C. G., & Nøremark, M. (2010). Automated generation of guidance lines for operational field planning. *Biosystems Engineering*, *107*(4), 294-306. https://doi.org/10.1016/j.biosystemseng.2010.09.001

Hameed, I. A., la Cour-Harbo, A., & Osen, O. L. (2016). Side-to-side 3D coverage path planning approach for agricultural robots to minimize skip/overlap areas between swaths. *Robotics and Autonomous Systems*, *76*, 36-45.

Han, X.-Z., Kim, H.-J., Moon, H.-C., Woo, H.-J., Kim, J.-H., & Kim, Y.-J. (2013). Development of a path generation and tracking algorithm for a Korean auto-guidance tillage tractor. *Journal of Biosystems Engineering*, *38*(1), 1-8.

Han, X., Kim, H.-J., Jeon, C. W., & Kim, J. H. (2019). Simulation Study to Develop Implement Control and Headland Turning Algorithms for Autonomous Tillage Operations. *Journal of Biosystems Engineering*, *44*(4), 245-257.

Han, X., Kim, H.-J., Jeon, C. W., Moon, H. C., Kim, J. H., & Yi, S. Y. (2019). Application of a 3D tractor-driving simulator for slip estimation-based path-

tracking control of auto-guided tillage operation. *Biosystems Engineering*, *178*, 70-85.

Han, X. Z., Kim, H. J., Kim, J. Y., Yi, S. Y., Moon, H. C., Kim, J. H., & Kim, Y. J. (2015). Path-tracking simulation and field tests for an auto-guidance tillage tractor for a paddy field. *Computers and Electronics in Agriculture*, *112*, 161-171.

Hart, P. E., Nilsson, N. J., & Raphael, B. (1968). A formal basis for the heuristic determination of minimum cost paths. *IEEE transactions on Systems Science and Cybernetics*, *4*(2), 100-107.

Hoy, R. M., Rohrer, R., Liska, A., Luck, J. D., Isom, L., & Keshwani, D. R. (2014). Agricultural industry advanced vehicle technology: Benchmark study for reduction in petroleum use.

Huang, P., Luo, X., & Zhang, Z. (2009). Headland turning control method simulation of autonomous agricultural machine based on improved pure pursuit model. International Conference on Computer and Computing Technologies in Agriculture,

Hunt, D. (2008). *Farm power and machinery management*. Waveland Press.

Jensen, M. A. F., Bochtis, D., Sørensen, C. G., Blas, M. R., & Lykkegaard, K. L. (2012). In-field and inter-field path planning for agricultural transport units. *Computers & Industrial Engineering*, *63*(4), 1054-1061. https://doi.org/10.1016/j.cie.2012.07.004

Jensen, M. F., Bochtis, D., & Sørensen, C. G. (2015). Coverage planning for capacitated field operations, part II: Optimisation. *Biosystems Engineering*, *139*, 149-164. https://doi.org/10.1016/j.biosystemseng.2015.07.002

Jeon, C.-W., Kim, H.-J., Yun, C., Han, X., & Kim, J. H. (2021). Design and validation testing of a complete paddy field-coverage path planner for a fully autonomous tillage tractor. *Biosystems Engineering*, *208*, 79-97.

Jeon, C. W., Kim, H.-J., Han, X. Z., & Kim, J. H. (2017). Fuzzy logic-based steering controller for an autonomous head-feed combine harvester. 2017 ASABE Annual International Meeting,

Jin, J., & Tang, L. (2010). Optimal Coverage Path Planning for Arable Farming on 2D Surfaces. *Transactions of the ASABE*, *53*(1), 283-295.

Jin, J., & Tang, L. (2011). Coverage path planning on three-dimensional terrain for arable farming. *Journal of Field Robotics*, *28*(3), 424-440. https://doi.org/10.1002/rob.20388

Johnson, D. A., Naffin, D. J., Puhalla, J. S., Sanchez, J., & Wellington, C. K. (2009). Development and implementation of a team of robotic tractors for autonomous peat moss harvesting. *Journal of Field Robotics*, *26*(6-7), 549-571. https://doi.org/10.1002/rob.20297

Kayacan, E., Kayacan, E., Ramon, H., & Saeys, W. (2014). Learning in centralized nonlinear model predictive control: Application to an autonomous tractor-trailer system. *IEEE Transactions on Control Systems Technology*, *23*(1), 197-205.

Kendall, A., Hawke, J., Janz, D., Mazur, P., Reda, D., Allen, J.-M., Lam, V.-D., Bewley, A., & Shah, A. (2019). Learning to drive in a day. 2019 International Conference on Robotics and Automation (ICRA),

Kim, H., Kim, S.-H., Jeon, M., Kim, J., Song, S., & Paik, K.-J. (2017). A study on path optimization method of an unmanned surface vehicle under

environmental loads using genetic algorithm. *Ocean Engineering*, *142*, 616-624.

Kise, M., Noguchi, N., Ishii, K., & Terao, H. (2001). Development of the agricultural autonomous tractor with an RTK-GPS and a FOG. *IFAC Proceedings Volumes*, *34*(19), 99-104.

Koyuncu, E., & Inalhan, G. (2008). A probabilistic B-spline motion planning algorithm for unmanned helicopters flying in dense 3D environments. 2008 IEEE/RSJ International Conference on Intelligent Robots and Systems,

Kraus, T., Ferreau, H. J., Kayacan, E., Ramon, H., De Baerdemaeker, J., Diehl, M., & Saeys, W. (2013). Moving horizon estimation and nonlinear model predictive control for autonomous agricultural vehicles. *Computers and electronics in agriculture*, *98*, 25-33.

Kurita, H., Iida, M., Cho, W., & Suguri, M. (2017). Rice autonomous harvesting: Operation framework. *Journal of Field Robotics*, *34*(6), 1084-1099.

Lee Jae Hoon, C. S. I., Lee Jeong Hoon. (1998). Autonomous SpeedSprayer Using DGPS and Fuzzy Control (II) - Real Operation -. *Agricultural and Biosystems Engineering*, *23*, 75-82.

Lenain, R., Thuilot, B., Cariou, C., & Martinet, P. (2005). Model predictive control for vehicle guidance in presence of sliding: application to farm vehicles path tracking. Proceedings of the 2005 IEEE international conference on robotics and automation,

Lenain, R., Thuilot, B., Cariou, C., & Martinet, P. (2006). High accuracy path tracking for vehicles in presence of sliding: Application to farm vehicle automatic guidance for agricultural tasks. *Autonomous robots*, *21*(1), 79-97.

Lenain, R., Thuilot, B., Cariou, C., & Martinet, P. (2007). Adaptive and predictive path tracking control for off-road mobile robots. *European journal of control*, *13*(4), 419-439.

Li, D., Zhao, D., Zhang, Q., & Chen, Y. (2019). Reinforcement learning and deep learning based lateral control for autonomous driving [application notes]. *IEEE Computational Intelligence Magazine*, *14*(2), 83-98.

Li, J., Liu, S., Zhang, B., & Zhao, X. (2014). RRT-A* motion planning algorithm for non-holonomic mobile robot. 2014 proceedings of the SICE annual conference (SICE),

Liu, C., Zhao, X., Du, Y., Cao, C., Zhu, Z., & Mao, E. (2018). Research on static path planning method of small obstacles for automatic navigation of agricultural machinery. *IFAC-PapersOnLine*, *51*(17), 673-677.

Luckow, A., Cook, M., Ashcraft, N., Weill, E., Djerekarov, E., & Vorster, B. (2016). Deep learning in the automotive industry: Applications and tools. 2016 IEEE International Conference on Big Data (Big Data),

Matsuo, Y., Yukumoto, O., & Noguchi, N. (2012). Enhanced Adaptability of Tilling Robot (Initial Report). *Japan Agricultural Research Quarterly: JARQ*, *46*(4), 295-303.

Mnih, V., Kavukcuoglu, K., Silver, D., Rusu, A. A., Veness, J., Bellemare, M. G., Graves, A., Riedmiller, M., Fidjeland, A. K., & Ostrovski, G. (2015). Human-level control through deep reinforcement learning. *nature*, *518*(7540), 529-533.

Nagasaka, Y., Saito, H., Tamaki, K., Seki, M., Kobayashi, K., & Taniwaki, K. (2009). An autonomous rice transplanter guided by global positioning system and inertial measurement unit. *Journal of field robotics*, *26*(6-7), 537-548.

Noguchi, N., Reid, J. F., Zhang, Q., Will, J. D., & Ishii, K. (1998). Development of robot tractor based on RTK-GPS and gyroscope. 2001 ASAE Annual Meeting,

Noguchi, N., & Terao, H. (1997). Path planning of an agricultural mobile robot by neural network and genetic algorithm. *Computers and electronics in agriculture*, *18*(2-3), 187-204.

Normey-Rico, J. E., Alcalá, I., Gómez-Ortega, J., & Camacho, E. F. (2001). Mobile robot path tracking using a robust PID controller. *Control Engineering Practice*, *9*(11), 1209-1214.

O'Rourke, J. (1985). Finding minimal enclosing boxes. *International Journal of Computer and Information Sciences*, *14*(3).

Oberti, R., & Shapiro, A. (2016). Advances in robotic agriculture for crops. *Biosystems Engineering*, *100*(146), 1-2.

Oksanen, T., & Visala, A. (2009). Coverage path planning algorithms for agricultural field machines. *Journal of Field Robotics*, *26*(8), 651-668. https://doi.org/10.1002/rob.20300

Precup, R.-E., & Hellendoorn, H. (2011). A survey on industrial applications of fuzzy control. *Computers in industry*, *62*(3), 213-226.

R Shamshiri, R., Weltzien, C., Hameed, I. A., J Yule, I., E Grift, T., Balasundram, S. K., Pitonakova, L., Ahmad, D., & Chowdhary, G. (2018). Research and development in agricultural robotics: A perspective of digital farming.

Rahman, M. M., Ishii, K., & Noguchi, N. (2019). Optimum harvesting area of convex and concave polygon field for path planning of robot combine harvester. *Intelligent service robotics*, *12*(2), 167-179.

Riedmiller, M., Montemerlo, M., & Dahlkamp, H. (2007). Learning to drive a real car in 20 minutes. 2007 Frontiers in the Convergence of Bioscience and Information Technologies,

Roberge, V., Tarbouchi, M., & Labonté, G. (2012). Comparison of parallel genetic algorithm and particle swarm optimization for real-time UAV path planning. *IEEE Transactions on industrial informatics*, *9*(1), 132-141.

Rodias, E., Berruto, R., Busato, P., Bochtis, D., Sørensen, C. G., & Zhou, K. (2017). Energy savings from optimised in-field route planning for agricultural machinery. *Sustainability*, *9*(11), 1956.

Sabelhaus, D., Röben, F., zu Helligen, L. P. M., & Lammers, P. S. (2013). Using continuous-curvature paths to generate feasible headland turn manoeuvres. *Biosystems engineering*, *116*(4), 399-409.

Saiz-Rubio, V., & Rovira-Más, F. (2020). From smart farming towards agriculture 5.0: a review on crop data management. *Agronomy*, *10*(2), 207.

Scarlett, A. J. (2001). Integrated control of agricultural tractors and implements: a review of potential opportunities relating to cultivation and crop establishment machinery. *Computers and electronics in agriculture*, *30*(1-3), 167-191.

Schrijver, R., Poppe, K., & Daheim, C. (2016). Precision agriculture and the future of farming in Europe. *Science and Technology options assessment*.

Sedighi, S., Nguyen, D.-V., & Kuhnert, K.-D. (2019). Guided Hybrid A-star Path Planning Algorithm for Valet Parking Applications. 2019 5th International Conference on Control, Automation and Robotics (ICCAR),

Seo, I.-H., Seo, D.-H., & Kim, K.-D. (2010). Development of working path formation program for autonomous tractor system. *Korean Journal of Agricultural Science*, *37*(1), 113-121.

Seyyedhasani, H., & Dvorak, J. S. (2017). Using the Vehicle Routing Problem to reduce field completion times with multiple machines. *Computers and Electronics in Agriculture*, *134*, 142-150. https://doi.org/10.1016/j.compag.2016.11.010

Shergold, I., Wilson, M., & Parkhurst, G. (2016). The mobility of older people, and the future role of Connected Autonomous Vehicles.

Song, R., Liu, Y., & Bucknall, R. (2019). Smoothed A* algorithm for practical unmanned surface vehicle path planning. *Applied Ocean Research*, *83*, 9-20.

Spekken, M., & de Bruin, S. (2012). Optimized routing on agricultural fields by minimizing maneuvering and servicing time. *Precision Agriculture*, *14*(2), 224-244. https://doi.org/10.1007/s11119-012-9290-5

Spekken, M., Molin, J. P., & Romanelli, T. L. (2015). Cost of boundary manoeuvres in sugarcane production. *biosystems engineering*, *129*, 112-126.

Stafford, J. V. (2000). Implementing precision agriculture in the 21st century. *Journal of Agricultural Engineering Research*, *76*(3), 267-275.

Thomasson, J. A., Baillie, C. P., Antille, D. L., Lobsey, C. R., & McCarthy, C. L. (2019). *Autonomous technologies in agricultural equipment: a review of the state of the art*. American Society of Agricultural and Biological Engineers.

Tillett, N. (2003). Robots on the farm. *Industrial Robot-an International Journal*, 396-397.

Tilman, D., Cassman, K. G., Matson, P. A., Naylor, R., & Polasky, S. (2002). Agricultural sustainability and intensive production practices. *Nature*, *418*(6898), 671-677.

Utamima, A., Reiners, T., Ansaripoor, A., & Seyyedhasani, H. (2018). The Agricultural Routing Planning in Field Logistics. In *Contemporary Approaches and Strategies for Applied Logistics* (pp. 261-283). IGI Global.

Utamima, A., Reiners, T., & Ansaripoor, A. H. (2019). Optimisation of agricultural routing planning in field logistics with Evolutionary Hybrid Neighbourhood Search. *Biosystems Engineering*, *184*, 166-180. https://doi.org/10.1016/j.biosystemseng.2019.06.001

Veres, S. M., Molnar, L., Lincoln, N. K., & Morice, C. P. (2011). Autonomous vehicle control systems—a review of decision making. *Proceedings of the Institution of Mechanical Engineers, Part I: Journal of Systems and Control Engineering*, *225*(2), 155-195.

Vougioukas, S. G. (2012). A distributed control framework for motion coordination of teams of autonomous agricultural vehicles. *Biosystems engineering*, *113*(3), 284-297.

Walker Jr, W. W., Westerberg, C. E., Schuler, D. J., & Bode, J. A. (1989). Design and evaluation of eutrophication control measures for the St. Paul water supply. *Lake and Reservoir Management*, *5*(1), 71-83.

Wang, S., Yin, X., Li, P., Zhang, M., & Wang, X. (2019). Trajectory Tracking Control for Mobile Robots Using Reinforcement Learning and PID. *Iranian*

Journal of Science and Technology, Transactions of Electrical Engineering, 1-10.

Wasala, A., Byrne, D., Miesbauer, P., O'Hanlon, J., Heraty, P., & Barry, P. (2020). Trajectory based lateral control: A Reinforcement Learning case study. *Engineering Applications of Artificial Intelligence*, *94*, 103799.

Watanabe, T. (2018). Paddy Fields as Artificial and Temporal Wetland. *Irrigation in Agroecosystems*.

Witney, B. (1988). *Choosing and using farm machines*. Longman.

Wu, T., & Hung, J. Y. (2017). Path following for a tractor-trailer system using model predictive control. SoutheastCon 2017,

Yin, X., Du, J., Noguchi, N., Yang, T., & Jin, C. (2018). Development of autonomous navigation system for rice transplanter. *International Journal of Agricultural and Biological Engineering*, *11*(6), 89-94.

Yu, X. (2015). *Optimization Approaches for a Dubins vehicle in coverage planning problem and traveling salesman problems*

Yu, X., Roppel, T. A., & Hung, J. Y. (2015). An optimization approach for planning robotic field coverage. IECON 2015-41st Annual Conference of the IEEE Industrial Electronics Society,

Zandonadi, R. S. (2012). Computational tools for improving route planning in agricultural field operations.

Zhang, Q., & Qiu, H. (2004). A dynamic path search algorithm for tractor automatic navigation. *Transactions of the ASAE*, *47*(2), 639.

Zhang, W., Gai, J., Zhang, Z., Tang, L., Liao, Q., & Ding, Y. (2019). Double-DQN based path smoothing and tracking control method for robotic vehicle navigation. *Computers and Electronics in Agriculture*, *166*, 104985.

Zhang, X., Fan, C., Cao, Z., Fang, J., & Jia, Y. (2020). Novel obstacle-avoiding path planning for crop protection UAV using optimized Dubins curve. *International Journal of Agricultural and Biological Engineering*, *13*(4), 172-177.

Zhou, K., Jensen, A. L., Sørensen, C. G., Busato, P., & Bothtis, D. (2014). Agricultural operations planning in fields with multiple obstacle areas. *Computers and electronics in agriculture*, *109*, 12-22.

수도작 자율 경운 및 균평·정지 농작업을 위한 전역 경로 생성 및 탐색 제어 기술 개발

전 찬 우

ABSTRACT IN KOREA

농업분야는 세계 인구 증가에 따른 생산량 증대 요구와 함께 농가 인구 감소 및 고령화로 지속 가능한 방법으로 농산물 생산을 위한 농가경영의 과제를 겪고 있으며, 이러한 효율적인 농업생산시스템에 대한 요구로 자율농기계가 농업 문제 해결방안 중 하나로 주목받고 있다. 소규모, 구획화 그리고 집약 농업 형태인 수도작 환경에서 자율주행 농기계 시스템의 적용은 농지 내 선회, 농지 형태에 따른 논둑 경계 작업, 논둑 지형적 특성으로 발생된 단일 출입구 등이 반영된 경로 계획 기술과 잦은 선회와 담수 환경에 의해 발생되는 동적환경변화 반영한 정밀제어 기술이 필요하다.

본 연구에서는 다변형 무논에서 경운 및 균평·정지 작업을 대상으로 자율주행 트랙터가 전역을 최적화 된 운행계획으로 효율적인 농작업을 수행할 수 있는 경로 생성기와 동적 환경변화를 감지해 주행전략의 실시간 변화가 가능한 지능형 경로 탐색기가 탑제 된 완전 자율작업 트랙터 시스템을 개발하고자 한다. 이를 위해 자율작업 트랙터 대상 경운 및 균평·정지 작업 경로 모델 제시 및 비정형 무논형태에 적용가능한 내외부 작업 경로 및 회경 방식을 개발하였으며, 경로 계획

성능향상을 위해 유전 알고리즘을 활용하여 비작업 거리의 최소화가 가능한 최적 왕복작업열 순서 결정 방법이 탑재되었다. 경로 계획 시뮬레이션 결과, 개발 된 경로생성기를 통해 최적 농작업 경로는 이전에 개발된 경로생성기와 비교하여 세 가지 다각형 포장 (삼각형, 사다리꼴, 오각형) 28%, 33.9% 및 45.0%의 비작업 거리를 줄임으로써 작업 효율성을 높이는 효과를 보여주었다. 더 나아가 농지 입구에 위치한 트랙터가 자동으로 농작업의 시작 지점으로 이동하고 농업 작업 완료 후 입구로 돌아갈 수 있도록 A* 알고리즘을 이용한 진출입 경로 생성기를 제안하여 농지 내 완전 자율작업이 가능하도록 하였다. 또한 다양한 속도 조건에서 트랙터의 주행 성능 (정확성, 안정성)을 향상시키기 위해 강화학습을 활용한 실시간 동적환경변화 대응 지능형 경로 탐색기를 설계 및 개발하였다. 가상현실에서 무인 농작업이 가능한 시뮬레이터를 이용하여 개발한 알고리즘을 평가하였으며 최종적으로는 개발 기술을 실제 농용트랙터에 탑재하여 실제포장에서 무인 경운 및 균평·정지작업 수행 및 주행·작업 성능을 검증하였다.

검증 결과, 자율작업 시스템 트랙터은 로터리 경운 작업 시 위치 오차 10.1cm 그리고 방향 오차 2.2° 미만인 RMSE 정확도로 세 가지 다각형 무논 (삼각형, (3020.3 m^2), 사다리꼴 (3451.3 m^2), and 오각형 (4361.3 m^2))에서 전체 면적의 1.7% 미만의 미경지로 자율 작업이 가능함을 보였다. 또한 자율 균평·정지 작업 시 횡방향 및 방향각 오차가 각각 -11.3cm ~ 13.7cm, -2.7^{o} ~ 1.8^{o}로 자율 작업기 가능함을 확인하였으며, 숙련 작업자에 비해 비해 주행 거리와 총 연료 소모량을 3039.6m 에서 1940.1m 그리고 17.1L 에서 16.3L 로 감소시킴으로써 주행거리 및 연료소모 효율을 개선 됨이 확인 되었다. 하지만 숙련 작업자(2.75km/h)보다 자율작업 트랙터(1.35km/h)는 느린 평균속도로 주행하여 20 분 정도 시간이 더 소요되었다. 그럼에도 불구하고, 비슷한 평준화 성능이 각각 39.61m 에서 39.85m(자율), 39.62m 에서 39.81m(수동)의 고도에서 측정되어 작업의 효용성이 확인되었다.

마지막으로, 강화학습 기반 지능형 경로 추적 제어기가 장착된 자율 트랙터 시스템의 RMS 주행 및 방향각 오차는 4km/h 주행 시 12.9 cm 와 3.8° 이내로 기존 슬립 추정 기반 탐색방법 (30.1 cm 와 8.6°)과 비교하여 우수한 추종경로 정확도 성능을 보였다. 이러한 결과들을 통해 개발 경운 및 균평·정지 경로 생성 및 지능형 탐색 제어 기술이 기존보다 효율적인 트랙터 운용으로 수도작 농업환경에서 무인 자율작업 트랙터의 잠재력을 보여주었다. 향후 보완 연구로서 곡선, 오목 포장형태 등 확대 된 다중 제약 영농조건을 고려한 경로생성 기술 보완이 필요하며, 자율작업 트랙터를 이용하여 농작업 시 토양조건으로 인하여 발생되는 부하 및 슬립 발생 시 탐색 매개변수를 가변적용하는 등의 무논에서 활용해 온 구형 농기계의 제원에 대응되는 보편적인 기능을 수행하면서도 높은 자동화 수준을 달성하기 위한 강인제어기술이 필요할 것으로 판단된다.

주요어: 자율주행 트랙터, 수도작 논, 경운, 균평·정지, 커버리지 경로 생성, 최적 경로 생성, 지능형 경로 탐색, 강화학습

학번 : 2015-21508